ISSN: 3102-0372 (Online)

Dec. 2025

Vol. 2, No. 2

Official Journal of

Nepal Society of Engineering Geology (NSEG)

Asian Journal of Engineering Geology

Vol. 2, No. 2, December 2025

The Official Journal of Nepal Society of Engineering Geology

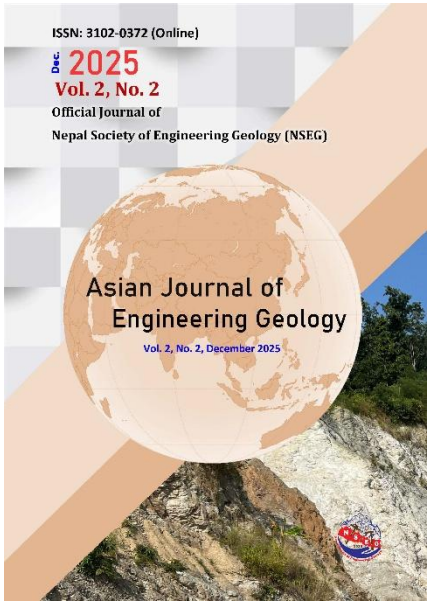

Asian Journal of Engineering Geology (AJEG)

Concept

The Asian Journal of Engineering Geology (**AJEG**), published by the Nepal Society of Engineering Geology (**NSEG**), is envisioned as a dedicated platform for advancing the understanding and application of engineering geology within the unique geological context of Asia, with a particular focus on the Himalayan region, while also welcoming contributions relevant to other parts of the world.

In recent years, research in engineering geology and related fields has seen significant progress. However, specialized publication platforms remain limited, especially in Asia, hindering the effective dissemination of research findings and knowledge sharing among engineering geologists. To address this gap, NSEG has launched the Asian Journal of Engineering Geology (AJEG), offering a professional and accessible forum for geoscientists, engineers, and environmentalists engaged in landslide studies, environmental geoscience, and engineering geological research.

AJEG aims to be a key resource for stakeholders seeking updated information on the geological challenges and engineering solutions relevant to seismically active and geologically complex regions like the Himalayas and beyond. The journal is committed to publishing original research, case studies, and technical notes that contribute to a deeper understanding of engineering geology in diverse terrains. Under the auspices of **NSEG**, **AJEG** places particular emphasis on:

- Slope stability and landslide hazard assessment
- Earthquake geology and seismic risk analysis
- Engineering geological aspects of infrastructure development
- Environmental and geotechnical investigations
- Integration of geological, geotechnical, and environmental knowledge for sustainable development

The journal actively promotes collaboration among researchers, engineers, and geologists from Asia and around the globe. By engaging regional experts and fostering interdisciplinary dialogue, **AJEG** seeks to address current and emerging challenges in engineering geology through shared knowledge and innovation.

In addition to peer-reviewed articles, **AJEG** will feature updates on conferences, research initiatives, and activities organized by the Nepal Society of Engineering Geology. This will position the journal not only as a scholarly publication but also as a hub for professional exchange and community building within the field of engineering geology in Nepal and across the region.

Aims and Scope

The Asian Journal of Engineering Geology (**AJEG**) serves as a common platform for the publication of integrated research covering all aspects of engineering geology. The journal welcomes original research articles, rapid reports on emerging engineering geology issues, case studies, and technical notes highlighting practical applications. Researchers and practitioners are encouraged to submit original, unpublished contributions. Subject areas include, but are not limited to, the following fields:

- Applied geomorphology
- Structural geology
- Applied geophysics and g
- Geochemistry
- Environmental geology
- Hydrogeology
- Land use planning
- Natural hazards
- Remote sensing techniques
- Soil and rock mechanics
- Applied geotechnical engineering
- Urban Engineering Geology
- Engineering Geology of marine and reservoir.
- Engineering geology in flash floods and tsunami
- Landslide hazard assessment and mapping
- GIS applications in engineering geology
- Landslide monitoring and landslide mitigation
- Engineering geology of the Himalayan slopes
- Rainfall-induced landslides
- Earthquake-induced landslides
- Anthropogenic controls on hazards
- Stability of dams and embankments
- Engineering geology of heritage areas, monitoring and mitigation
- Groundwater monitoring
- Seismic Hazard and Risk
- Disaster Risk Reduction and Management
- Engineering geology of Tunnels and bridges
- Foundations on slopes and plains

- Early warning of multi-hazard risk
- Landslide hazard management at community level
- Physical and numerical modeling in engineering geology
- High altitude engineering geological issues.
- Economics of natural hazards and related climate change
- Agricultural geology
- Snow avalanche
- Engineering geology and infrastructure development
- Snow cover in the Himalaya
- Environment friendly low cost infrastructure development
- Rural infrastructures and engineering geology
- Geotechnical engineering, modeling and ground improvement
- Nature-based solutions for disaster risk reduction

These topics suggest a multidisciplinary approach, encompassing various aspects of geology and engineering that have practical applications in fields such as environmental management, land planning, and geotechnical engineering.

Publication program

The Asian Journal of Engineering Geology (**AJEG**) publishes two issues each year. It is a peer-reviewed journal committed to disseminating the latest developments across various fields of engineering geology. **AJEG** is an open-access online journal, freely available to readers worldwide.

The Nepal Society of Engineering Geology promotes open access publishing to broaden the journal's global reach, enhance the visibility and impact of published research, and improve indexing across major search engines. Researchers and professionals from all relevant disciplines are invited to submit high-quality manuscripts presenting cutting-edge research or innovations in engineering geology and related areas. **AJEG** welcomes both individual and institutional submissions aligned with the journal's aims and scope.

Editorial Team

Associate Editor-in-Chief

Editorial Board Members

Editors for online handling

We invite researchers specializing in engineering geology to become part of the editorial board and contribute to our publication. If you are interested in joining, kindly send an email to nsegnepal@gmail.com.

Instructions to Contributors

All manuscripts submitted for publication, including original articles, rapid reports on recent engineering geology issues, case studies, and technical notes, will undergo a rigorous peer review by at least two independent experts in the relevant field. A member of the Editorial Board may also serve as a reviewer when appropriate expertise is required.

Authors' Responsibilities

Only individuals who have made significant intellectual contributions to the content of the manuscript should be listed as authors. Authorship should be based on contributions to the conception and design of the study, active involvement in drafting or critically revising the manuscript, and participation in the final revision process.

The corresponding author is responsible for submitting the final version of the manuscript following the peer review process. Any external support, such as funding, equipment, or institutional assistance, must be clearly acknowledged in the Acknowledgment section.

In the Comments to the Editor section during submission, authors must disclose any prior or duplicate publication of the manuscript's content. All submissions to AJEG are subject to plagiarism screening, and the acceptable similarity index is limited to a maximum of 20%. Author should use given Template in the web site for preparation of manuscript.

Manuscript Preparation Overview

All submissions to the Asian Journal of Engineering Geology (AJEG) must be written in International English. Authors whose first language is not English are strongly encouraged to have their manuscripts reviewed by a native English speaker or to use a professional English editing service prior to submission. All references, including online sources, must be formatted according to the journal's referencing guidelines outlined in this document. Each submitted article must include an abstract that briefly summarizes the key content and findings of the study. The name,

institutional address, and email address of the corresponding author must be clearly indicated on the title page.

Figures and tables should be embedded within the manuscript after the list of references. Original figures should be at least half the size of A4 paper in their longest dimension. Acceptable formats for figures and images are TIFF (TIF) with a resolution of 300–600 pixels per inch (ppi). Monochrome images should be saved in grayscale mode, while color images must be in RGB mode. Only single-layer images are accepted. Authors should make every effort to avoid jargon, clearly define all nonstandard abbreviations upon first use, and present the content in a clear, concise, and accessible manner.

Manuscript Preparation Guidelines for AJEG

Authors must use the official manuscript template available on the AJEG website for preparing their submissions.

Title Page

The **title page** should include the following details:

- **Title** of the article
- **Full name(s)** of all authors (first name, middle initial(s), and surname)
- **Affiliations** of the authors, including department or division, institution or organization, city, and country. Do not use abbreviations for affiliations.
- If multiple authors share the same affiliation, list all authors first, followed by the shared affiliation.
- **Email addresses** of all authors must be included.
- The **corresponding author** should be clearly identified with an asterisk (*).

Abstract and Keywords

The manuscript should begin with an **Abstract** of approximately **300 words**, clearly summarizing:

- The research problem
- The methods used
- Major findings
- Conclusions

Immediately following the abstract, list **up to five keywords or phrases** for indexing purposes as per the template provided.

Figures, Tables, and Symbols

- Special characters, mathematical symbols, and Greek letters not available on a standard keyboard must be created using the **Symbol** font.
- **Figures and tables** should be **embedded** at appropriate locations within the text **after the list of references**.
- After the manuscript is accepted, authors must also submit **figures as separate high-resolution files**.
- Figures should follow the formatting requirements outlined in the submission guidelines (e.g., TIFF format, 300–600 dpi, RGB/grayscale mode, single-layer).

Pagination, Line Numbering, and Equations

- Authors must insert both page numbers and continuous line numbers throughout the manuscript to facilitate the review process. Page numbers should appear in the footer of each page.
- Equations should be left-aligned, with reference numbers aligned to the right margin.
- For long equations, break the right side into approximately equal parts and align to the right. Place the equation number on the last line only.
- All equations must be numbered sequentially as they appear in the text.

Units

Use **SI units** throughout the manuscript. If alternative units are provided, they should appear in parentheses following the SI units.

Acknowledgments

Acknowledgments should be included before the list of References, and the title should read "Acknowledgments." Author/s should obtain a permission to acknowledge from all those mentioned in the Acknowledgements.

References

In the list of references, provide complete information of each reference material. Cite a symposium paper only from published proceedings. Do not cite an article or book only accepted for publication but not published. Do not use ibid. Please avoid excessive referencing.

Unpublished data, unpublished abstracts and personal communications should not be included in the reference list. Footnotes are not acceptable.

AJEG prefers maximum 60 references per article. The journal follows the Harvard system for citation, with author name/s and year of publication in parentheses, such as one author: (Hungr 2003) or Hungr (2003), two authors: (Doe and Morris, 2009) or Doe and Morris (2009), and three authors or more: (Rahardjo et al., 2002) or Rahardjo et al. (2002).

APA-Style Reference Examples

Journal article

van Westen, C. J., Rengers, N., and Soeters, R. (2003). Use of geomorphological information in indirect landslide susceptibility assessment. Natural Hazards, 30, 399–419.

Multiple works by same author(s) in same year

Dahal, R. K., Hasegawa, S., Nonomura, A., Yamanaka, M., and Dhakal, S. (2008a). DEM-based deterministic landslide hazard analysis in the Lesser Himalaya of Nepal. Georisk: Assessment and Management of Risk for Engineered Systems and Geohazards, 2(3), 161–178.

Dahal, R. K., Hasegawa, S., Nonomura, A., Yamanaka, M., Dhakal, S., and Paudyal, P. (2008b). Predictive modelling of rainfall-induced landslide hazard in the Lesser Himalaya of Nepal based on weights-of-evidence. Geomorphology, 102(3–4), 496–510.

Journal article with DOI

Hasegawa, S., Dahal, R. K., Yamanaka, M., Bhandary, N. P., Yatabe, R., and Inagaki, H. (2009). Causes of large-scale landslides in the Lesser Himalaya of central Nepal. Environmental Geology, 57, 1423–1434. https://doi.org/10.1007/s00254-008-1420-z

Journal article in press

Dahal, R. K., and Hasegawa, S. (2008). Representative rainfall thresholds for landslides in the Nepal Himalaya. Geomorphology. https://doi.org/10.1016/j.geomorph.2008.01.014 (in press)

Maps and Pamphlets

Amatya, K. M., and Jnawali, B. M. (1994). Geological map of Nepal (Scale 1:1,000,000). Department of Mines and Geology, Kathmandu, Nepal.

Books (authored)

Dahal, R. K. (2006). Geology for technical students. Bhrikuti Academic Publication, Kathmandu.

Same author, multiple books same year

Krahn, J. (2004a). Seepage modeling with SEEP/W: An engineering methodology (1st ed.). Geo-Slope International Ltd., Alberta.

Krahn, J. (2004b). Stability modeling with SLOPE/W: An engineering methodology (1st ed.). Geo-Slope International Ltd., Calgary.

Edited Book

Wohletz, F., and Aaron, G. (Eds.). (1992). Sedimentology. California Press, CA.

Book Chapter

Ward, T. J., Li, R.-M., and Simons, D. B. (1981). Use of a mathematical model for estimating potential landslide sites in steep forested basin. In T. R. H. Davis and A. J. Pearce (Eds.), Erosion and sediment transport in pacific rim steep lands (pp. 21–41). Institute of Hydrology, Wallingford, Oxon, UK.

Proceedings as a Book

Sassa, K. (1998). Recent urban landslide disasters in Japan and their mechanisms. In Proceedings of the 2nd International Conference on Environmental Management, Environmental Management (Vol. 1, pp. 47–58), Australia, 10–13 February. Elsevier, Amsterdam.

Proceedings with an editor, no publisher

Rahardjo, H., Leong, E. C., and Rezaur, R. B. (2002). Studies of rainfall-induced slope failures. In P. Paulus and H. Rahardjo (Eds.), Proceedings of the National Seminar, Slope 2002 (pp. 15–29). Bandung, 27 April 2002.

Proceedings without editor, with publisher

Doe, S.-T., and Morris, R. L. (1998). Rainfall-induced slope failures and damming of ravines. In Abstracts of international symposium on water-induced disasters. Tribhuvan University, Kathmandu, 4–9 June 1998.

Proceedings in CD/DVD format

Yatabe, R., Yagi, N., Yokota, K., and Bhandary, N. P. (2000). Influence of expansive chlorite on the strength of weathered Green Rock at Mikabu Belt of Japan. Proceedings of International Conference on Geotechnical and Geological Engineering, Melbourne, Australia, 19–24 November 2000 (CD format).

Publicly Available Unpublished Report

Wagner, A. (1983). The principal geological factors leading to landslides in the foothills of Nepal: A statistical study of 100 landslides – steps for mapping the risk of landslides. HELVETAS-Swiss Technical Cooperation and ITECO-Company for International Cooperation and Development.

Online Document

Hungr, O. (2003). Flow slides and flows in granular soils. In Proceedings of international workshop on occurrence and mechanisms of flows in natural slopes and earth fills (15 p.). http://www.unina2.it/flows2003/flows2003/articoli/Hungr-Flows.pdf (Accessed 15 January 2024)

Dissertation

Khanal, R. K. (1991). Historic landslides of Nepal during 1902–1990 A.D.: Extent and economic significance (M.Sc. dissertation). Central Department of Geology, Tribhuvan University, Nepal.

Standard

ASTM D3385-03. (2003). Standard test method for infiltration rate of soils in field using double-ring infiltrometer. ASTM International.

Review and Production Process

All manuscripts submitted for publication, including original articles, rapid reports on recent engineering geology issues, case studies, and technical notes, will undergo a rigorous peer review by at least two independent experts in the relevant field. A member of the Editorial Board may also serve as a reviewer when appropriate expertise is required. Accepted materials are subject to copyediting to ensure clarity, consistency, and adherence to journal standards. Authors will receive galley proofs of their article prior to publication and are expected to respond promptly to any editorial queries. Proof corrections must be limited to typographical or printer's errors; substantial revisions or rewriting at the proof stage will not be permitted.

Page Charges

There is **no page charge/s** for papers submitted to the AJEG. The upper limit on length of a paper is approximately 35 manuscript pages, including tables and references. This limit may be exceeded at the discretion of the Editor-in-chief.

Online Submission

Please note that the online manuscript submission system is available through the journal's official website. This system is essential for preparing and submitting your manuscript electronically to the Asian Journal of Engineering Geology via its web-based peer-review platform.

Manuscripts should be submitted at https://ajeg.nseg.org.np . The submission portal also allows authors to track the progress of their manuscript throughout the peer-review and editorial process.

Author should use given Template in the web site for preparation of manuscript.

Quick Report DOI: https://doi.org/10.64862/ajeg.2025.202.01.322 Open Access

Report on the 15th Asian Regional Conference of the International Association for Engineering Geology and the Environment (ARC-15), Kathmandu, Nepal, 27–29 November 2025

Anjila Babu Malla[1], Ranjan Kumar Dahal[2], ATM Shakhawat Hossain[3], Feruj Alam[4], Kanchan Chaulagain[5], Sunil Poudel[6], Ujjwal Krishna Raghubansa[2], Sweata Sijapati[7], Manita Timilsina[8], Sunam Kumar Sharma[8], Praveen Upadhyaya Kandel[8], Dhruba Tiwari[8], Sajeev Kumar Regmi[9], Kumud Raj Kafle[10]

[1]Shimane University, Matsue, Shimane, Japan
[2]Central Department of Geology, Tribhuvan University, Kirtipur, Kathmandu 44618, Nepal
[3]Jahangirnagar University, Savar, Dhaka-1342, Bangladesh
[4]Geological Survey of Bangladesh, Segunbagicha, Dhaka-1000, Bangladesh
[5]Underground Space Engineering, Jwagal, Lalitpur, Nepal
[6]Hong Kong University of Science and Technology, Hong Kong
[7]GeoHazards International, 6701 Koll Center Pkwy, Suite 250, Pleasanton, CA 94566, USA
[8]Geotech Solutions International, Dhobighat, Lalitpur, Nepal
[9]Nepal Electricity Authority, Ratnapark, Kathmandu, Nepal
[10]Department of Environmental Science and Engineering, Kathmandu University, Nepal

(*Corresponding E-mail: mallaanjila22@gmail.com)

Received: December 07, 2025, Accepted: December 21, 2025

Abstract: The 15th Asian Regional Conference of the International Association for Engineering Geology and the Environment (ARC-15) was held in Kathmandu, Nepal, from 27 to 29 November 2025 under the theme "Geological Engineering for Societal and Sustainable Development." Jointly organized by the Nepal Society of Engineering Geology (NSEG) and the IAEG Bangladesh National Group (IBNG), the conference hosted more than 340 participants from over 25 countries representing academia, industry, governmental institutions, and students. While ARC-15 is an Asian regional conference, the program and participation reflected strong global engagement. A total of 217 scientific presentations were delivered, including 190 oral and 27 poster contributions. The conference also included keynote and invited lectures, parallel technical sessions, poster exhibitions, training workshops, Women in Engineering Geology (WEG) and Young Engineering Geologists (YEG) activities, and pre- and post-conference field excursions in Nepal and Bangladesh. This report summarizes the main components of ARC-15 and highlights key outcomes and lessons relevant to future regional and international conferences.

Keywords: ***IAEG, Asian Regional Conference, ARC-15, WEG, YEG. Kathmandu, NSEG, Engineering geology.***

Introduction

Engineering geology has become increasingly important for societies facing rapid development and intensifying natural hazards. In many parts of Asia, expanding infrastructure networks, including roads, hydropower projects, tunnels, and urban developments, are being constructed in complex geological environments. At the same time, landslides, debris flows, floods, and earthquakes continue to affect lives and economies, particularly in mountain belts such as the Himalayas.

The International Association for Engineering Geology and the Environment (IAEG) promotes international collaboration and the advancement of engineering geology through global and regional conferences, technical commissions, and professional networks (IAEG, 2025). Among its major regional events, the Asian Regional Conference (ARC) series has served as an important platform for fostering scientific exchange and professional cooperation across Asia. The 15th Asian Regional Conference (ARC-15) was held in Kathmandu, Nepal, from 27 to 29 November 2025, and was jointly organized by the Nepal Society of Engineering Geology (NSEG) and the IAEG Bangladesh National Group (IBNG) under the theme "Geological Engineering for Societal and Sustainable Development." Although regional in scope, ARC-15 attracted internationally renowned keynote and invited speakers and welcomed more than 340 participants from over 25 countries. This report summarizes the conference organization, participation, scientific program, workshops, Women in Engineering Geology (WEG) and Young Engineering Geologists (YEG) activities, field excursions, and major outcomes, highlighting its

contributions to advancing engineering geology and strengthening international collaboration.

Conference program structure

ARC-15 was jointly organized by NSEG and IBNG. The conference theme, "Geological Engineering for Societal and Sustainable Development," guided the scientific sessions, workshops, and field activities.

Program overview

The program was designed to combine scientific exchange with training, networking, and field-based learning. The overall structure consisted of three phases (Figure 1).

Figure 1, Overall program structure of ARC-15.

Inaugural ceremony and institutional engagement

The inaugural ceremony was a major highlight of ARC-15, reflecting the growing recognition of engineering geology in national development and disaster risk reduction. The presence of high-level government representatives, including a ministerial guest, emphasized the importance of integrating engineering geology into sustainable infrastructure planning and resilience initiatives (Figure 2a). The ceremony also celebrated individuals who made significant contributions to strengthening the activities and global presence of both IAEG and NSEG. A Certificate of Appreciation was presented to Ms. Anjila Babu Malla in recognition of her outstanding efforts in promoting membership growth, enhancing member engagement, and supporting the continued development of the engineering geology community through IAEG and NSEG initiatives (Figure 2b).

Participation and demographics

ARC-15 brought together more than 340 participants from over 25 countries (Table 1), creating an international forum for engineering geology. Participants represented universities, research institutions, consulting and engineering companies, government agencies, and student communities. This diverse professional and geographical representation enriched technical discussions, strengthened international collaboration, and promoted valuable exchanges between academic research and engineering practice, reflecting the growing global engagement and scientific capacity of the engineering geology community.

Figure 2, Inaugural ceremony highlights: (a) opening session with ministerial participation and distinguished guests, and (b) Certificate of Appreciation awarded to Ms. Anjila Babu Malla in recognition of contributions supporting IAEG and NSEG.

Table 1, National Group and Regional Group-wise distribution of ARC-15 participants (top contributing countries and others).

Country	Participants
Nepal	178
Bangladesh	44
Japan	30
China	24
Chinese Taipei (RG)	21
India	6
Malaysia	6
South Korea	6
Canada	4
Germany	4
Others	24
TOTAL	343

Scientific sessions and technical contributions

Scientific presentations

A total of 217 scientific presentations were delivered during ARC-15, including 190 oral and 27 poster presentations. In addition, the conference featured keynote and invited lectures delivered in dedicated sessions. Figure 3 presents the country-wise distribution of oral and poster contributions based on the available presenter dataset, which also includes keynote and invited lecture entries.

Keynote and invited lectures

The conference featured keynotes and invited lectures from internationally recognized experts (Table 2). These lectures addressed major contemporary challenges in engineering geology, including:

- Engineering geology in tunneling and underground construction
- Deep-seated landslides and slope instability
- Climate change and geo-environmental risks
- Advances in remote sensing and monitoring technologies

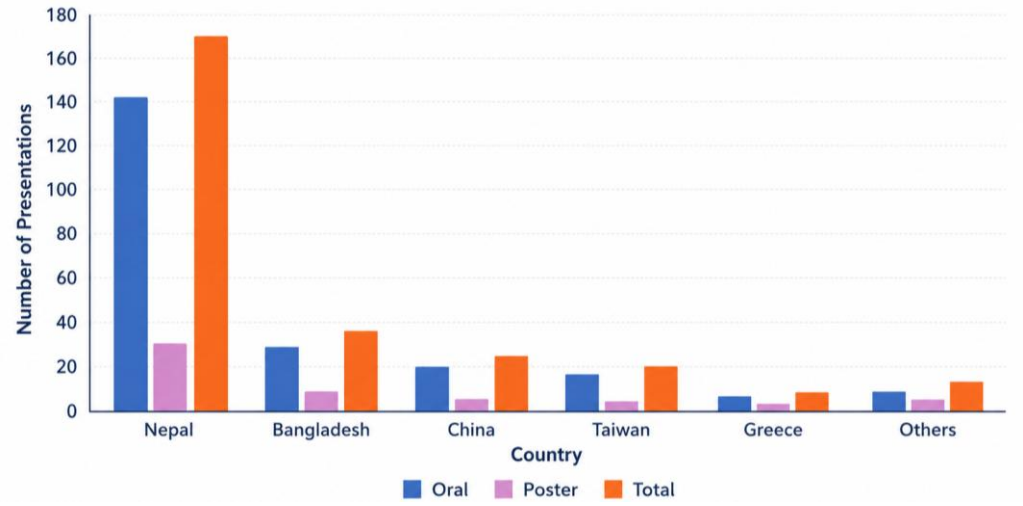

Figure 3, Country-wise distribution of ARC-15 presentations (oral and poster).

Parallel technical sessions

Parallel technical sessions were conducted throughout the three main conference days, forming the core of the scientific program. A total of 22 parallel technical sessions were organized, complemented by keynote and invited lectures, as well as two dedicated poster sessions. The program showcased the latest advances in engineering geology, geotechnical engineering, and geohazard research, providing an excellent platform for knowledge exchange among researchers, practitioners, consultants, industry professionals, and students from across Asia and beyond.

The technical sessions covered a broad spectrum of topics, with particular emphasis on engineering geological challenges in the Himalayan region. Major themes included landslide mechanisms, hazard and risk assessment, debris flows, rockfalls, active tectonics, earthquake-induced geohazards, groundwater and hydrogeology, tunneling, hydropower development, transportation infrastructure, urban geology, and climate change impacts. Several sessions highlighted innovative approaches in geological mapping, remote sensing, numerical modeling, monitoring technologies, and field investigations for improving hazard evaluation and infrastructure resilience. A distinctive feature of ARC-15 was its strong commitment to professional development and inclusivity. Dedicated technical sessions were organized by the Women in Engineering Geology (WEG) Committee on the first conference day and the Young Engineering Geologists (YEG) Committee on the second day. In addition, a special session focused on engineering geology education, professional training, and scientific communication, promoting capacity building and international collaboration. Overall, the parallel technical sessions successfully fostered scientific exchange, strengthened regional partnerships, and highlighted the growing contribution of engineering geology to sustainable infrastructure development and disaster risk reduction across Asia.

Workshops and training programs

Pre-conference workshops

Several pre-conference workshops and training sessions were organized to strengthen technical capacity and provide hands-on learning. The program included a full-day software-based workshop on tunneling and rock slope engineering, a technical workshop on engineering geological modeling using IAEG Commission 25 guidelines, and a training session on manuscript preparation for international journals (Table 3).

Table 2, Summary of keynote and invited lectures at ARC-15 (NSEG, 2025).

Category	Speaker	Lecture title
Keynote	Dr. Vassilis P. Marinos	Advancements in Tunneling: the Role of Engineering Geology in Design and Construction over the Last 30 Years
Keynote	Prof. Dr. Shuichi Hasegawa	Significance of Dissected Deep-seated Landside Topography and Hydrothermal Alteration in Active Mountain Belts
Keynote	Dr. Ann Williams	Climate Change: closing the gap between challenges faced by developing and developed countries
Keynote	Prof. Dr. rer. nat. Muhammad Qumrul Hassan	Smart Water Management for Sustainable Development: Bridging Groundwater–Surface Water Dynamics Amid Climate Change
Keynote	Er. Keshav Kumar Sharma	Slope Stability and Resilient Roads in the Himalayas: Nepal's Challenges and Initiatives
Keynote	Prof. Dr. Christian Zangerl	Deep-Seated Rock Slides: Understanding Processes and Assessing Impacts on Settlements and Infrastructure
Keynote	Dr. Shahid Azam	New Methods for Characterizing and Modeling the Engineering Behavior of Expansive Soils
Keynote	Prof. Dr. Trilok Nath Singh	Rockfall Prediction and Prevention in High Hills of Deccan Trap
Keynote	Dr. Shengwen Qi	Geological Environment and Geohazards in the Qinghai–Xizang Plateau, China
Keynote	Dr. Daniele Giordan	Glacier instabilities identification and monitoring: case studies in the Alps
Keynote	Prof. Dr. Keh-Jian (Albert) Shou	On the Catchment Sedimentation and Landslides Induced by 1999 Taiwan Chi-Chi Earthquake
Keynote	Mr. Anil Pokhrel	An Interdisciplinary Approach to Disaster Risk Reduction and Management and Sustainable Development in Nepal
Keynote	Prof. Dr. Giovanna Vessia	Neo Deterministic Seismic Hazard Approach (NDSHA) for Seismic Response Analyses in urban areas: a case study from Italian territory
Keynote	Prof. Dr. Tümay Kadakci Koca	Erosion and Mass Wasting Processes in Post-Wildfire Mountainous Terrains: Impacts and Challenges
Keynote	Dr. Scott Andersen	The evolution of remote sensing for regional characterization and response to geohazards and extreme events
Keynote	Mr. Dinesh Napit	Role of the Department of Mines and Geology (DMG) in Advancing Engineering Geological Sciences in Nepal
Invited	Dr. Mike Winter	Debris Flow Risk to Roads and Road Users
Invited	Dr. Ko-Fei Liu	Wave Dynamics and Geohazards Monitoring
Invited	Prof. Dr. Tetsuya Sakai	Potential Natural Hazards in Kathmandu, Nepal: Lessons from Stratigraphic Analysis of the Pleistocene Succession in the Kathmandu Valley
Invited	Prof. Dr. Younus Ahmed Khan	Progressive failure analysis based on a method of non-vertical slices *(presented in closing ceremony in Dhaka)*
Invited	Dr. Md. Shofiqul Islam	Tectonic Evolution and Seismic Hazards in Bangladesh: Insights from Geophysical and Geotechnical Studies
Invited	Dr. H. M. Sayem	Role of Suction in Unsaturated soils
Invited	Dr. Arvind Kumar Jha	Development of a Laboratory-Scale Model to Evaluate Rainfall-Induced Surface Erosion Mitigation in MICP-Treated Sand
Invited	Prof. Dr. Toru Terao	Asian Monsoon, Climate and Climate-Induced Hazards in the Asia and Pacific Region
Invited	Dr. Sultana Nasrin Nury	Quantitative Analysis for Greening as an option for Sustainable City
Invited	Dr. Mahmuda Khatun	Establishment of Rainfall Thresholds for Shallow Landslide in Rangamati Sadar, Bangladesh
Invited	Prof. Dr. Tomochika Tokunaga	Land Subsidence and Subsurface Environmental Changes in the Tokyo Metropolitan Area, and Possible Groundwater Management for Urban Sustainability
Invited	Prof. Dr. Jia-Jyun Dong	Random Field Modeling of Subsurface Stratigraphic/Parameters and Its Applications: Using the Taipei Basin as an Example
Invited	Dr. Abd Rasid Jaapar	Emerging Roles of Engineering Geologist in Geotourism Industry: Some Case Studies from Malaysia

Table 3, Workshops and training programs conducted during ARC-15.

Date	Title	Mentor
25 Nov 2025	Enhancing Tunneling and Rock Slope Engineering with Rocscience Software Tools	Dr. Manoj Verman (Rocscience India)
26 Nov 2025	Engineering Geological Models – Traditional and Digital Approaches Using IAEG Commission 25 Guidelines	Fred Baynes, Mark Eggers, Anthony Bowden
26 Nov 2025	Preparing a Manuscript for an International Scientific Journal – What Editors and Reviewers Look For	Janusz Wasowski

Women in Engineering Geology (WEG) activities

ARC-15 included a strong Women in Engineering Geology (WEG) program under the theme "The Role of Women in the Development of Engineering Geology." The WEG session was convened by Dr. Ann Williams (IAEG-WEG Chair) and coordinated by Ms. Anjila Babu Malla (NSEG-WEG Chair, IAEG-WEGC Member) and Dr. Mahmuda Khatun (IBNG-WEG Chair). The activities brought together women engineering geology professionals, researchers, and students and aimed to strengthen professional networking, visibility, mentorship, and collaboration.

Pre-conference virtual networking (17 November 2025)

The WEG program began with an informal virtual networking session held via Zoom on 17 November 2025. This introductory networking session allowed participants to connect prior to arriving in Kathmandu and helped create a welcoming environment for the in-person activities.

Outdoor "Walk and Talk" geological session (26 November 2025)

The first in-person WEG activity was the Outdoor Walk and Talk Session, held on 26 November 2025 in the Chovar area of Kathmandu Valley (Figure 4). The event brought together participants for a guided geological walk, introducing the area's unique geology and geomorphology while fostering informal discussions on professional experiences, career development, and shared challenges in engineering geology. Field notes and educational handouts were provided to enhance learning and encourage active participation. The program also included a visit to the Central Department of Geology, Tribhuvan University, where participants interacted with faculty members and students, strengthening academic collaboration, professional networking, and knowledge exchange between experienced practitioners and the next generation of engineering geologists.

Figure 4, WEG Walk and Talk session in the Chovar area.

WEG technical session, panel discussion, and career development workshop

The WEG Technical Session was held on 27 November 2025 and included an invited lecture and multiple technical presentations covering diverse topics relevant to engineering geology. The session concluded with a panel discussion titled "Global Perspectives on Women's Careers in Engineering Geology: Overcoming Barriers and Creating Opportunities."

The panel included Dr. Ann Williams, Prof. Ranjan Kumar Dahal, Dr. Mahmuda Khatun, and Dr. Hiromi Kaji, and was moderated by Dr. Sweata Sijapati and Ms. Anjila Babu Malla. The discussion addressed leadership, mentorship, field challenges, institutional barriers, and pathways for strengthening women's participation across regions. Tokens of appreciation were presented to presenters and panelists in recognition of their contributions (Figure 5a). The final WEG event was a career development workshop held on 29 November 2025, focusing on essential professional skills including communication, leadership, negotiation, and allyship (Figure 5b).

Figure 5, WEG activities (a) Panel discussion at ARC-15 and (b) Career development workshop at ARC-15.

Young Engineering Geologists (YEG) program

The Young Engineering Geologists (YEG) program at ARC-15 attracted strong participation and provided early-career professionals and students with opportunities for technical exchange, networking, and professional development. The program was coordinated by Mr. Shankar Pantha (NSEG-YEG Chair), Mr. Om Prasad Dhakal (NSEG-YEG; IAEG-YEG), and Mr. Shafiqul Islam Sany (IBNG-YEG Secretary).

A pre-conference online "Meet and Greet" session was held on 16 November 2025 to introduce participants and support early connections. The main YEG session was conducted on 28 November 2025 and included a panel discussion titled "Past, Present and Future of Engineering Geology," moderated by Mr. Om Prasad Dhakal, followed by a recorded presentation on AI in engineering geology (Figure 6). The session also featured a Quick-fire YEG Research Session with short presentations and interactive discussion, including a Best Quick-fire YEG Presentation Award supported by the IAEG-YEG committee.

Figure 6, YEG panel discussion at ARC-15.

The YEG program concluded with a networking dinner and cultural evening on 28 November 2025 (Figure 7), strengthening international connections among young engineering geologists.

Figure 7, YEG networking dinner and cultural evening at ARC-15.

Pre- and post-conference field excursions

Field excursions were a key component of ARC-15 and provided participants with direct exposure to engineering geological conditions in Nepal and Bangladesh. The excursions strengthened the applied character of the conference and allowed participants to connect technical discussions with real geological settings, infrastructure corridors, and hazard processes.

Pre-conference excursions

Pre-conference excursions were conducted in the Kathmandu Valley on 26 November 2025. The program included two parallel day tours: Ex-2, a Kathmandu Valley tour focusing on ground response and reconstruction aspects following the 2015 Gorkha earthquake, and Ex-3, a day tour exploring the engineering geological setting of the Kathmandu Valley.

Post-conference excursions

Post-conference field excursions were conducted from 30 November to 2 December 2025, providing participants with opportunities to examine engineering geological conditions and geohazards in the field. Two major multi-day excursions were organized in Nepal. Ex-5, covering the Kathmandu–Pokhara corridor, focused on engineering geological conditions, geotechnical characteristics and infrastructure challenges, and was organized by the Women in Engineering Geology (WEG) team of NSEG under the field leadership of Dr. Manita Timilsina and Dr. Sweata Sijapati (Figure 8). Ex-6, exploring the Koshi River, Jhapa, and Ilam corridor in eastern Nepal, was led by Prof. Shuichi Hasegawa and Mr. Praveen Upadhyaya Kandel, highlighting landslide processes, geological diversity, and infrastructure development (Figure 9). Additional excursion programs were also organized in Bangladesh, reflecting the joint organizational framework and regional collaboration of ARC-15.

Figure 8, Field excursion Ex-5 (Kathmandu–Pokhara corridor) led by the WEG team of NSEG.

Figure 9, Field excursion Ex-6 in Far Eastern Nepal (Koshi River–Jhapa–Ilam corridor).

Awards and recognition

ARC-15 included presenter awards to recognize outstanding technical contributions and encourage high-quality scientific communication. Awards were presented for outstanding oral and poster presentations, with encouragement for early-career contributors (Figure 10). The awardees and their countries are summarized in Table 4.

Table 4, Presenter awardees at ARC-15.

Award category	Awardee	Country
Best Oral Presentation	**Tunisha Gyawali**, Prajwal Timsina, Bhim Kumar Dahal and Ellen B. Robson	UK
Best Oral Presentation	**Yong-Zhi Huang**, Chia-Hong Chiu, and Tai-Tien Wang	Taiwan
Best Poster Presentation	**Hiroyuki Hashimoto**, Akira Sato and Reiko Kuwano	Japan
Best Poster Presentation	**Aonan Dong** and Jie Dou	China
Best Quick-fire YEG Presentation	**Jui-Ming Chang**	Taiwan

Institutional support and sponsorship

ARC-15 benefited from strong institutional support from IAEG leadership, national groups, commissions, and international sponsors. Their guidance, encouragement, and best wishes contributed significantly to the scientific quality and organizational success of the conference. Sponsorship support enabled the delivery of workshops, special sessions, field excursions, and WEG and YEG programs, reinforcing the collaborative spirit of the global engineering geology community.

Figure 10, Presenter awardees recognized during ARC-15.

Conclusion

ARC-15 successfully combined scientific exchange, global participation, capacity building, and inclusive professional engagement. The conference hosted more than 340 participants from over 25 countries and featured 217 scientific presentations, including 190 oral and 27 poster contributions. Although it was organized as an Asian regional conference, ARC-15 demonstrated strong international relevance through its international participation and globally connected scientific program.

The integration of workshops, WEG and YEG activities, and extensive field excursions in Nepal and Bangladesh strengthened the overall impact of ARC-15 and set a strong benchmark for future Asian Regional Conferences of IAEG. The outcomes of ARC-15 contribute to advancing engineering geology in support of societal resilience and sustainable development.

Acknowledgement

The authors acknowledge the International Association for Engineering Geology and the Environment (IAEG), the Nepal Society of Engineering Geology (NSEG), and the IAEG Bangladesh National Group (IBNG) for organizing ARC-15. The authors also acknowledge international sponsors, supporting organizations, session conveners, volunteers, and all participants who contributed to the success of the conference.

References

IAEG, (2025). International Association for Engineering Geology and the Environment (IAEG) website, Available at: http://www.iaeg.info/

NSEG, (2025). Conference Program Book of the 15th Asian Regional Conference of the International Association for Engineering Geology and the Environment (ARC-15), Kathmandu, Nepal. Nepal Society of Engineering Geology (NSEG) website, Available at: http://www.nseg.org.np/

Research Article DOI: https://doi.org/10.64862/ajeg.2025.202.02.265 Open Access

Comparative Evaluation of SVM and MLC for Land Use and Land Cover Change Mapping Using Landsat Data: A Case Study of Bhaktapur District, Nepal

Nirmal Kafle[1*]

[1]Khwopa College of Engineering, Bhaktapur, Nepal

(*Corresponding E-mail: nirmalkafle1917@gmail.com)

Received: August 08, 2025, Accepted: November 15, 2025

Abstract: **The availability of reliable land cover maps is vital for effective planning, as their absence can compromise project validity. This study investigates the land use and land cover (LULC) changes in Bhaktapur district, Nepal, from 2015 to 2025 using Landsat imagery employing Support Vector Machine (SVM) and Maximum Likelihood Classifier (MLC). The primary objective is to compare the performance of SVM and MLC in LULC mapping and to calculate changes between two time periods. The results show increase in Built-up area and a reduction in barren land between the two time periods. Built-up area is increased by 12.36% (SVM) and 3.59% (MLC), between 2015 and 2025. Vegetation areas showed substantial gains, while forest area remained relatively stable. SVM achieved an overall accuracy of 79% (kappa = 0.69) whereas MLC achieved 73% (kappa = 0.60) indicating slightly higher classification accuracy for SVM. This study provides a comparative evaluation of two commonly used classifiers for LULC mapping and change analysis in Bhaktapur district. It also provides baseline spatial information for future planning studies.**

Keywords: ***Bhaktapur, LULC, Support Vector Machine.***

Introduction

The growth of human populations and settlements is a common global drift influenced by human necessities and activities, which ultimately led to land-cover changes due to growing land-use requirements. While Land Use Land Cover (LULC) is frequently used interchangeably, these terms have distinct meanings (Dimiyati et al., 1996). A thorough spatial knowledge of urban expansion is essential for actual urban planning (Subasinghe et al., 2016). Accurate land cover information is vital for assessing these changes, enabling planners to implement up-to-date strategies for sustainable growth (Alharthi et al., 2020).

Encouraged by economic growth and infrastructure development, urbanization has emerged as a major inclination in developing countries. The conversion of vegetation land for urban purposes has become a topic for sustainable urban expansion. Accessibility and infrastructure development have further influenced settlement growth and urbanization (Xian and Crane, 2005).

Urban expansion studies have been key research since the 1990s (Batty and Xie, 1997). Remote sensing data has become a valuable resource for assessing LULC changes across various scales (Johnson and Iizuka, 2016). A common and effective way to obtain this information is through LULC classification of multispectral satellite imagery (Gibril et al., 2017). Remote sensing enables effective monitoring of both short-term and long-term land use processes, patterns, and their impacts (Wellmann et al., 2018). The understandings derived from remote sensing and Geographic Information Systems (GIS) such as spatial patterns and the extent of urban land changes (e.g., conversion of vegetation to Built-up area) can support urban planners (Simwanda and Murayama, 2018). Tracking land cover changes has remained a prominent research area in remote sensing and GIS over the past decade (MohanRajan et al., 2020). Various LULC change models have been developed to improve the accuracy of change (Maleki et al., 2020).

This study employs Maximum Likelihood Classifier (MLC) and Support Vector Machines (SVM) for change mapping and comparison between two classifiers. MLC is a widely used classification method for satellite image analysis which has demonstrated high accuracy in land-cover classification and change monitoring, often exceeding 80% (Huang et al., 2002; Kanellopoulos et al., 1992). In remote sensing, enhancing classification accuracy remains a key concern using advanced algorithms like Neural Networks and SVM. SVM is a supervised classification technique which have gained importance in remote sensing due to its ability to improve classification (Kavzoglu and Colkesen, 2009). Classes with large extents suffer from real-world variability and affects the MLC performance, while SVM is less dependent on data distribution (Naghadehi et al., 2021).

Bhaktapur is a historically significant city in Kathmandu Valley, Nepal (Figure 1). It has experienced various physical changes in recent decades marked by rapid urban expansion and internal transformation. The increase in Built-up area is prominent in Bhaktapur district over the years (1989-2015). The Built-up area increased from 1.8% to 24.0% between 1988 and 2015

(Chhetri and Moriwaki, 2017). The conversion of vegetation area into Built-up area reflects the pressure of population growth and shifting toward nuclear families (Yadav, 2013). In recent years, Bhaktapur has transitioned from a farming economy to a rapidly urbanizing District (Timsina, 2020). The land use and population analysis of Bhaktapur District (2001–2019) show significant urban expansion showing the increment to population growth and economic development. The Built-up area has been increased especially around Bhaktapur city and nearby municipalities (Prajapati, 2024). Additionally, population growth driven by rural-to-urban migration for better living has further increased these changes (Ishtiaque et al., 2017). Bhaktapur risks deteriorating into overcrowded and poorly managed settlements for its residents if urbanization remains unmanaged.

Despite several previous studies in Bhaktapur (e.g., Chhetri and Moriwaki, 2017; Prajapati, 2024), none of the studies have compared two classifiers (SVM vs. MLC). Therefore, the novelty of this study lies in providing a decade-based LULC comparison (2015–2025), and evaluating the relative classification performance of SVM and MLC under similar preprocessing and training conditions.

Materials and methods

Case study

Bhaktapur is the smallest district in Nepal (Figure 1) which lies on the eastern edge of the Kathmandu Valley. It lies between 27°36' N to 27°44' N latitude and 85°21' E to 85°32' E longitude, with an area of 119 km^2. The altitude of Bhaktapur varies between 1,331 m and 2,191 m above sea level. A significant portion of Bhaktapur's eastern region, along with nearly half of its northern and southern area, is covered by Mahabharat range and Midlands. The district has a moderate temperate climate, with an average annual rainfall of 1300 mm (DHM, 2023). The variations in temperature range from a maximum of 33°C to a minimum of 0°C with an average temperature of 23°C throughout the year.

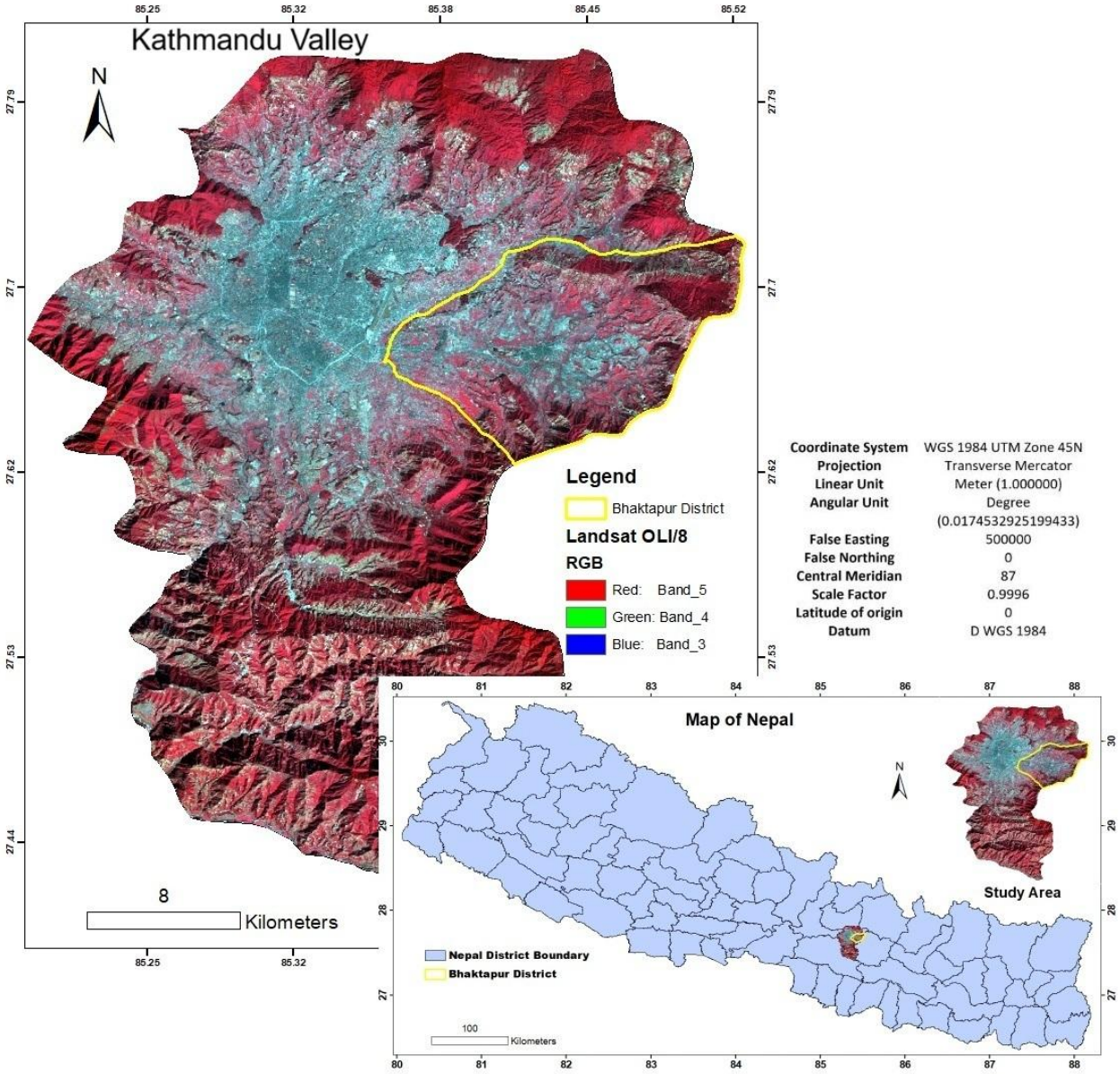

Figure 1, Landsat image of Kathmandu Valley showing the study area (Bhaktapur district).

Table 1, Detailed data on Landsat images used in the study (USGS).

Year	Spacecraft ID	Sensor ID	Path/Row	Resolution (m)	Acquisition Date	Cloud Cover
2015	LANDSAT_8	OLI_TIRS	141/41	30	9 February 2015	17.57 % (not in the study area)
2025	LANDSAT_8	OLI_TIRS	141/41	30	20 February 2025	9.57 % (not in the study area)

Data acquisition and preparation

Landsat imagery was used to analyze LULC changes, selecting data based on quality, availability, and the dry season (Table 1). Two Landsat images (2015 and 2025) were extracted from the United States Geological Survey (USGS) Earth Explorer (https://earthexplorer.usgs.gov/) specific Path/Row coordinates. The images were processed in ArcGIS 10.4, to generate LULC maps. All image had a 30 m spatial resolution, captured by OLI_TRIS at varying times. The selected images were pre-processed to ensure radiometric and geometric consistency before classification. Atmospheric correction was carried out using Landsat Surface Reflectance Code (LaSRC) which minimizes the atmospheric effects. Layer stacking, clipping to the Bhaktapur district boundary, and visual inspection for radiometric consistency were carried out before classification. Throughout the study and data preparation, the spatial reference provided in Figure 1 was employed.

Classification and change analysis

Two different supervised classifiers, SVM and MLC were used for digital classification. Comparison with high-resolution images revealed misclassifications, which were refined through post classification techniques for improved accuracy using Google Earth Pro, field verification and previous LULC maps. The study area was categorized into 5 LULC classes: Built-up area, Vegetation area, Forest area, Barren area, and Water bodies for each image (Table 2). Assessment of LULC changes was carried out using a post-classification comparison method where classified images from two different years were compared to identify transitions between land cover classes. This approach minimizes radiometric inconsistencies between multi-temporal images providing a detailed change matrix. The raster calculator was utilized to compare images from different years (Figure 2).

Using overlay procedures in GIS, a change matrix was generated which quantifies the gains and losses in each LULC category. The transitions between LULC classes were analyzed to understand the spatial extent and pattern of changes using SVM and MLC (Figure 3). The diagrams representing change in each class with gains and losses area were prepared implementing both techniques (Figure 4 and Figure 5).

Accuracy assessment

Accuracy assessment is crucial for evaluating individual classifications which ensures the reliability of classification data for change (Owojori and Xie, 2005). Typically, this assessment involves comparing two datasets: one derived from reference information, known as "ground truth," and the other obtained from analyzing remotely sensed data (Congleton, 1991). In the case of LULC maps generated from satellite imagery, a random sampling approach was employed for each of the four LULC maps to represent the various land cover classes. Training and validation samples were selected separately for the accuracy assessment to avoid bias. Approximately 100 training samples per class were used to develop the classifiers. An independent set of randomly distributed validation points was then used to generate the confusion matrix. These validation points were identified through visual interpretation of Google Earth imagery.

Table 2, LULC classification scheme.

LULC Category	Description
Built-up area	Includes residential, commercial, industrial, transportation infrastructure, and other structures.
Vegetation area	Includes grasslands, croplands and cultivated vegetation cover including agricultural lands.
Forest area	Densely wooded areas, including natural and planted forests.
Barren area	Land with little to no vegetation, including exposed rock or soil.
Water bodies	Represents surface water features such as rivers and ponds.

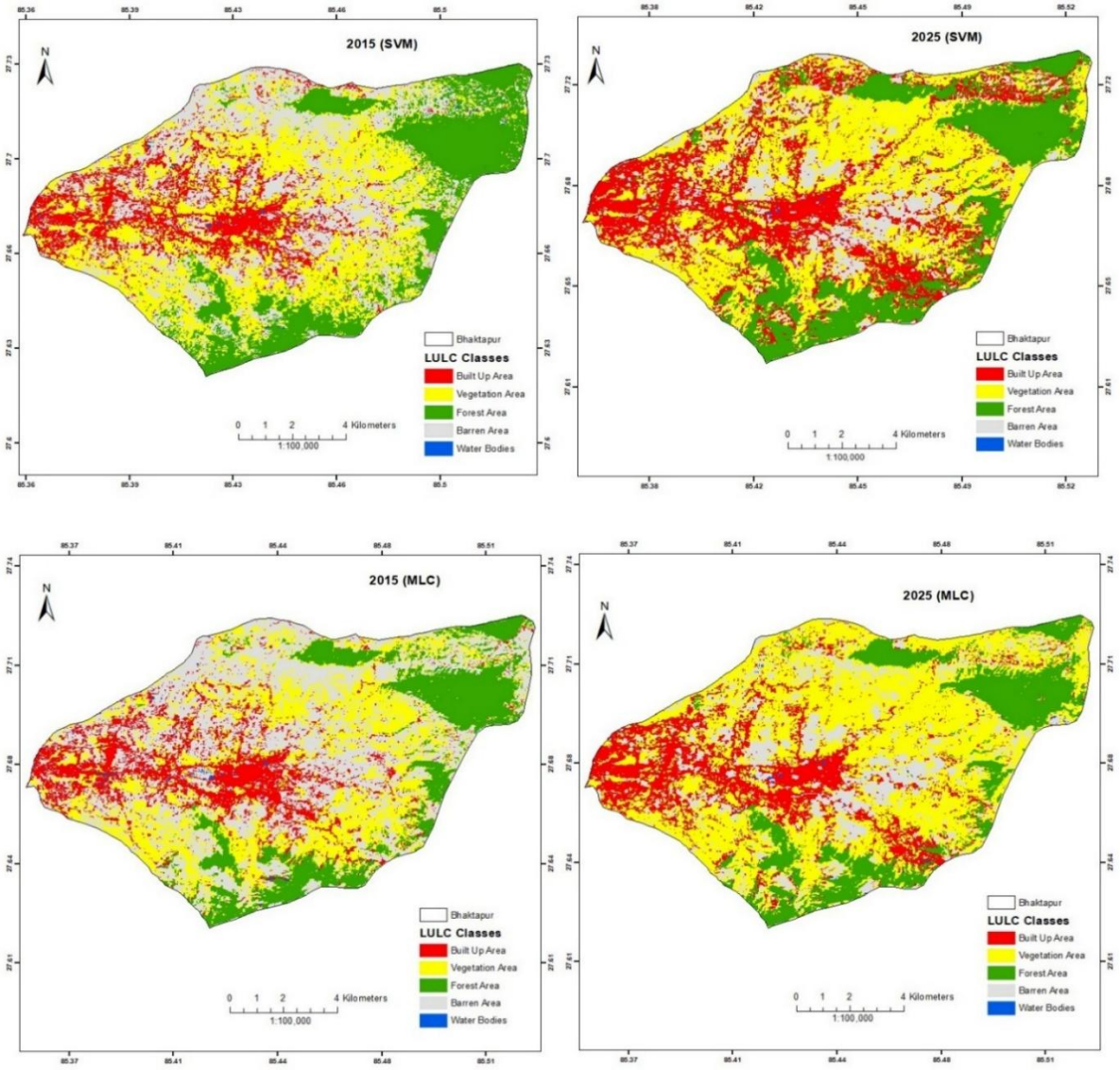

Figure 2, Status of LULC maps of Bhaktapur district in 2015 and 2025 with SVM and MLC classifier.

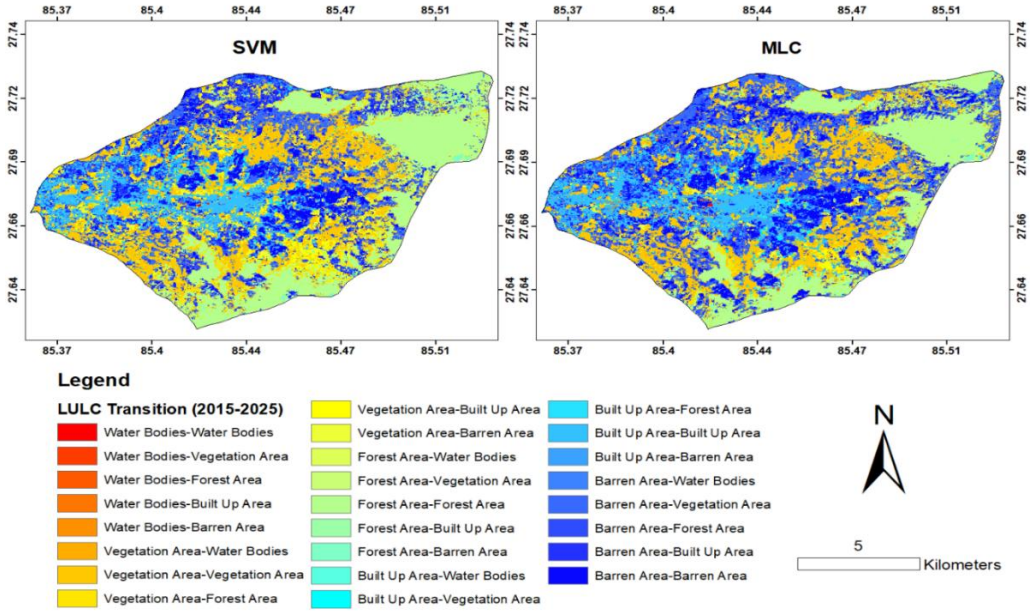

Figure 3, LULC change map from 2015 to 2025.

Result and discussion

LULC changes (2015-2025)

The results from the analysis indicate important transformations in the LULC patterns of Bhaktapur district between 2015 and 2025. The classification results using both SVM and MLC show an increase in Built-up area and a decrease in vegetation and forest cover (Figure 6 and Figure 7). Table 3 shows the Built-up area revealed substantial growth over the study period with an increment from 12.36% (SVM) and 3.59% (MLC) in 2015 to 2025 respectively. The expansion of urban infrastructure, including residential, commercial, and industrial areas, is evident from the classification results. These results are consistent with previous studies (Chhetri and Moriwaki, 2017; Prajapati, 2024), which reported a steady urban expansion in Bhaktapur. Vegetation area also showed an increase over the decade with 4.92% (SVM) and 21.09 % (MLC). This expansion suggests important transformation of previously barren area into vegetation area. The forest area does not show noteworthy changes (0.5%) which might be due to government policies. The analysis also revealed a decline in barren area, decreasing from -16.83 % (SVM) and -24.21% (MLC), indicating a substantial increase in vegetation area.

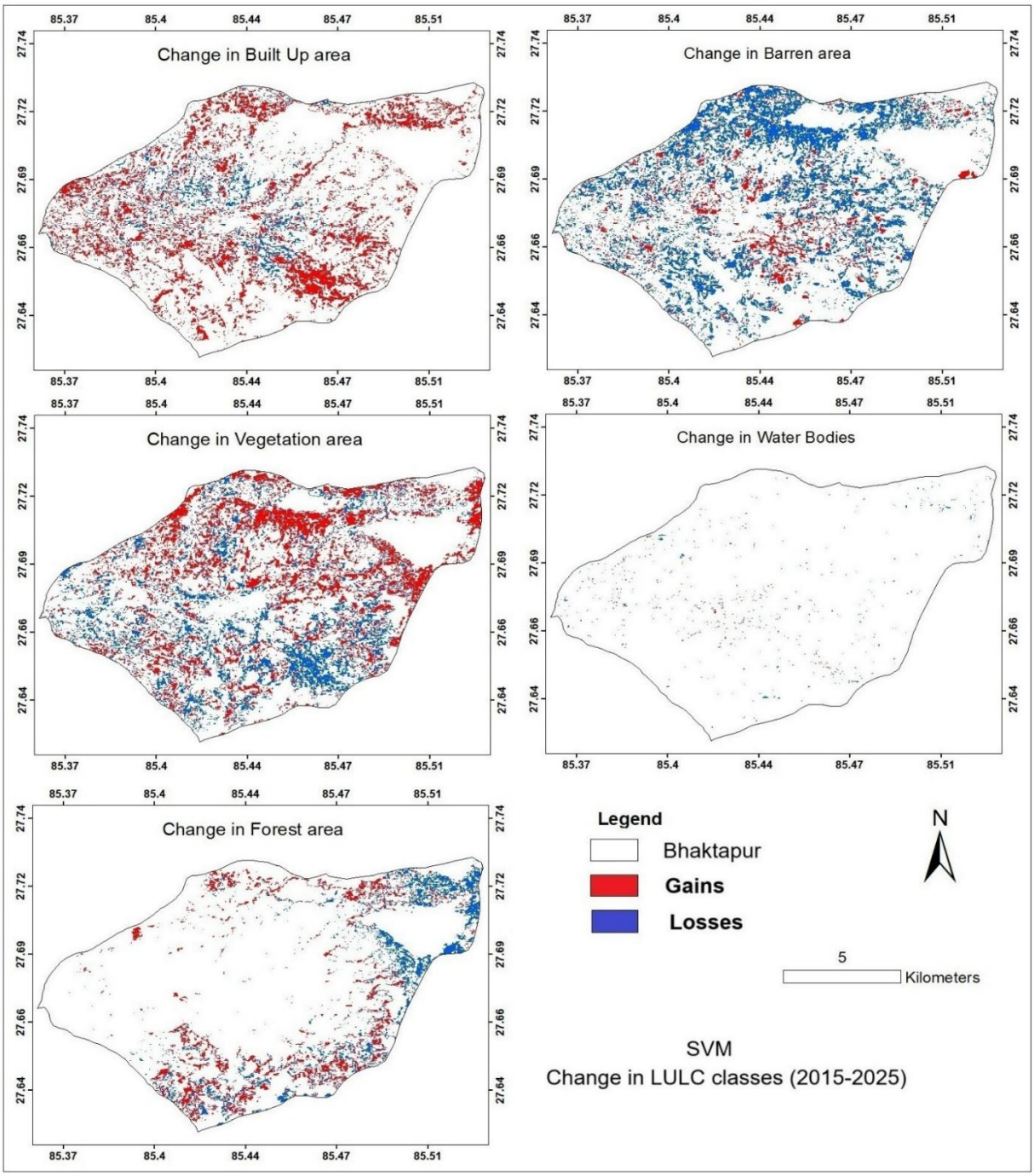

Figure 4, LULC change in different classes during 2015-2025 (SVM).

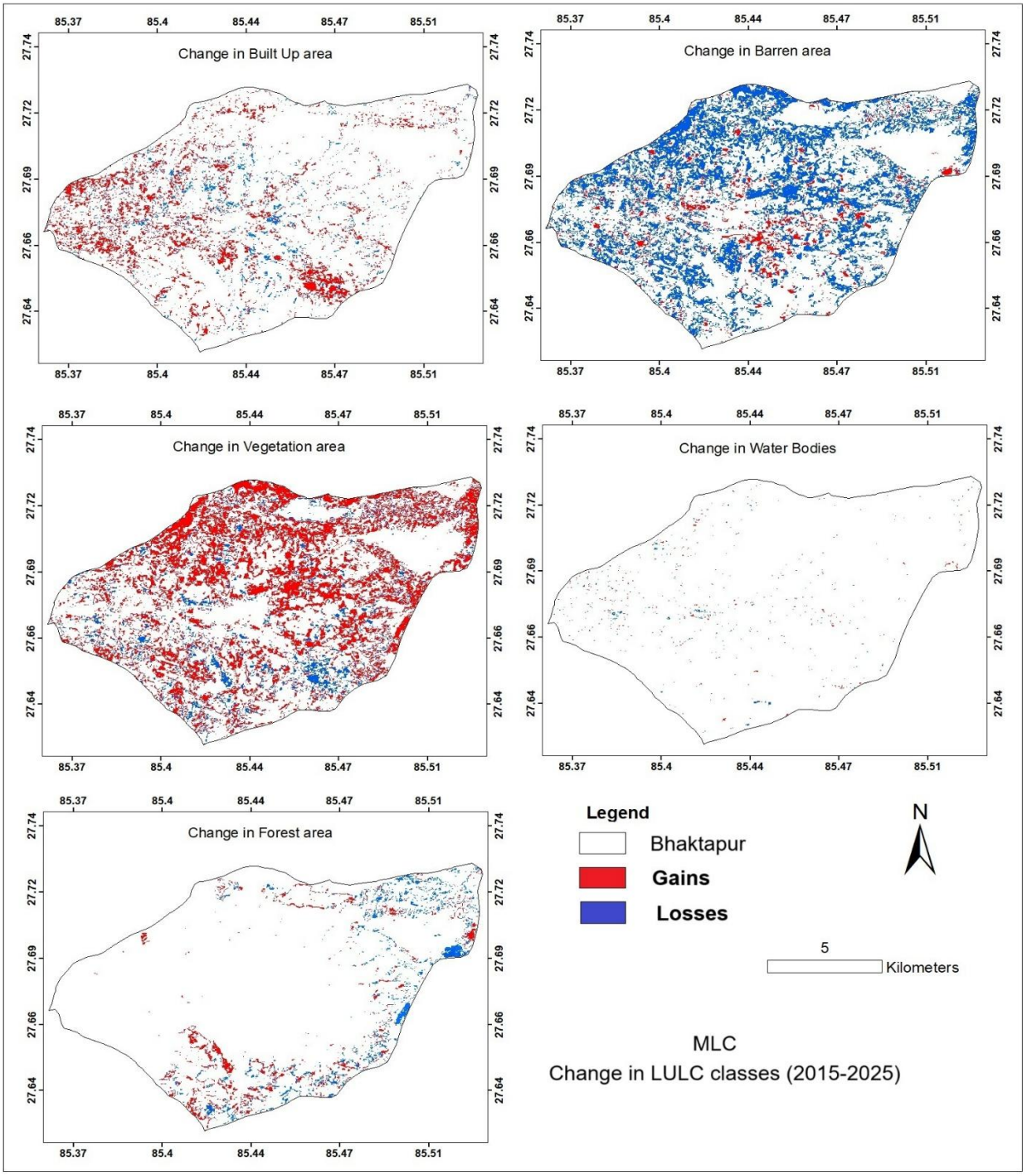

Figure 5, LULC change in different classes during 2015-2025 (MLC).

Table 3, Change area (%) on LULC classification in 2025 and 2015.

		Built-up area	Vegetation area	Forest area	Barren area	Water bodies
% Change Area	**SVM**	12.36	4.92	-0.45	-16.83	-0.01
	MLC	3.59	21.09	-0.52	-24.21	0.06

This reduction is the result of expanded vegetation area, afforestation efforts, and urban encroachment, as barren area were converted into vegetation, or Built-up area. Meanwhile, it is important to mention that the water bodies class showed very low classification accuracy, mainly because it occupies only a small portion of the study area. As a result, any interpretation regarding the stability or change of water bodies should be considered with caution. From a spatial perspective, the increase in Built-up area is mainly observed around the central parts of

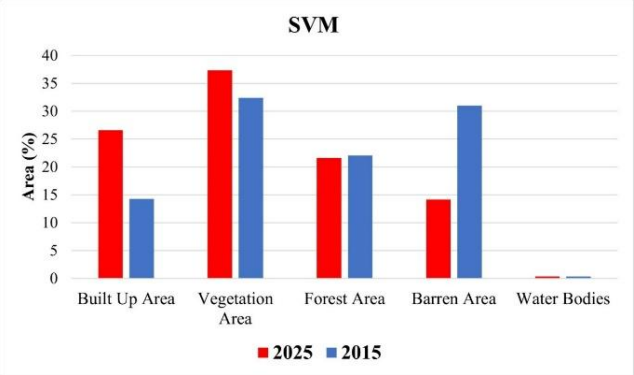

Figure 6, Status (%) on LULC classification in 2025 and 2015 (SVM).

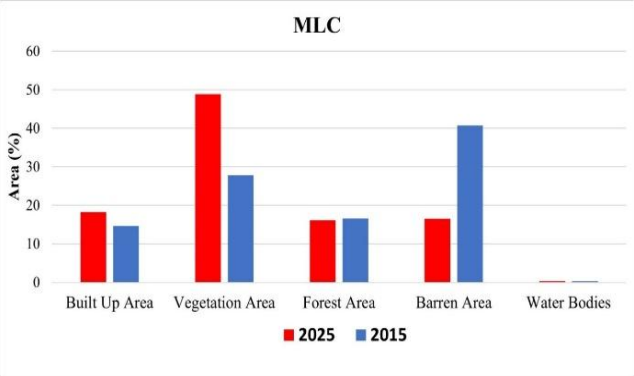

Figure 7, Status (%) on LULC classification in 2025 and 2015 (MLC).

Bhaktapur and its surrounding peri-urban zones. Overall, the pattern indicates gradual outward expansion from the existing core urban area rather than scattered developments. Conversion was primarily observed from previously barren or vegetated area.

Analysis of LULC transition and gains/losses (2015-2025)

Both classifiers agree on a reduction in barren area, with SVM showing 12.44% to vegetation and 8.09% to Built-up area, while MLC reports 22.01% to vegetation and 5.79% to built-up. This points towards the reclamation of marginal areas for expansion of vegetation and urban areas. Built-up area expanded primarily at the expense of vegetation (SVM: 6.65%; MLC: 2.39%), supporting rapid infrastructural growth. Forest area shows negligible net change (~0.5%) but internal shifts (e.g., forest-to-vegetation: SVM 3.46 %; MLC 2.31%) suggest minor degradation (Figure 8).

The LULC gain-loss analysis from both SVM and MLC classifications highlights consistent and significant landscape transformations. Vegetation Area recorded the highest gains, 17.87% in SVM and 26.91% in MLC, indicating re-vegetation or reclamation of previously unused areas in both cases. Barren Area consistently showed the highest losses, with 22.20% in SVM and 28.59% in MLC, suggesting noteworthy conversions into vegetated or urban areas. Built-up area expanded noticeably in both classifications (16.52% gain in SVM and 8.76% in MLC), reflecting rapid urbanization and infrastructure development (Figure 9 and Figure 10).

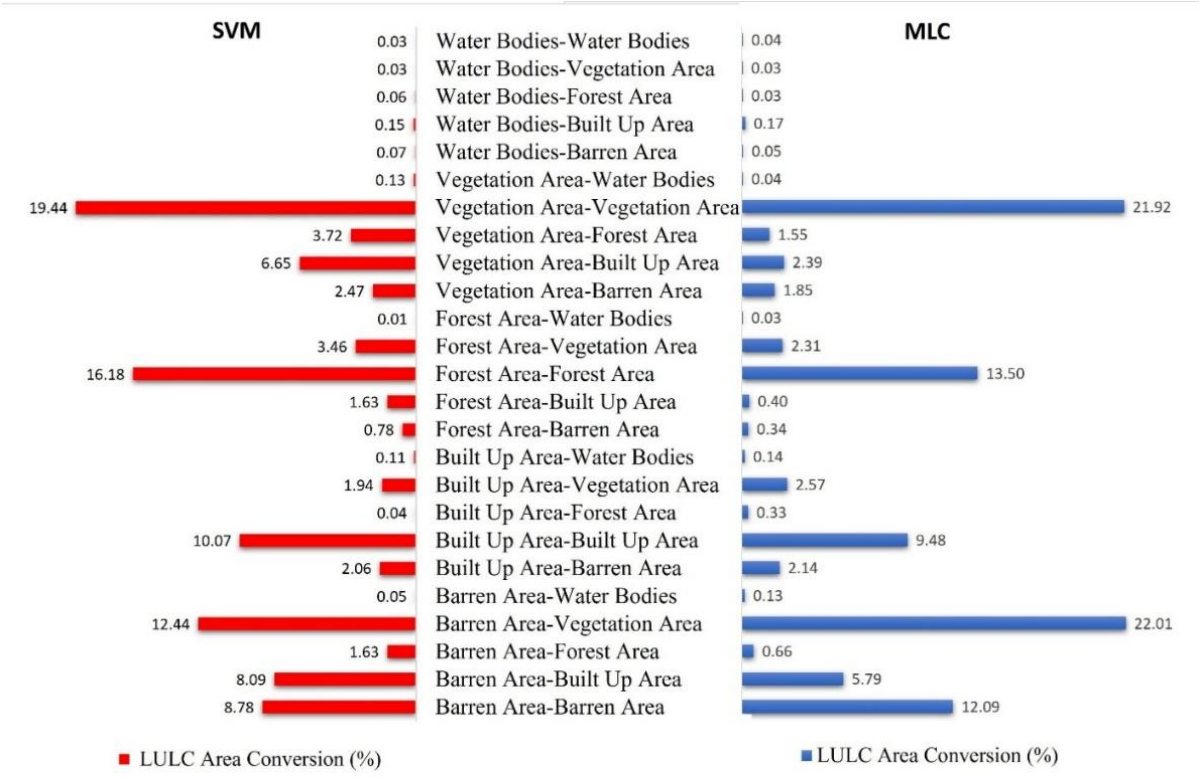

Figure 8, Transition (%) between LULC classes from 2015-2025.

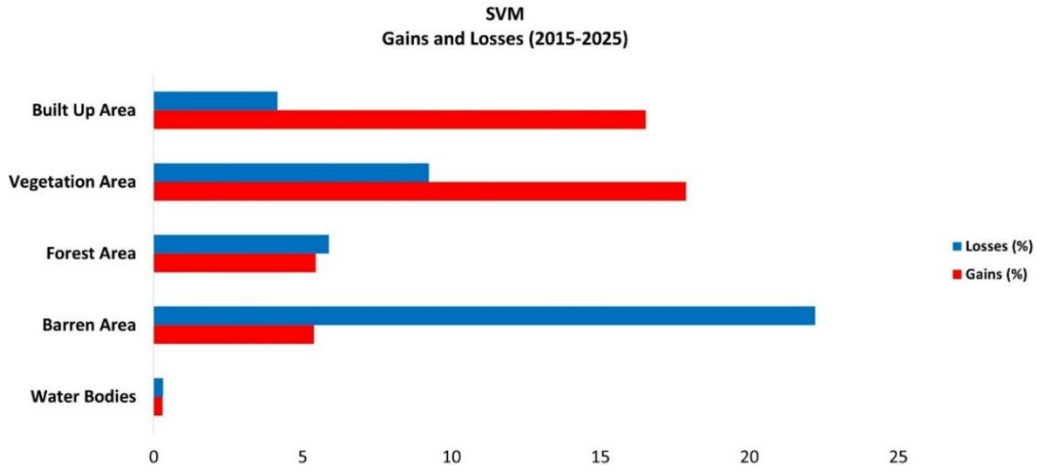

Figure 9, Gains and losses of LULC classes from 2015 to 2025 (SVM).

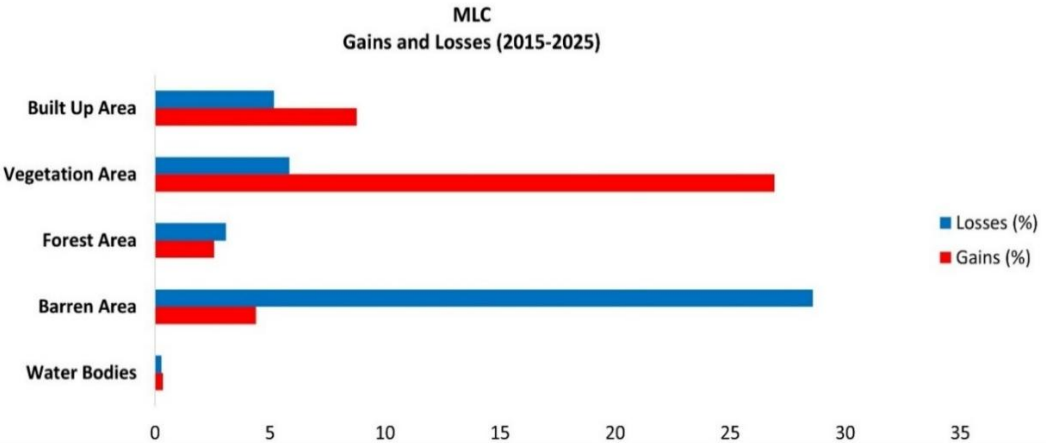

Figure 10, Gains and losses of LULC classes from 2015 to 2025 (MLC)

Accuracy assessment and comparative analysis: SVM vs. MLC classification

A comparative evaluation of accuracy assessment suggests that SVM provides slightly higher classification reliability compared to MLC. The overall accuracy for SVM-based classification was 79% in 2025, compared to 73% for MLC. The kappa coefficient for SVM (0.69) was higher than that of MLC (0.60), demonstrating improved agreement with ground truth data (Table 4). The major advantage of SVM lies in its ability to effectively differentiate similar classes, such as Built-up area and barren area. MLC tends to classify more transitions toward vegetative categories (e.g., Barren to Vegetation, Built-Up to Vegetation), while SVM shows stronger internal class consistency. Both classifiers identify transitions among LULC classes, but the magnitude and direction vary notably. It suggests the advantage of SVM over MLC in remote sensing applications. The kappa coefficient for both classifiers shows substantial agreement based on the commonly used interpretation scale (Landis and Koch, 1977).

This study employs a two-date post-classification comparison using data from 2015 and 2025. While this method effectively captures the overall changes that occurred between these two years, it does not fully reflect the gradual or year-to-year dynamics of LULC transformation. As a result, short-term fluctuations or intermediate transitions may not be represented. Future research that incorporates multi-year time-series datasets would provide a more comprehensive understanding of continuous LULC changes and help reveal long-term transformation patterns more clearly. This study also did not directly examine the environmental consequences behind the changes and no statistical significance tests were conducted.

Conclusion

These are exclusive concluding remarks from this study:

1. Utilizing freely available Landsat imagery enabled the quantification and mapping of LULC changes in Bhaktapur district, Nepal, with a particular focus on variations between SVM and MLC classifiers.
2. Analysis of Landsat imagery of 2015 and 2025 revealed variations in LULC change patterns. During the study decade, much of the land was converted into Built-up area and vegetation areas, with substantial reductions in barren area, and negligible reduction in forest area. These changes indicate ongoing urban expansion in the area. However, it is important to note that this study did not directly examine the specific causes such as environmental consequences behind these changes.

Table 4, Accuracy assessment of the LULC classification

	SVM				MLC			
	2015		2025		2015		2025	
LULC	Producers Accuracy	User Accuracy	Producers Accuracy	User Accuracy	Producers Accuracy	User Accuracy	Producers Accuracy	User Accuracy
Built-up area	66.66	80	80	64	70	58.33	65	76.47
Vegetation area	51.51	85	74.5	92.68	52.63	100	87.8	67.92
Forest area	89.28	96.15	100	94.73	77.77	87.5	73.68	93.33
Barren area	95.23	52.63	63.63	46.66	91.17	59.61	52.63	66.66
Water bodies	0	0	0	0	0	0	0	0
Overall	74		79		72		73	
Kappa	0.65		0.69		0.60		0.60	

3. SVM achieved an overall accuracy of 79% with a kappa coefficient of 0.69, while MLC recorded 73% accuracy with a kappa coefficient of 0.60. These results suggest that SVM provides slightly higher agreement compared to MLC. Both classifiers fall within the substantial agreement category.

Overall, the study presents a comparative analysis of the SVM and MLC techniques for LULC mapping in Bhaktapur district using Landsat imagery. The analysis shows measurable changes in Built-up area, vegetation, and barren areas between 2015 and 2025. SVM achieved slightly higher classification accuracy compared to MLC. The results provide useful baseline spatial information that can support planners in monitoring future land-use changes.

Acknowledgements

The author would like to thank two anonymous reviewers for their valuable comments and suggestions, which helped to rectify the manuscript. The author also expresses sincere gratitude to Khwopa College of Engineering for its continuous support.

Data availability

The Landsat imagery used in this study is publicly available from the United States Geological Survey (USGS) Earth Explorer platform. Derived datasets and classification outputs generated during the study are available from the corresponding author upon reasonable request.

Declarations

The author declares that he has no known competing financial interests or personal relationships that could have appeared to influence the work reported in this article.

References

Alharthi, A., El-Sheikh, M.A., Elhag, M., Alatar, A.A., Abbadi, G.A., Abdel-Salam, E.M., Arif, I.A., Baeshen, A.A. and Eid, E.M., (2020). Remote sensing of 10 years changes in the vegetation cover of the northwestern coastal land of Red Sea, Saudi Arabia. Saudi Journal of Biological Sciences, 27(11), 3169–3179. https://doi.org/10.1016/j.sjbs.2020.07.021

Batty, M. and Xie, Y., (1997). Possible urban automata. Environment and Planning B: Planning and Design, 24(2), 175–192. https://doi.org/10.1068/b240175

Chhetri, D.B.T. and Moriwaki, R., (2017). Monitoring urban growth, land use and land cover using remote sensing and GIS techniques: A case study of Bhaktapur District, Nepal. Engineering Science and Technology International Journal (ESTIJ), 7(1).

Congleton, R.G., (1991). A review of assessing the accuracy of classifications of remotely sensed data. Remote Sensing of Environment, 37(1),35–46. https://doi.org/10.1016/0034-4257(91)90048-B

Dimyati, M., Mizuno, K., Kobayashi, S. and Kitamura, T., (1996). An analysis of land use/cover change in Indonesia. International Journal of Remote Sensing, 17(5),931–944. https://doi.org/10.1080/01431169608949056

DHM (2023). Department of Hydrology and Meteorology, Annual climate report. Government of Nepal, Ministry of Energy, Water Resources and Irrigation. https://www.dhm.gov.np

Gibril, M.B.A., Bakar, S.A., Yao, K., Idrees, M.O. and Pradhan, B., (2017). Fusion of RADARSAT-2 and multispectral optical remote sensing data for LULC extraction in a tropical agricultural area. Geocarto International, 32(7), 735–748. https://doi.org/10.1080/10106049.2016.1170893

Huang, C., Davis, L.S. and Townshend, J.R.G., (2002). An assessment of support vector machines for land cover classification. International Journal of Remote

Sensing, 23(4), 725–749. https://doi.org/10.1080/01431160110040323

Ishtiaque, A., Shrestha, M. and Chhetri, N., (2017). Rapid urban growth in the Kathmandu Valley, Nepal: Monitoring land use land cover dynamics of a Himalayan city with Landsat imageries. Environments, 4(4), 72. https://doi.org/10.3390/environments4040072

Johnson, B.A. and Iizuka, K., (2016). Integrating OpenStreetMap crowdsourced data and Landsat time-series imagery for rapid land use/land cover (LULC) mapping: Case study of the Laguna de Bay area of the Philippines. Applied Geography, 67, 140–149. https://doi.org/10.1016/j.apgeog.2015.12.006

Kanellopoulos, I., Varfis, A., Wilkinson, G.G. and Mégier, J., (1992). Land-cover discrimination in SPOT HRV imagery using an artificial neural network—a 20-class experiment. International Journal of Remote Sensing, 13(5), 917–924. https://doi.org/10.1080/01431169208904164

Kavzoglu, T. and Colkesen, I., (2009). A kernel functions analysis for support vector machines for land cover classification. International Journal of Applied Earth Observation and Geoinformation, 11(5), 352–359. https://doi.org/10.1016/j.jag.2009.06.002

Landis, J.R. and Koch, G.G., (1977). The measurement of observer agreement for categorical data. Biometrics, 33(1), 159–174.

Maleki, M., Van Genderen, J.L., Tavakkoli-Sabour, S.M., Saleh, S.S. and Babaee, E., (2020). Land use/cover change in Dinevar rural area of west Iran during 2000–2018 and its prediction for 2024 and 2030. Geographia Technica, 15(2), 93–105. https://doi.org/10.21163/GT_2020.152.10

MohanRajan, S.N., Loganathan, A. and Manoharan, P., (2020). Survey on Land Use/Land Cover (LU/LC) change analysis in remote sensing and GIS environment: Techniques and challenges. Environmental Science and Pollution Research, 27(24), 29900–29926. https://doi.org/10.1007/s11356-020-09091-7

Naghadehi, S.Z., Asadi, M., Maleki, M., Tavakkoli-Sabour, S.M., Van Genderen, J.L. and Saleh, S.S., (2021). Prediction of urban area expansion with implementation of MLC, SAM and SVM classifiers incorporating artificial neural network using Landsat data. ISPRS International Journal of Geo-Information, 10(8). https://doi.org/10.3390/ijgi10080513

Owojori, A. and Xie, H., (2005). Landsat image-based LULC changes of San Antonio, Texas using advanced atmospheric correction and object-oriented image analysis approaches. In: Proceedings of the 5th International Symposium on Remote Sensing of Urban Areas, Tempe, Arizona, USA, 14–16 March 2005. Available at: https://www.researchgate.net/publication/253839686

Prajapati, R.N., (2024). Land Use Land Cover and Population Changes in Bhaktapur District. PhD Centre Nepal. Available at: www.phdcentre.edu.np

Simwanda, M. and Murayama, Y. (2018). Spatiotemporal patterns of urban land use change in the rapidly growing city of Lusaka, Zambia: Implications for sustainable urban development. Sustainable Cities and Society, 39, 262–274. https://doi.org/10.1016/j.scs.2018.01.039

Subasinghe, S., Estoque, R. and Murayama, Y., (2016). Spatiotemporal analysis of urban growth using GIS and remote sensing: A case study of the Colombo Metropolitan Area, Sri Lanka. ISPRS International Journal of Geo-Information, 5(11),197. https://doi.org/10.3390/ijgi5110197

Timsina, N.P., (2020). Trend of urban growth in Nepal with a focus in Kathmandu Valley: A review of processes and drivers of change. Tomorrow's Cities Working Paper 001. Available at: www.tomorrowscities.org

Wellmann, T., Haase, D., Knapp, S., Salbach, C., Selsam, P. and Lausch, A., (2018). Urban land use intensity assessment: The potential of spatio-temporal spectral traits with remote sensing. Ecological Indicators, 85, 190–203. https://doi.org/10.1016/j.ecolind.2017.10.029

Xian, G. and Crane, M., (2005). Assessments of urban growth in the Tampa Bay watershed using remote sensing data. Remote Sensing of Environment, 97(2), 203–215. https://doi.org/10.1016/j.rse.2005.04.017

Yadav, R.K., (2013). Ageing population in Nepal: Challenges and management. Academic Voices: A Multidisciplinary Journal, 2, 48–53. https://doi.org/10.3126/av.v2i1.8287

Research Article DOI: https://doi.org/10.64862/ajeg.2025.202.03.269 Open Access

Study on Spatio-Temporal Changes in River Dynamics and Land Cover along the Seti River Floodplain, Kaski, Nepal

Bikash Adhikari[1], Aastha Singh Bhandari[2], Ram Chandra Tiwari[3*] and Aanchal Tiwari[4]

[1,2]Department of Environmental Science and Engineering, Kathmandu University, Nepal
[3,4]Department of Civil Engineering, Institute of Engineering, Pulchowk Campus, Tribhuvan University, Lalitpur, Nepal

(*Corresponding E-mail: rct2075ce_rctiwari@pcampus.edu.np)

Received: August 14, 2025, Accepted: December 22, 2025

Abstract: **In a geographically diverse country like Nepal, changes in river dynamics and land use/land cover are common phenomena. Kaski District, located in the hilly region of central Nepal, exhibits significant variations in river morphology and landform characteristics over time. This study analyzes the decadal changes in river dynamics and land cover along the Seti floodplain from 1989 to 2017 using Geographic Information System (GIS) and Remote Sensing (RS) techniques. Landsat images from four decades were used, followed by radiometric correction, reclassification, and combination for analysis. River dynamics were evaluated through parameters such as sinuosity and bankline shift, while land cover classification employed unsupervised segmentation and indices-based methods. Six land cover categories were identified: water body, built-up area, barren land, agriculture and grassland, shrub and forest, and snow and glacier. The Seti River showed a decreasing trend in sinuosity, with the highest value in 1989 and the lowest in 2017. The maximum bank shift of 42.7 m occurred in the mid-right bank between 1999 and 2009, while the minimum shift of 6.7 m was observed in the upper right bank between 1989 and 1999. Water body area increased from 7.60 km^2 in 1989 to 8.34 km^2 in 2017, and built-up area expanded from 32.44 km^2 to 80.98 km^2. Barren land decreased from 353.80 km^2 to 332.07 km^2, while agriculture and grassland increased from 251.21 km^2 to 320.15 km^2. Shrub and forest areas declined from 984.75 km^2 to 889.05 km^2, whereas snow and glacier cover increased from 458.05 km^2 to 477.55 km^2.**

Keywords: ***Land Use and Land Cover change (LULC), Seti floodplain, Remote sensing and GIS, Bankline shift, Spatio-temporal changes***

Introduction

Nepal River dynamics refers to the study of water and sediment movement within a river channel and its adjacent areas, focusing on how natural processes and human activities influence channel morphology (Hazarika et al., 2015). Natural phenomena such as earthquakes and floods, along with anthropogenic interventions, often modify river behavior, affecting sediment transport, erosion, and deposition patterns. Understanding river dynamics is crucial for predicting channel deformation, assessing associated hazards, and managing floodplains effectively.

Floodplains, defined as low-lying lands adjacent to rivers that experience periodic flooding, serve vital ecological and socio-economic functions. They provide fertile soil for agriculture, habitats for biodiversity, and space for human settlement, especially in densely populated regions of South and Southeast Asia (Hazarika et al., 2015). However, floodplains are dynamic systems constantly reshaped by lateral and vertical river movements, which in turn influence land use and land cover (LULC) patterns.

In the current study, the Seti River in Kaski District, Nepal is taken into account to identify decadal changes in the dynamics of the river and land use/land cover (LULC) from 1989 to 2017. The Seti River passes through major settlement areas such as Pokhara, serving livelihoods, agricultural activities, and water needs. Even after being so important, little effort has been made to assess its geomorphological, ecological, and LULC change aspects. Thus, the main objectives of the study are: (1) to identify the decadal changes in sinuosity and bank shift of the Seti River using GIS and remote sensing technology; (2) to map and analyse the decadal LULC changes of Kaski District from 1989 to 2017; and (3) to highlight the spatial and temporal changes and their relationship with natural and anthropogenic drivers. The current study aims to contribute to the scientific knowledge of river morphology evolution and landscape transformation of the basin. The results of the research can be used for flood hazard prediction and land management, as well as policy-making. The limitations of the study include low resolution of satellite data and lack of field data for validation. The findings provide baseline spatial information for future studies in the Seti River basin.

River dynamics and land use land cover (LULC) pattern

River dynamics phenomena

The study of river flow, sediment transport, and channel evolution has been ongoing for centuries. However, the scientific foundation of river dynamics was established when DuBoys (1879) introduced a bed-load formula and

Rouse (1937) described suspended sediment distribution, advancing river dynamics as a distinct discipline (Wu, 2007). Since then, numerous studies have enhanced understanding in river engineering and floodplain management.

Human activities such as dam construction, channel modification, and land-use change have significantly altered river systems. Müller (1996) observed that engineering interventions disrupted natural morphodynamics and floodplain vegetation, leading to habitat loss and reduced biodiversity. Restoration and conservation efforts therefore emphasize re-establishing natural river processes. Similarly, Dufour et al. (2015) found that anthropogenic control along the Magra River after WWII caused channel narrowing and morphological changes, shifting from braided to meandering patterns and affecting riparian landscapes.

Urbanization increases impervious surfaces, reducing infiltration and enhancing surface runoff. Petchprayoon et al. (2010) noted that urban land expansion along the Yom River accelerated peak-flow discharge, elevating flood risks compared to rural basins.

Shrestha (2010) reported that decreased precipitation in the Bagmati River basin reduced stream power and discharge, increasing sinuosity. Global warming is expected to further alter rainfall patterns, causing intensified floods or river drying (Hassan et al., 2016).

Vegetation strongly influences runoff and erosion. Matheussen et al. (2000) found that reduced forest cover and lower leaf area index increased snow accumulation and runoff in the Columbia River Basin. Similarly, Kalliola and Puhakka (1988) observed that riparian vegetation along Finland's Kamajohka River was shaped by fluvial processes, with primary successions continually renewed by erosion and deposition.

Land use and land cover (LULC) pattern

Land cover change is a global phenomenon driven by both natural and anthropogenic activities, resulting in temporal and spatial modifications of land features (Zewdu et al., 2016). These changes influence surface characteristics such as albedo, roughness, leaf area index, soil texture, and structure (Lambin et al., 2003). Analyzing LULC provides baseline data to understand past land-use patterns, climate change impacts, and human-induced environmental changes.

Urbanization is a major force altering LULC patterns (Xiao et al., 2006). Deng et al. (2009) reported that in Hangzhou, China, 27.4% of land transformed within a decade, primarily from agricultural to urban use. Similarly, Mohan et al. (2011) found that Delhi's population growth and unplanned expansion led to a 16.86% increase in built-up area at the expense of agricultural and open lands. Land-use changes also influence river systems. Klocking and Haberlandt (2002) found that afforestation and valley-floor restoration affected water availability in the Elbe Basin. In the Brahmaputra floodplain, Hazarika et al. (2015) observed that unstable river courses caused significant erosion and deposition, altering settlement and agricultural areas. Such changes highlight the interplay between river dynamics and human adaptation in flood-prone regions.

Walker and Homma (1996) showed that in the Brazilian Amazon, land concentration, rural violence, and deforestation were closely linked. Land-use dynamics are thus not only environmental but also deeply social, demanding consideration of ecological sustainability to ensure social well-being.

Tools for river dynamics and indices used for LULC

Tools for river dynamics

Remote sensing is a technique for obtaining information about the Earth's surface without direct contact. It involves sensing and recording reflected or emitted energy, followed by processing, analysis, and interpretation of the data (Barnsley, 1999). Remote sensing is widely used for mapping, monitoring, and managing natural hazards as well as studying land cover and river dynamics. Commonly used remote sensing software includes ERDAS IMAGINE, eCognition Developer, OSSIM, InterImage, E-foto, and ILWIS.

A Geographic Information System (GIS) is a computer-based technology used for capturing, storing, manipulating, analyzing, and displaying spatial or geo-referenced data (Burrough and McDonnell, 1998). In the study of land and river dynamics, GIS enables the creation of interactive map overlays that support developmental planning, resource management, and hazard assessment. Widely used GIS software includes ArcMap, ArcView, Arc/Info, GRASS GIS, QGIS, and MapInfo.

Indices used for LULC

Various indices are used for the proper delineation of land cover in GIS. NDVI is a simple graphical indicator used to determine whether the target being observed contains live green vegetation or not. Generally, plants show low reflectance in the blue and the red portion of the spectrum because of chlorophyll absorption (Wang et al., 2005). However, they have a slightly high reflectance in green, hence, appearing green to our eyes. Spectral reflectance of a crop varies substantially in the near infrared region (λ=700-1300nm) and in the visible red range (λ=550-700nm) of the electromagnetic spectrum. The plant surface strongly reflects near infrared radiant energy and the properties of the leaf tissues like cellular structure, and the air-cell wall-protoplasm-chloroplast interfaces are the key determinant of the reflectance amount. The NDVI is hence calculated from reflectance measurements in

the red and near infrared (NIR) region of the spectrum by the following relation.

$$NDVI = \frac{R_{NIR}-R_{Red}}{R_{NIR}+R_{Red}} = \frac{Band_4-Band_3}{Band_4+Band_3} \quad (1)$$

Where R_{NIR} is the reflectance of NIR radiation and RRED is the reflectance of visible red radiation (Govaerts and Verhulst, 2010).

The main purpose of NDSI is to identify the snow cover from a given target imagery. Snow has high reflectance in the visible and near-infrared region of the spectrum. However, it can decrease with age of the snow and contamination by aerosols, soot, pollen, etc., yet its reflectance is higher than any other surfaces. It has a high absorbance in infra-red part, resulting in low reflectance. Based on these reflectance properties the MODIS snow cover algorithm was made. The NDSI is hence calculated from reflectance measured in the green and shortwave infrared (SWIR) region of the spectrum by the following relation.

$$NDSI = \frac{R_{Green}-R_{SWIR}}{R_{Green}+R_{SWIR}} = \frac{Band_2-Band_5}{Band_2+Band_5} \quad (2)$$

Where R_{Green} is the reflectance of visible green radiation and R_{SWIR} is the reflectance of shortwave infrared radiation (Riggs et al., 1994).

The Normalized Difference Water Index (NDWI) serves as an indicator to delineate open water features and enhance their presence in remotely sensed images. The reflectance of near infrared radiation and visible green light are operated to delineate the water features while eliminating the presence of soil and terrestrial vegetation features side by side. It may also provide the turbidity estimations of the water bodies (McFeeters, 1996). The NDWI is hence calculated from reflectance measured in the green and near infrared (NIR) region of the spectrum by the following relation.

$$NDWI = \frac{R_{Green}-R_{NIR}}{R_{Green}+R_{NIR}} = \frac{Band_2-Band_4}{Band_2+Band_4} \quad (3)$$

Where R_{Green} is the reflectance of visible green radiation and R_{NIR} is the reflectance of near infrared radiation. The observed river changes, vegetation loss, and urban expansion increase flood and erosion risks, highlighting the need for regular monitoring and sustainable management.

Material and method

Study area

Kaski district is located in the Gandaki region of the Western Development Region of Nepal (Figure 1) and falls under Province 4. It lies between 28.2622° N latitude and 84.0167° E longitude, covering an area of 2,017 km^2. The district's elevation ranges from 450 m to 8,901 m above sea level. The administrative center and district headquarters is Pokhara.

Kaski district majorly has upper tropical climate. Its annual rainfall is around 3876mm. However, the pattern was fluctuating between 1985 and 2013 A.D. The minimum average annual temperature ranges from 0.5 to 5.5˚C while the yearly maximum average temperature has fluctuated from 33 to 37.4˚C (AEPC, 2017).

Vegetation in Kaskivary according to its altitude. Sub-tropical zone (1000-1800masl) is rich in Schimawallichii and Castanopsisindica vegetation type. Other trees like oak, birch, maple, alder are also found. Riverine forests are mostly dominated by simal (Bombaxmalbaricum). On slopes above 1800m evergreen coniferous forests are found containing pine, fir, spruce and larch trees. Rhododendron species occupies the main temperate zone forest at an altitude between 1800-4000masl. The alpine region includes plant species like Juniperusrecurva, Ephedra gerardiana, Rhododendron lepidotumetc (HIMALDOC, 2017).

Kaski is rich in multiple cultures,language and religion. According to the census of 2068 B.S. Kaski has 84 castes, 44 languages and 11 religions. The major ethnic group includes Gurung, Brahmin, Chhetri, Newar, Thakali and Kumal. The major sources of income include agriculture, business and tourism.

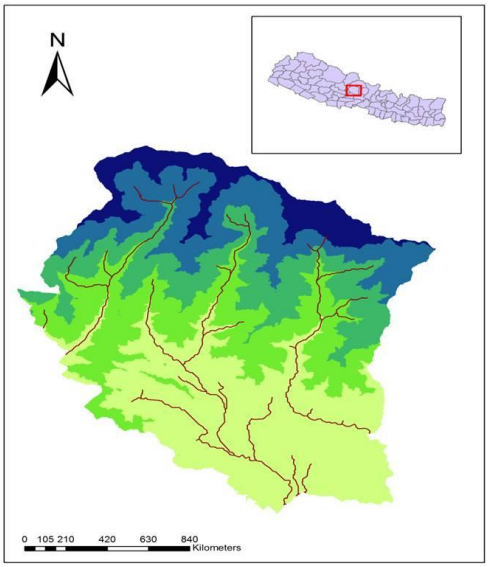

Figure1, Study area- Kaski district with its drainage patterns

Data Collection

Images with least cloud cover were extracted from the official site of U.S Geological Survey. Satellite images of years 1989, 1999, 2009 and 2017 were downloaded. Further information was obtained from related corresponding articles, reports, publications, books, literatures from various sources like a University library, ICIMOD library, HICCDRC, Department of Hydrology and Meteorology and World Wide Web. After the collection of all the desired data and information, they were analyzed using tools like Remote Sensing and GIS.

Landsat images for the stated years, i.e. 1989, 1999, 2008, 2017 were downloaded from the official site of the U.S. geological survey. Best images from the dry season

were selected to obtain images with least cloud cover and also to avoid the overestimation of the river channel. Landsat sensors L4-5 and L8 OLI/TIRS were used. Information about the Landsat images used for the study is given below in Table 1.

Table 1, Detail Information of the Landsat used

Year	Sensor	Acquisition date	Path/Row	Res. (m)
1989	L4-5 TM	7th Nov	142/40	30<10%
1999	L4-5 TM	13th Dec	142/40	30<10%
2009	L4-5 TM	15th Feb	142/40	30<10%
2017	L8 OLI/TIRS	21st Feb	142/40	30<10%

Image processing

The acquired raw images were unzipped and hence processed in QGIS at initial. Pre-processing basically refers to radiometric corrections which involves correction of digital numbers (DN) of the images. It is carried out in order to improve the interpretability and quality of remotely sensed data (Radiometric Corrections).

The sensors, Landsat Thematic Mapper ™ and Enhanced Thematic Mapper (ETM+) after capturing the reflected solar energy, convert the data to radiance. Later they are rescaled into 8-bit digital numbers (DN). These DN can be converted to Top of Atmosphere (ToA) radiance first and ToA reflectance later. Hence, the radiance correction at ToA was carried out using the algorithm.

$$ToA(\lambda) = M_L * Q_{cal} + A_L \qquad (4)$$

Where M_L=Band specific multiplicative rescaling factor from Landsat Metadata, A_L= Band-specific additive rescaling factor from Landsat Metadata and Q_{cal}=Quantized and calibrated standard product pixel values (DN).

After the computation of ToA radiance, reflectance correction at ToA was operated. The following algorithm was used.

$$ToA(\rho_p) = (\pi * L_\lambda * d^2)/(ESUN_\lambda * cos\theta_s) \qquad (5)$$

Where L_λ= Spectral radiance at the sensor's aperture (at-satellite radiance), d=Earth-sun distance in astronomical units, $ESUN_\lambda$= mean solar exo-atmospheric irradiances and θ_s= Solar zenith angle in degrees. The Landsat OLI sensor, however, converts the DN data directly to reflectance compared to TM and ETM+ where two steps computation of radiance and reflectance needs to be carried out.

In order to derive wind, vapor, cloud, rain, and SST products the brightness temperatures are used at remote sensing. This is one of the important radiometric corrections to improve the quality of the image. The conversion of DN to At-Satellite Brightness Temperature is given by the following relation.

$$T_B = k_2/ln[(\frac{k_1}{L_\lambda}) + 1] \qquad (6)$$

Where k_1=Band-specific thermal conversion constant (in watts /meter squared*ster*μm) and k_2= Band-specific thermal conversion constant (in kelvin) and L_λ is the Spectral Radiance at the sensor's aperture measured in watts (meter squared*ster*μm).

After the completion of radiometric corrections, False Color Composite (FCC) was employed for better visualization.

The characteristics of local features such as color, texture, edge and contour are naturally ambiguous. They do not really show the same level of homogeneity or notability at the same spatial scale (Yang et al., 2008). After the preprocessing of the images, Kaski district was clipped from the entire Landsat image with the help of projected shape file of the district. Then an unsupervised segmentation method was operated in ArcMap 10.3 in which the colors of the image were quantized to several representative classes that could be used to differentiate various regions in the image. With the help of image pixels, corresponding color class labels were formed hence forming the class map of the image.

Three main indices were further employed for proper delineation of the land features in Table 2.

Table 2, Main indices employed for the proper delineation of the land features

Index used	Equation
Normalized Difference Vegetation Index	$DVI = \frac{Band4 - Band3}{Band4 + Band3}$
Normalized Difference Snow Index	$NDSI = \frac{Band2 - Band5}{Band2 + Band5}$
Normalized Difference Water Index	$NDWI = \frac{Band2 - Band4}{Band2 + Band4}$

Finally, individually operated raster dataset was combined into a single raster dataset. After the classification, 3x3 Majority Filter was run for further editing using ArcMap tools. This tool basically replaces cells in a raster based on the majority of their adjoining neighboring cells.

Finally, the raster was converted to polygon and some manual editing was carried out as a final touch prior to image analysis.

The area of each individual polygon representing a single class was summed using ArcMap tools. Hence area for each class was obtained. The detail working procedure is included in the flow chart (Figure 2).

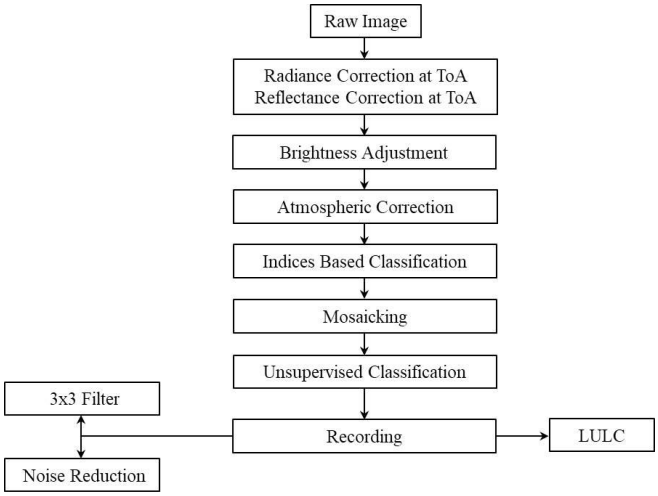

Figure 2, Flow chart of the methodology

Change in River dynamics

Iso-cluster unsupervised classification was used to perform the classification process in the raster band, hence classifying the image and enabling us to locate the desired feature, i.e. River .

With the help of reclassify tool, the classified image was further processed in order to distinguish river course and extract it eventually (Figure 3). With the help of conversion tools, the obtained river raster was ultimately converted to polygon. Manual editing was done to enhance the river features. Ultimately, the river polygon was converted into polylines, and hence bank lines were delineated.

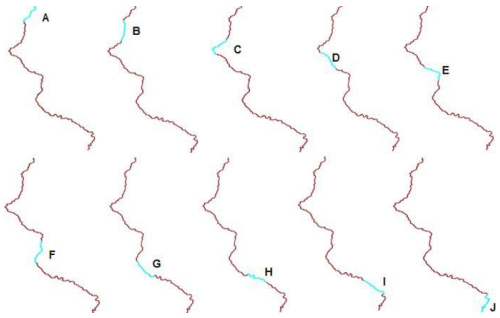

Figure 3, Sections of River

With the help of the obtained bank lines, the channel centerline was generated through detailed on-screen digitization using GIS tools. To ensure a more systematic and unbiased assessment of river dynamics, the entire river channel was divided into ten nearly equal segments for analysis (Hazarika et al., 2015). The sinuosity index and bank line shift were then measured for each segment, allowing a comparative evaluation of channel migration, curvature variation, and the degree of lateral shifting along different reaches of the river.

The extent to which a river channel departs from a straight line is known as river sinuosity (Ebisemiju, 1994). It is calculated as follows.

$$Sinuosity\ (S) = \frac{L}{l} \qquad (7)$$

Where L=Total length of a reach and l= length of straight line between the two points. For the analysis of bank shift, first, points were created on the vertices of the bank. Then, minimum distance between the vertices and next bank (corresponding to the bank with vertices) was calculated. Suppose, points were created on the vertices of the left bank of 1989, then the nearest distance between those vertices and left bank of 1999 bank was calculated. Then again points were created on 1999 bank and minimum distance was measured with 2009 bank and so on. The same process was continued for the right bank. Hence, the entire shift in each segment of each bank was obtained, along with sinuosity.

Result and discussion

After the application of the radiometric corrections, clear and good quality images were obtained for the analysis (Figure 4).

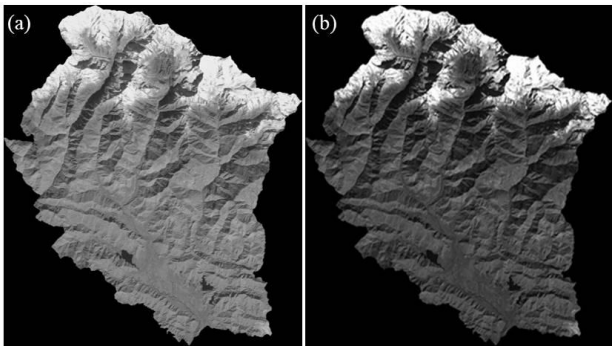

Figure 4, Image correction: (a) Before and (b) After.

Sinuosity of Seti

Since the river was divided into 10 sections, sinuosity for both banks in each section was obtained. Section A refers to the uppermost part of the river channel where the river originates and section B to J are the downstream adjacent parts (Table 3 and Figure 5).

The sinuosity value decreases gradually from 1989 to 2017. The river shows high sinuosity in H section of 1989 bank. The lowest sinuosity is seen in D section of 2017 bank. High sinuosity (>1.50) value means the part of the channel is meandering while the range between 1.05-1.25 suggests the channel is winding. Sediment transport, bed load together with the slope of the floodplain are the basic factors that influence sinuosity (Smith, 1998).

Bank shift

Decadal bank shifts of both right and left bank have been assessed section wise (Table 4 and Figure 6). The bank shift is quite fluctuating in each decade. However, compared to 1989-1999, the other two decades show greater shift. There is a high shift of 42.7 m in the right bank of F-section during the decade 1999-2009. The shift may result due to the river flowing into wider plain after flowing from the narrow channel. Similarly, rivers

tend to spread laterally towards the lower region of the valley. Therefore, most of the high values of bank shifts are seen in lower sections.

Table 3, Decadal sinuosity of Seti

S. No	Section	Left_1989	Right_1989	Left_1999	Right_1999	Left_2009	Right_2009	Left_2017	Right_2017
1.	A	1.56	1.58	1.54	1.59	1.51	1.50	1.63	1.64
2.	B	1.38	1.39	1.36	1.34	1.38	1.35	1.38	1.47
3.	C	1.74	1.74	1.74	1.68	1.68	1.73	1.54	1.54
4.	D	1.45	1.44	1.42	1.39	1.36	1.38	1.26	1.24
5.	E	1.73	1.70	1.75	1.71	1.64	1.64	1.57	1.59
6.	F	1.40	1.38	1.38	1.32	1.31	1.28	1.28	1.32
7.	G	1.52	1.46	1.53	1.49	1.48	1.45	1.37	1.35
8.	H	1.79	1.81	1.71	1.79	1.66	1.74	1.64	1.53
9.	I	1.45	1.39	1.47	1.45	1.47	1.42	1.31	1.29
10	J	1.68	1.68	1.79	1.68	1.65	1.67	1.52	1.42

Table 4, Decadal Bank shift of Seti in meters

S. No	Section	1989 to 1999_L	1989 to 1999_R	1999 to 2009_L	1999 to 2009_R	2009 to 2017_L	2009 to 2017_R
1	A	11.5	9.5	13.1	12.5	18.9	19.3
2	B	7.7	6.7	10.4	12.2	20.5	19.2
3	C	7.9	8.1	13.1	10.3	14.9	17.1
4	D	8.2	10.0	9.1	9.1	11.5	13.1
5	E	9.6	9.8	11.1	12.2	17.2	17.8
6	F	15.5	25.1	29.9	42.7	27.9	19.7
7	G	15.5	16.7	17.1	17.3	24.7	20.9
8	H	12.5	12.3	16.6	19.1	22.8	23.7
9	I	24.8	30.1	22.6	19.4	24.5	27.4
10	J	14.5	15.1	36.1	20.2	36.7	23.6

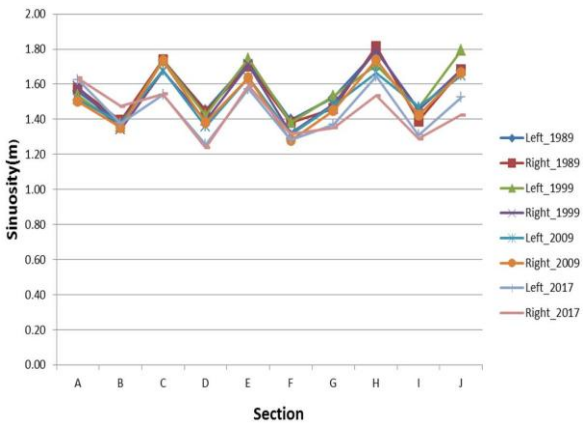

Figure 5, Section wise sinuosity of Seti from 1989 to 2017

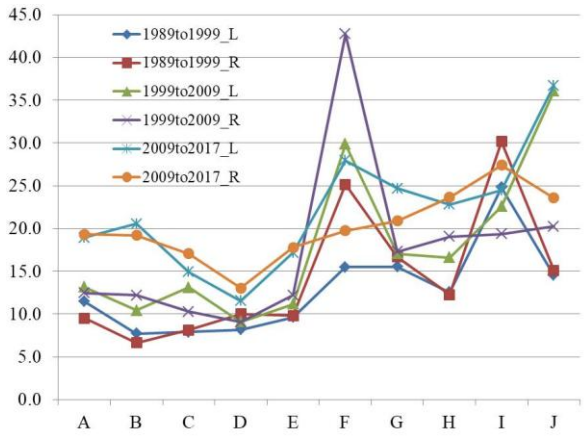

Figure 6, Section wise bank shift of Seti from 1989 to 2017

Threshold values of land class

The following threshold values were determined and land classes were separated accordingly with the help of the three major indices. Table 5 shows the land use classes and their respective threshold values (reflectance).

Table 5, Land use classes and their reflectance

S. No.	Land Class	Indices Used	Threshold values (Reflectance)
1.	Built up area	NDVI	0.11-0.3
2.	Barren land		0.3-0.36
3.	Agriculture and Grassland		0.36-0.5
4.	Shrub and forest		>0.5
5.	Water Bodies	NDWI	>0.35
6.	Snow and glacier	NDSI	>0.5

LULC classification

Land use cover classification was done for the following years and was divided into 6 major classes. Table 6 shows the area occupied by each class in the following years.

Table 6, The area occupied by land use class in sq km

S. No.	Land Class	1989	1999	2009	2017
1	Water Body	7.60	7.9	7.34	8.34
2	Builtup Area	32.44	54.39	74.15	80.98
3	Barren land	353.802	341	355.66	332.07
4	Agriculture and grassland	251.207	274.03	299.76	320.15
5	Shrub and forest	984.753	916.48	911.50	889.05
6	Snow and Glacier	458.052	495.95	439.37	477.55
Total		2088	2088	2088	2088

Figure 7, Figure 8, Figure 9 and Figure 10 respectively show the LULC of Kaski from the 1989 to 2017. The overall result delineates that there was a huge change in shrub and forest area from 984.753km^2 (1989) to 889.05km^2 (2017). The land class that was least changed was water bodies from 7.60 km2 in 1989 to 8.34 km^2 in 2017.The barren land decreased from 353.802 to 332.07 km^2 while agriculture land seems to increase proportionately every decade starting from 251.207 km^2 in 1989 to 320.15 km^2 in 2017. Builtup area seems to increase gradually from 32.44 to 80.98 km^2. The decreasing trend of shrub and forest land seems prominent in every decade. The area coverage of snow and glaciers seems to fluctuate every decade. However, there is an overall increase in its area from 458.052 km^2 (1989) to 477.55 km^2 (2017). These changes can mainly be attributed to anthropogenic activities and to some extent the natural causes as well. Rapid urbanization is one of the main causes that drives changes in land cover patterns (Xiao et al., 2006). To meet the demands of increasing population the vegetation land is rapidly cleared out and is replaced with builtup areas. Such trend is seen in the above results too. With the decadal increase in builtup areas, a decrease in shrub and forest area is quite evident. The barren land has also decreased subsequently and resulting into conversion of built up areas.

LULC map of Kaski indicates a lot of changes in the land use and cover pattern of the area under study in different periods of time. From Figure 7, the initial pattern of land use and cover of the area can be noticed, which is dominated by extensive presence of shrubs, forest, and glacial areas with few infrastructural developments. In Figure 8, an increase in built-up areas has been observed, mainly in the southern and central part of the district. Figures 7, Figure 8, Figure 9 and Figure 10 present the LULC maps of Kaski for 1989, 1999, 2009, and 2017, respectively, whereas Figure 11 summarizes the temporal changes in the area of each land-cover class..

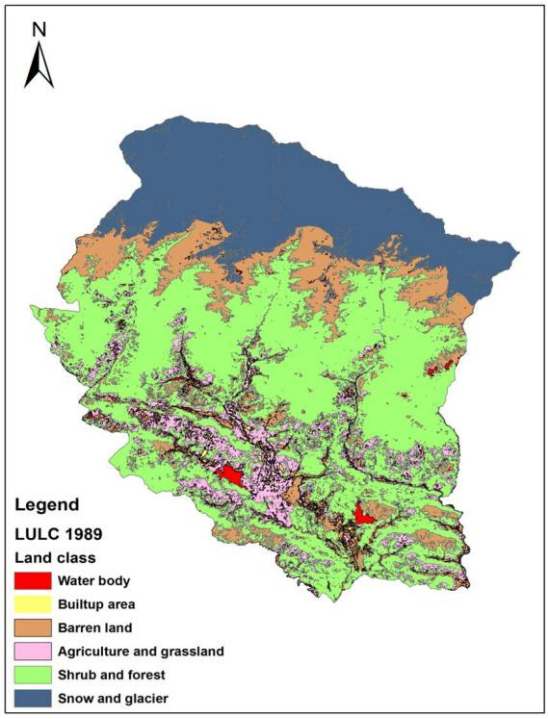

Figure 7, LULC of Kaski in 1989

Natural phenomenon such as floods, change in river courses and other such river and Riverine hazards also trigger land use changes. The 2012 Seti flash flood resulted in conversion of the settlement area into the debris filled land. The meandering pattern of Seti is also responsible for the conversion of cultivated land into sand area. Certain areas of the district, especially Pokhara city is vulnerable to flooding, riverbank erosion and slope undercutting and sinkhole hazards since the river flows beneath the city weakening/undermining the stability of the ground materials.

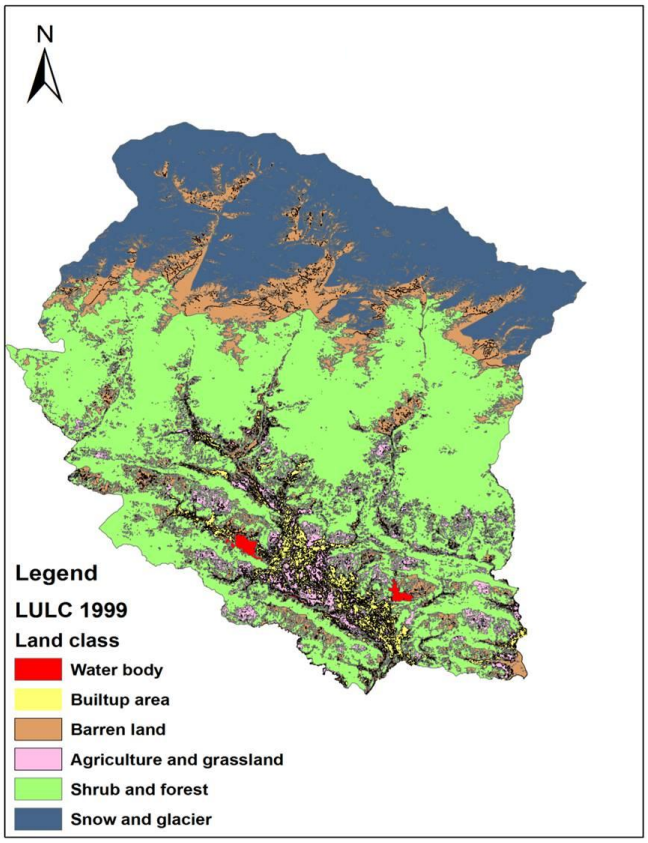

Figure 8, LULC of Kaski in 1999

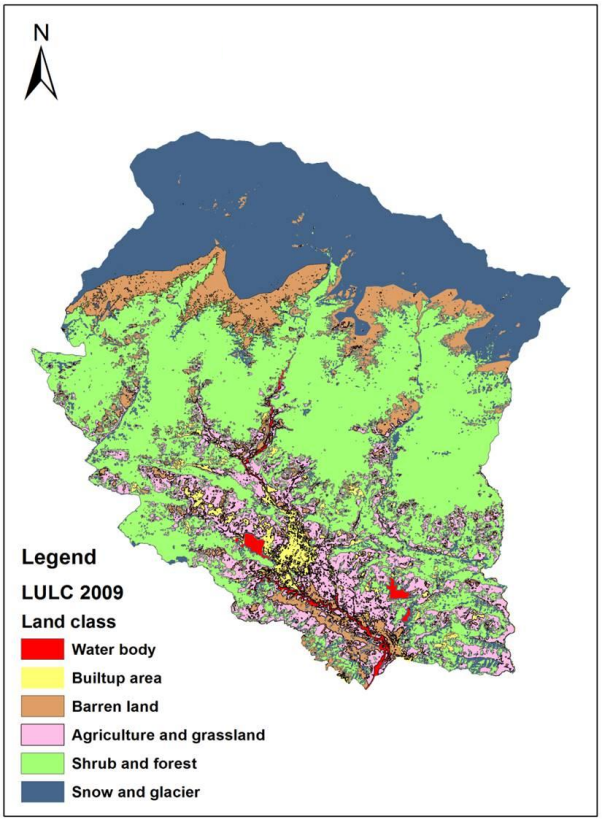

Figure 9, LULC of Kaski in 2009

Agricultural land is most vulnerable to such Riverine hazards, including some settlements located on unstable or flood-prone terrain. Such events are eventually responsible changing landforms and land patterns (Rimal et al., 2015).

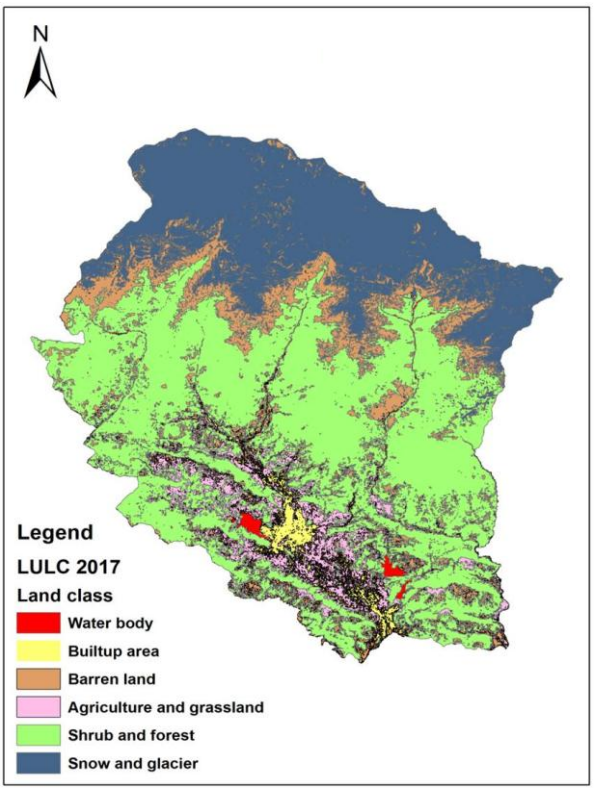

Figure 10, LULC of Kaski in 2017

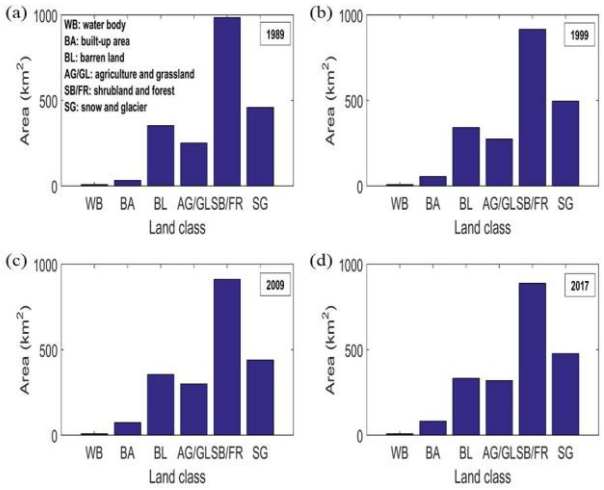

Figure 11, Area covered by each land class between the period of 1989-2017 (a) In 1989, (b) In 1999, (c) In 2009 and (d) In 2017

Furthermore, the interaction between the Seti River and surrounding landforms reveals the fragile geomorphic stability of the region. Continuous erosion, sediment deposition, and channel shifting have altered the landscape and affected local livelihoods, underscoring the need for integrated river basin management and sustainable land use planning in Kaski district. In particular: (a) The overall tendency towards a reduction in sinuosity in sections D, H, and J may be associated with increased straightening of the channel, which may lead to higher flow velocities and flood risk

downstream. (b) The bank shifts, especially the 42.7 m bank shift at Section F (1999–2009) may indicate the presence of some level of channel instability with the potential danger to nearby agricultural and built-up areas in the valley. (c) A very slight increase in water body size may point to channel widening. (d) The nearly doubled built-up area (32.44 km^2 to 80.98 km^2) will further increase people's exposure to flood risk. (e) The reduction in shrubs and forests will reduce the amount of interception and will make more land available for erosion and surface runoff. (f) The small net increase in the amount of snow and glaciers on the territory of the river is locally unusual when compared to global trends; it is explained by the inter-decadal fluctuations in snow cover mapping using Landsat satellite images, not by any proven glacier expansion.

Conclusion

This study employed GIS and remote sensing techniques to evaluate decadal changes in river morphology and land use/land cover (LULC) in the Seti River corridor, Kaski District, Nepal, from 1989 to 2017. The results demonstrate the effectiveness of geospatial technologies for long-term environmental monitoring and provide valuable insights into the interactions between river dynamics and landscape transformation.

The LULC analysis revealed significant changes over the study period. Shrubland and forest cover declined from 47.17% in 1989 to 42.17% in 2017, indicating continued land cover transformation. In contrast, built-up areas expanded markedly from 32.44 km^2 to 80.98 km^2, reflecting rapid urbanization and infrastructure development. Agricultural land also increased gradually, suggesting continued cultivation expansion. Snow and glacier cover showed interdecadal fluctuations with a slight overall increase; however, this trend should be interpreted cautiously because Landsat-based snow classification is influenced by seasonal variation and classification uncertainty.

Morphological analysis indicated that the Seti River largely maintained its meandering planform, although localized channel adjustments were evident. Reduced sinuosity at Sections D, H, and J indicates channel straightening, while spatial variations in bank migration highlight the river's dynamic nature. The maximum bank shift of 42.7 m occurred at Section F during 1999–2009, demonstrating active lateral migration. An increase in water surface area further suggests localized channel widening associated with erosion, sediment redistribution, and flood processes. Overall, the study highlights increasing human influence through declining shrubland and forest cover and expanding built-up and agricultural areas, while confirming that the Seti River remains geomorphologically active. These findings provide valuable baseline information for sustainable land use planning, river corridor management, flood hazard mitigation, and environmental conservation in the rapidly developing Seti River basin and other Himalayan river systems.

Article Note

This article is a full-length paper developed from **Extended Abstract #211**, entitled "**Spatio-Temporal Changes in River Dynamics and Land Cover Along the Seti River Floodplain, Kaski District, Nepal (1989–2017)**", which was presented at the 15th Asian Regional Conference of the International Association for Engineering Geology and the Environment (ARC-15 of IAEG), held in Kathmandu, Nepal, from 27 to 29 November 2025.

Reference

AEPC. (2017). Alternative Energy Promotion Centre. Available at: http://aepc.gov.np/

Barnsley, M. (1999). Digital remotely-sensed data and their characteristics. In Geographical Information Systems (Vol. 1, pp. 451–466). Available at: https://www.geos.ed.ac.uk/~gisteac/gis_book_abridged/files/ch32.pdf

Burrough, P. A. and McDonnell, R. A. (1998). Principles of Geographical Information Systems. Oxford University Press, Oxford, 333p.

Deng, J. S., Wang, K., Hong, Y., and Qi, J. G. (2009). Spatio-temporal dynamics and evolution of land use change and landscape pattern in response to rapid urbanization. Landscape and Urban Planning, 92(3), 187–198. https://doi.org/10.1016/j.landurbplan.2009.05.001

Dufour, S., Rinaldi, M., Piégay, H., and Michalon, A. (2015). How do river dynamics and human influences affect the landscape pattern of fluvial corridors? Lessons from the Magra River, Central-Northern Italy. Landscape and Urban Planning, 134, 107–118. https://doi.org/10.1016/j.landurbplan.2014.10.007

Ebisemiju, F. S. (1994). The sinuosity of alluvial river channels in the seasonally wet tropical environment: Case study of River Elemi, southwestern Nigeria. Catena, 21(1), 13–25. https://doi.org/10.1016/0341-8162(94)90028-0

Govaerts, B., and Verhulst, N. (2010). The normalized difference vegetation index (NDVI) GreenSeeker™ handheld sensor: Toward the integrated evaluation of crop management. Part A—Concepts and case studies. Available at: https://www.nue.okstate.edu/GreenSeeker/NDVI-PartA-mayo.pdf

Hassan, Z., Shabbir, R., Ahmad, S. S., Malik, A. H., Aziz, N., Butt, A., and Erum, S. (2016). Dynamics of land use and land cover change (LULCC) using geospatial techniques: A case study of Islamabad, Pakistan. SpringerPlus, 5(1), 1–11. Available at:

https://link.springer.com/article/10.1186/s40064-016-2414-z

Hazarika, N., Das, A. K., and Borah, S. B. (2015). Assessing land-use changes driven by river dynamics in chronically flood-affected Upper Brahmaputra plains, India, using RS-GIS techniques. The Egyptian Journal of Remote Sensing and Space Science, 18(1), 107–118. https://doi.org/10.1016/j.ejrs.2015.02.001

HIMALDOC. (2017). Retrieved September 3, 2017, from http://lib.icimod.org/Kalliola, R., and Puhakka, M. (1988). River dynamics and vegetation mosaicism: A case study of the River Kamajohka, northernmost Finland. Journal of Biogeography, 703–719. https://doi.org/10.2307/2845334

Klöcking, B., and Haberlandt, U. (2002). Impact of land use changes on water dynamics: A case study in temperate meso- and macroscale river basins. Physics and Chemistry of the Earth, Parts A/B/C, 27(9), 619–629. https://doi.org/10.1016/S1474-7065(02)00046-3

Lambin, E. F., Geist, H. J., and Lepers, E. (2003). Dynamics of land-use and land-cover change in tropical regions. Annual Review of Environment and Resources, 28(1), 205–241. https://doi.org/10.1146/annurev.energy.28.050302.105459

Matheussen, B., Kirschbaum, R. L., Goodman, I. A., O'Donnell, G. M., and Lettenmaier, D. P. (2000). Effects of land cover change on streamflow in the interior Columbia River Basin (USA and Canada). Hydrological Processes, 14(5), 867–885. https://doi.org/10.1002/(SICI)1099-1085(20000415)14:5%3C867::AID-HYP975%3E3.0.CO;2-5

McFeeters, S. K. (1996). The use of the Normalized Difference Water Index (NDWI) in the delineation of open water features. International Journal of Remote Sensing, 17(7), 1425–1432. https://doi.org/10.1080/01431169608948714

Mohan, M., Pathan, S. K., Narendrareddy, K., Kandya, A., and Pandey, S. (2011). Dynamics of urbanization and its impact on land-use/land-cover: A case study of megacity Delhi. Journal of Environmental Protection, 2(9), 1274–1283. https://doi.org/10.4236/jep.2011.29147

Müller, N. (1996). River dynamics and floodplain vegetation and their alterations due to human impact. River Systems, 9(3-4), 477-512. https://doi.org/10.1127/lr/9/1996/477

Petchprayoon, P., Blanken, P. D., Ekkawatpanit, C. and Hussein, K. (2010). Hydrological impacts of land use/land cover change in a large river basin in central–northern Thailand. International Journal of Climatology, 30(13), 1917-1930. https://doi.org/10.1002/joc.2131

Riggs, G. A., Hall, D. K., and Salomonson, V. V. (1994). A snow index for the Landsat thematic mapper and Moderate Resolution Imaging Spectroradiometer. In Geoscience and Remote Sensing Symposium, 1994. IGARSS '94. Surface and Atmospheric Remote Sensing: Technologies, Data Analysis and Interpretation (Vol. 4, pp. 1942–1944). https://doi.org/10.1109/IGARSS.1994.399618

Rimal, B., Baral, H., Stork, N. E., Paudyal, K. and Rijal, S. (2015). Growing city and rapid land use transition: Assessing multiple hazards and risks in the Pokhara Valley, Nepal. Land, 4(4), 957-978. https://doi.org/10.3390/land4040957

Rouse, H. (1937). Modern conceptions of the mechanics of fluid turbulence. Transactions of the American Society of Civil Engineers, 102, 463-543. https://doi.org/10.1061/TACEAT.0004872

Shrestha, P. (2010). Climate change impact on river dynamics of the Bagmati Basin, Kathmandu, Nepal. Report submitted to the National Adaptation Programme of Action (NAPA) to Climate Change Project, Government of Nepal.

Smith, C. E. (1998). Modeling high sinuosity meanders in a small flume. Geomorphology, 25(1), 19–30. https://doi.org/10.1016/S0169-555X(98)00029-4

Walker, R., and Homma, A. K. O. (1996). Land use and land cover dynamics in the Brazilian Amazon: An overview. Ecological Economics, 18(1), 67–80. https://doi.org/10.1016/0921-8009(96)00033-X

Wang, J., Rich, P. M., Price, K. P., and Kettle, W. D. (2005). Relations between NDVI, grassland production, and crop yield in the central Great Plains. Geocarto International, 20(3), 5–11. https://doi.org/10.1080/10106040508542350

Wu, W. (2010). Computational river dynamics. CRC Press. 509p.

Xiao, J., Shen, Y., Ge, J., Tateishi, R., Tang, C., Liang, Y., and Huang, Z. (2006). Evaluating urban expansion and land use change in Shijiazhuang, China, by using GIS and remote sensing. Landscape and Urban Planning, 75(1), 69–80. https://doi.org/10.1016/j.landurbplan.2004.12.005

Yang, A. Y., Wright, J., Ma, Y., and Sastry, S. S. (2008). Unsupervised segmentation of natural images via lossy data compression. Computer Vision and Image Understanding, 110(2), 212–225. Available at: https://people.eecs.berkeley.edu/~sastry/pubs/Pdfs%20of%202008/YangUnsupervised2008.pdf

Zewdu, S., Suryabhagavan, K. V., and Balakrishnan, M. (2016). Land-use/land-cover dynamics in Sego Irrigation Farm, southern Ethiopia: A comparison of temporal soil salinization using geospatial tools. Journal of the Saudi Society of Agricultural Sciences, 15(1), 91–97. https://doi.org/10.1016/j.jssas.2014.03.001

Asian Journal of Engineering Geology, 2025, Vol. 2 No. 2, 29-40

Research Article DOI: https://doi.org/10.64862/ajeg.2025.202.04.301 Open Access

SWAT-Based Hydrological Modeling and Water Balance Dynamics of West Rapti River Basin, Nepal

Rabindra Bahadur Thapa[1], Kumud Raj Kafle[2*] and Kundan Lal Shrestha[3]

[1]Department of Water Resources and Irrigation, Jawalakhel, Lalitpur, Nepal
[2]Department of Environmental Science and Engineering, Kathmandu University, Dhulikhel, Nepal
[3]Department of Chemical Engineering, Kathmandu University, Dhulikhel, Nepal

([*]Corresponding E-mail: krkafle@ku.edu.np)

Received: June 04, 2025, Accepted: December 15, 2025

Abstract: This study simulated the hydrological and sediment dynamics of Nepal's West Rapti River Basin (WRB) using the Soil and Water Assessment Tool (SWAT) to quantify water balance components and sediment yield. The model integrated a 30 m resolution digital elevation model (DEM), soil maps, and land use data, delineating the basin into 21 sub-basins and 180 hydrological response units (HRUs). Sensitivity analysis identified the curve number (CN2), baseflow recession coefficient (ALFA_BF), and surface runoff lag time (SURLAG) as the most influential hydrological parameters. The SWAT model was calibrated (2003–2011) and validated (2012–2020) using observed discharge at Jalkundi station. The model showed strong performance, with coefficient of determination (R^2) values of 0.95 and 0.91 and Nash–Sutcliffe efficiency (NSE) values of 0.76 and 0.75 during calibration and validation, respectively. Percent bias (PBIAS) ranged from −7.7% to −13.5%, indicating slight overestimation of baseflow. Sediment simulation achieved R^2 and NSE values of approximately 0.60, representing satisfactory performance. Long-term simulation (2000–2022) estimated a mean annual precipitation of 1,676 mm, with about 55% contributing to streamflow, resulting in an average annual water yield of 951 mm, while 42% was lost through evapotranspiration. Surface runoff averaged 573 mm yr^{-1} and peaked during the monsoon season. Mean annual sediment yield was 166 t ha^{-1} yr^{-1}, varying from 15.68 to 468.05 t ha^{-1} yr^{-1} across sub-basins. Sub-basin 8 recorded the highest sediment yield because of steep slopes (>40%) and erosive land use. Approximately 68% of annual streamflow and 85% of sediment yield occurred during the monsoon (June–September). These findings demonstrate the capability of the SWAT model to support watershed management, sediment control, and sustainable water resource planning in the WRB.

Keywords*: Hydrology, SWAT, Water balance, Model performance, Model calibration, Model validation*.

Introduction

River basins are key ecosystems for the sustenance of human civilization by providing basic resources to millions of people, among them indigenous ethnic minorities who directly depend on these ecosystems for their livelihood (Bohara et al., 2025). A river basin can be understood as the whole surface area drained by a river and its feeders, sustaining both ecosystems and human populations, with an accentuation on indigenous communities within its benefits. Hydrologically, river basins play the most crucial role in regulating water availability for agriculture and infrastructure (Basnet et al, 2024). The pressure on water resources, accompanied by changes in the hydrological cycle and degradation of basin ecosystems due to rapid development and population increase, was articulated by the UN in 2016. Inappropriate land use, deforestation activities, and climatic variations have disturbed natural dynamics related to water balance components both at upstream and downstream areas (Moges and Bhat, 2020). Precipitation partitioning into surface runoff, evapotranspiration, and groundwater recharge defines the hydrological resilience of a basin since it takes place within it. Anthropogenic activities like building dams and diverting rivers, which change flow regimes, call for strong hydrological modeling to assess such impacts (Owens, 2020; de Oliveira Serrão et al., 2022).

Hydrological simulation, together with the analysis of the water balance, forms the core element in sensitivity studies of the impacts of land use and climate variability on water resources within river basins (Nepal et al., 2024; Thapa et al., 2005). Changes in infiltration, surface runoff, and recharge of groundwater induced by urbanization or intensified agriculture directly control hydrological response at the basin scale (Ren et al., 2021). Accurate quantification of these dynamics is a prerequisite for modeling approaches applicable to simulate fluxes and storage variations involved in available water resource management. Possible imbalances caused by altered precipitation patterns or increased irrigation demand will also challenge the existing components' water security (Vercruysse et al., 2017). An assessment that would fully document the hydrological processes that take place in streamflow variation and seasonal water budgets (Van Oost et al., 2002).

Combining physical hydrological models with geospatial data has made a comprehensive understanding of the impact catchment-scale transformations, such as afforestation or urbanization, have on water cycling and nutrient transport possible (Schweizer et al., 2018; Pant et al., 2025). Land Use Change simulation or climate projections provide

potential impacts on river discharge and groundwater recharge as well as ecosystem stability, for scientifically informed policy decisions. Advancements in the Geographic Information System and hydrological modeling brought dramatic improvements to water balance evaluations through accurate simulations of complex hydrological processes (Liu and Jiang, 2019; Bishwakarma et al., 2024). The Soil and Water Assessment (SWAT) model is known to be one of the best physically based models used for simulating surface and subsurface runoff generation mechanisms with accompanying soil moisture variations and actual evapotranspiration components at various spatial and temporal scales (Ayele et al., 2021; Bekele and Abate, 2020; Subedi et al.,2024). By using climate data, land-use maps, and soil features as input, SWAT provides reliable predictions of water resources in ungauged basins to support the assessment of management options, for example, the optimization of irrigation or afforestation (Toma et al., 2023). As observed by Rahman et al. (2024) and Sinha et al. (2019), remote sensing is also found to contribute towards these through providing spatial detail information on precipitation and evapotranspiration that goes into better model performance, and also real-time tracking of hydrological changes at the basin scale. When used together with climate and land use scenarios, SWAT has been found effective in making forecasts of future vulnerabilities in water resources, thus informing adaptive management strategies in regions highly pressured climatically, such as those identified by Chilagane et al. (2021) and Li et al. (2022).

In the West Rapti River Basin, climate projections for South Asia indicate erratic monsoon and rising temperatures, posing significant threats to streamflow trend, intensifying drought risks, and reducing groundwater recharge (Shi et al., 2018). These challenges are further compounded by unsustainable practices such as deforestation and inefficient irrigation, which accelerate soil erosion and diminish the basin's capacity to retain water (Van Oost et al., 2002; Vercruysse et al., 2017). However, the localized hydrological effects of these combined climatic and human-induced pressures remain insufficiently quantified, limiting the effectiveness of targeted mitigation strategies. To address these gaps, this study utilizes the SWAT model to: (1) establish a baseline assessment of the basin's hydrological dynamics, including runoff, evapotranspiration, water yield, sediment yield, and groundwater recharge, and (2) analyze the basin's response to projected climate change scenarios. Establishing a baseline is crucial for identifying existing stressors, such as erosion-prone areas or inefficiencies in water allocation, while climate simulations (IPCC scenarios) will provide insights into shifts in streamflow seasonality, flood frequency, and aquifer behavior.

Methodology and materials

Description of the study area

The West Rapti River Basin is situated in the southwestern part of Nepal in Lumbini Province. It covers an area of approximately 6,380 km^2. Geographically, the basin extends between 27°45'10" N to 28°35'35" N and 81°40'10" E to 83°10'55" E. The length of the main river is 260 km from its origin to the basin outlet (Figure 1). The West Rapti River originates from the middle mountains region of Nepal and flows southward through rugged highlands into the lowlands, eventually draining into the Ghagra River in India. Jhimruk and Madi Rivers are two major tributaries of the west Rapti. Rainfall and groundwater are the primary contributors to its flow. The basin is characterized by its diverse topography, with elevations ranging from 70 m to 3,609 m above sea level (asl). The upstream portion of the basin exhibits a temperate climate, while the lower areas experience a tropical climate. The south region of the basin, primarily below 500 masl, consists of lowlands and accounts for approximately 34% of the total basin area. Geographically, the basin is wide in its headwaters and narrows toward the lower reaches. This has caused distinct variation in landscape and climate. The average annual precipitation for the basin is 1500 mm (Figure 2).

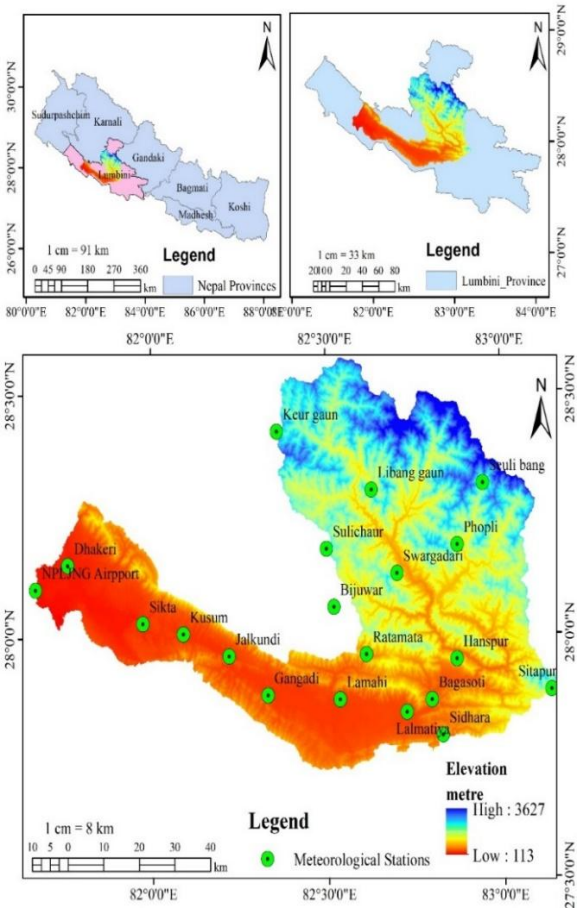

Figure 1, Map showing the study area of the Rapti River basin

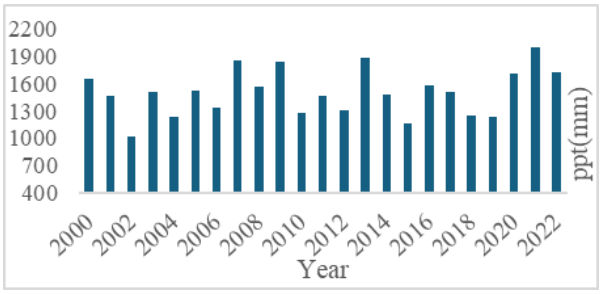

Figure 2, Average annual precipitation trend of the West Rapti River Basin

Data used

Different types of data are required to simulate the river basin hydrology using SWAT model. In this study, Digital Elevation Model (DEM), Land use/land cover, and Soil map are used as spatial data, the meteorological data, such as temperature and precipitation, have been used for this study. The Hargreaves method was used for the estimation of potential evapotranspiration (PET). Flow and sediment data obtained from the DHM Nepal are also used during the process of model calibration and validation.

Table 1, Sources of data used

S.N.	Data	Source	Type
1	DEM	ASTERGDEM website (https://gdemdl.aster.jspacesystems.or.jp/index_en.html)	Spatial grid
2	Soil Map	FAO (https://www.fao.org/soils-portal/data-hub/soil-maps-and-databases/harmonized-world-soil-database-v20/en/)	Spatial grid
3	LULC Map	ICIMOD (https://rds.icimod.org/DatasetMasters/Download/1972729)	Spatial grid
4	Precipitation and Temperature	Department of Hydrology and Meteorology, Nepal	Time series
5	River Flow and Sediment	Department of Hydrology and Meteorology, Nepal	Time series

Spatial data

Digital elevation model (DEM)

The DEM of 30-meter resolution was downloaded from the ASTER Global Digital Elevation Model website (Bhatta et al., 2019). The analysis of DEM shows that the elevation of the basin extends from 113 m to 3627 masl. The ASTER GDEM has good vertical accuracy for the root mean square error (RMSE) of 24 meters in Indian and Nepalese regions (Thomas et al., 2014). ASTER DEM could meet the demand in India and Nepal because it is accurate, easily obtainable, and suitable for the complex territorial structure of the Himalayas. With a resolution of 30 meters and a high level of vertical accuracy, ASTER DEM is capable of providing detailed information on the elevation, especially in regions with mountainous terrain, compared to other datasets such as SRTM (Thomas et al., 2014). This data set provides accurate topography information, which makes it useful in hydrology, sediment research, and disaster management. Free and easily accessible, ASTER DEM is a viable and cheaper option as compared to LiDAR data, for instance, making it easily accessible to researchers and policy makers in India and Nepal for applications in flood modeling, watershed management, and sustainable development (Shinde et al., 2013). These features make it a crucial application in environmental as well as scientific research in these areas. Further, the slope map was also derived from the DEM. During HRU analysis, multiple slope classes were designated as 0-5%, 5-15%, 15-25%, 25-40%, and more than 40%.

Land use land cover map

Land use/ land cover data in this study have been taken from the Forest Research Training Centre (FRTC) Nepal, with 30 m resolution (FRTC, 2022). The total LULC class classes were 8 among which the highest and lowest area covered by forest (69.61%) and barren land (0.001%) as shown in Figure 3.

Table 2, Land use land cover (LULC) data

SN	LULC type	Area %
1	Water	0.450
2	Forest	63.658
3	Riverbed	1.704
4	Built-up	0.220
5	Cropland	23.018
6	Barren	0.001
7	Rangeland	5.002
8	Woodland	5.947

Soil map

Soil map, along with soil data properties, was cited from the Food and Agriculture Organization (FAO). HWSD (Harmonized world soil data) was applied for soil properties classification (FAO, 2002). The map originally obtained in vector form was rasterized with pixel matching that of the DEM, i.e., 30 m resolution. Soil map of the basin has 4 soil types viz., I-Bh-U-c (lithic/rock debris), Bd34-2bc (stony), Rd30-2d, and Je75-2a, and as shown in Figure 3 and Table 3.

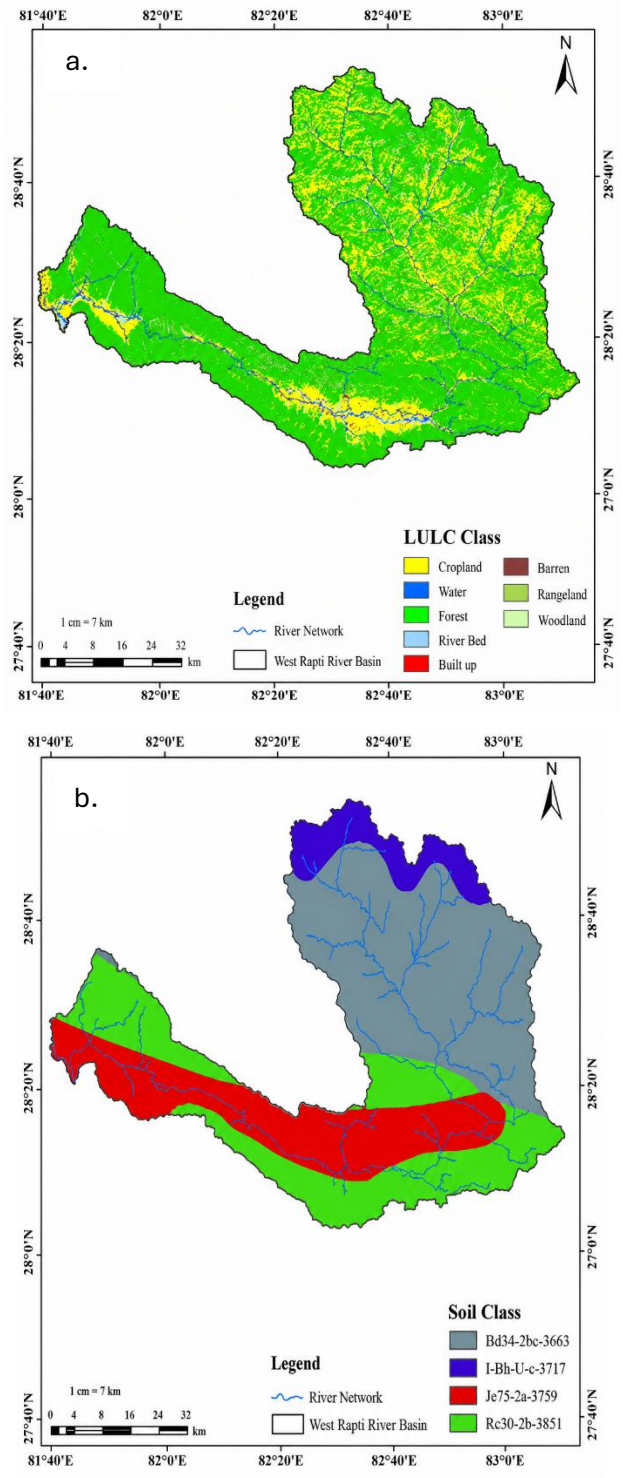

Figure 3, a. Land use land cover map and b. FAO soil map

Hydro-meteorological data

The daily observed meteorological data (maximum and minimum temperature, and average precipitation) for the basin were acquired from the Department of Hydrology and Meteorology (DHM) for 13 spatially distributed stations within the basin, covering the period from 2000 to 2022. Missing precipitation data were estimated using the Arithmetic Mean Method (Abdullah and Al-Ansari, 2022). Additionally, the simulation algorithm in the SWAT model was employed to derive the data for relative humidity, solar radiation, and wind speed across the river basin. The availability of high-resolution meteorological data is essential for accurately simulating hydrological processes such as runoff generation and water yield (Srivastava et al., 2020).

Table 3, FAO soil data

SN	Soil type	Area%
1	I-Bh-U-c	7.424
2	Bd34-2bc	42.020
3	Rd30-2b	26.994
4	Je75-2a	23.562

Observed monthly discharge data at Jalkundi station, which lies in sub-basin 18 as per the watershed delineation, was obtained from DHM for 2000 to 2022 to process flow calibration and validation of the model. Similarly, the monthly sediment concentration data for the Jalkundi station were obtained from the DHM for the calibration and validation of sediment in the model.

The Department of Hydrology and Meteorology provided historical sediment concentration data for the discharge measuring station Jalkundi (Station ID 360) since the most recent time series sediment for the river could not be located. Data on sediment concentration are dispersed. The 1985–1989 data is available. Using the available sediment load and outflow data from Jalkundi Station (Station 360), a sediment rating curve was created, and the sediment load, expressed in tonnes per day, was estimated. The developed rating curve, represented by a power equation, is given as S (tonnes/day) = 2.7081 × $Q^{1.5557}$, where S denotes the sediment load, and Q represents the daily discharge in cubic meters per second (m^3/s). The equation exhibited a correlation coefficient (R^2) of 0.65, indicating a moderate relationship between discharge and sediment load (Figure 4).

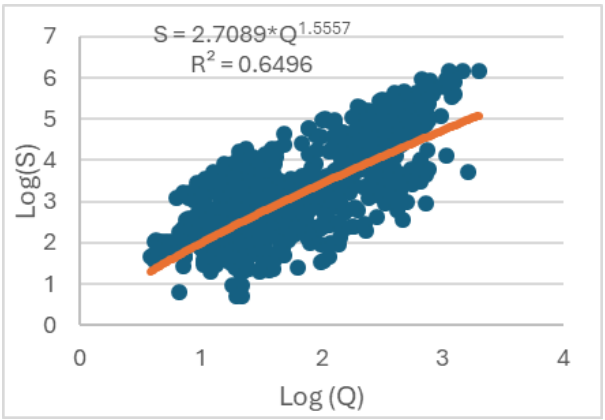

Figure 4, Sediment Rating Curve

Using the finalized sediment discharge rating equation, the sediment load (tonnes per day) was estimated. A daily data series was then generated, from which monthly sediment data were derived. This

dataset was subsequently utilized for the calibration and validation of the SWAT model.

Hydrological modeling of the west Rapti river basin

The SWAT model (Figure 5) was used for hydrological modeling of the West Rapti River basin (Figure 6). It is a semi-distributed, process-oriented, continuous-time watershed model created by the USDA to evaluate how different management strategies affect nonpoint source pollution and water resources in extensive catchment areas (Toma et al., 2023). The SWAT model deals with major components such as hydrology, vegetation growth, reservoir dynamics, land use management, pesticide behavior, and sediment transport in a river basin. The hydrological cycle of SWAT is governed by the following water balance equation (Arnold et al, 1998):

$$SWt = SW0 + \sum_{i=1}^{n}(Rday - Qsurf - Ea - Wseep - Qgw) \quad (1)$$

Where *SWt*: soil water content at time step t, *SW0*: initial soil water content, *Rday*: daily precipitation, *Qsurf*: runoff, *Ea*: evapotranspiration, *Wseep*: percolation and *Qgw*: groundwater flow.

Watershed delineation, HRU analysis, model set-up, and run

The SWAT initially delineates the watershed and further subdivides it into smaller sub-basins based on a predefined area threshold determined during model setup. The selection of this threshold is a subjective but critical process, as it directly influences model performance, computational efficiency, and spatial resolution (Pandey et al., 2019). A smaller threshold results in a greater number of sub-basins, improving spatial detail but substantially increasing computational demands. In this study, an area threshold of 15,000 hectares was applied (Chinnasamy and Sood, 2020), leading to the classification of the watershed into 21 sub-basins.

Subsequently, HRUs were defined by applying a 10% threshold for LULC, soil type, and slope, ensuring the retention of dominant hydrological characteristics while filtering out less significant spatial variations (Becker and Braun, 1999). This approach resulted in the generation of 180 unique HRUs, each representing a distinct combination of these three physiographic factors. The accurate delineation of sub-basins and HRUs is crucial for capturing spatial heterogeneity in hydrological processes, thereby enhancing the reliability of SWAT-based simulations.

The SWAT model was configured to simulate hydrological processes for the period 2000–2022, with the initial three years (2000–2002) designated as a warm-up period. This warm-up phase is essential for stabilizing key hydrological parameters such as soil water storage, groundwater levels, and aquifer recharge before generating model outputs.

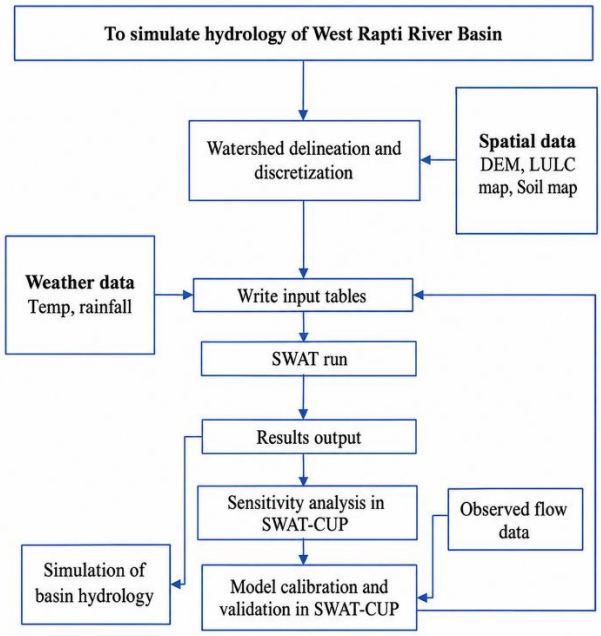

Figure 5, Workflow of research

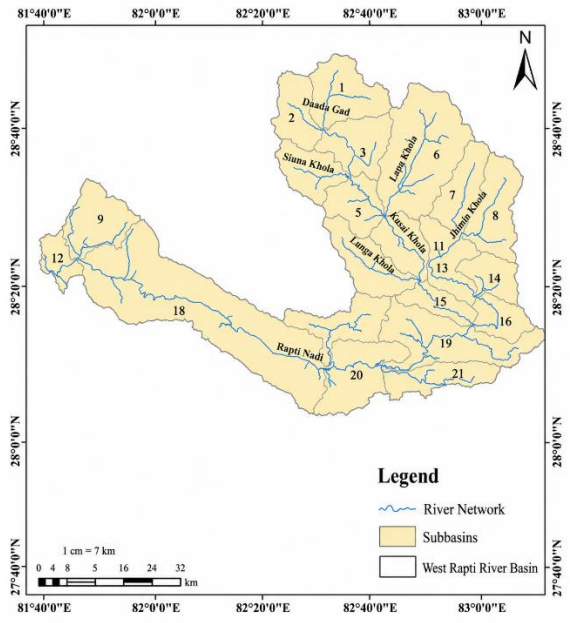

Figure 6, Sub-basins of the West Rapti River Basin

The inclusion of a warm-up period ensures that the model reaches a quasi-steady state, thereby minimizing initialization biases and improving the accuracy of subsequent hydrological simulations. Research by SWAT developers, including Douglas-Mankin et al. (2010), suggests that an optimal warm-up period typically ranges between one and three years, depending on the availability of input data and the complexity of the watershed. Given the availability of long-term observational data, this study adopted a three-year warm-up period (2000–2002) to enhance model reliability. Following this initialization stage, the model was calibrated for the years 2003–2011 and then validated for the years 2012–2020 using data on observed river discharges to evaluate its performance. Similarly, as there is observable sediment data up to

2015, the sediment was calibrated for 2003–2008 and validated for 2008–2014. By adjusting parameters to reflect observed hydrological responses, calibration and validation enhance the model's prediction power, making them essential phases in hydrological modeling.

Sensitivity analysis and model performance evaluation

The SWAT Calibration and Uncertainty Program (SWAT-CUP), a widely recognized tool for SWAT model calibration, was applied to adjust model parameters (Arnold et al., 2012). SWAT-CUP is extensively employed in hydrological research for model calibration, sensitivity analysis, and uncertainty analysis. In this study, the Sequential Uncertainty Fitting (SUFI-2) algorithm was applied to assess model uncertainty and optimize parameterization. The built-in Global Sensitivity Analysis tool in SWAT-CUP was employed for parameter sensitivity assessment and optimization. Global sensitivity analysis evaluates the collective impact of multiple parameters through multiple regression analysis. The degree of parameter sensitivity varied depending on watershed characteristics, model structure, hydrological state variables, and the spatial and temporal resolution of input data. The sensitivity analysis results were crucial in refining model calibration by optimizing parameter values to align with local hydrological conditions, thereby minimizing computational complexity and prediction uncertainty. Additionally, this process facilitated the evaluation of parameter interactions, range constraints, and spatial heterogeneity, contributing to improved model accuracy.

Initially, 23 parameters were shortlisted based on an extensive literature review, and the model simulation was executed for 400 iterations. From this analysis, the 11 most sensitive parameters were selected using statistical significance criteria, including p-values and t-test rankings. These parameters were then subjected to an additional 500 simulation runs with updated values for further refinement. Similarly, 18 sediment-sensitive parameters were studied to determine calibration and validation of sediment concentration in the model.

To evaluate model performance, two statistical indicators were employed: the coefficient of determination (R^2) and the Nash–Sutcliffe Efficiency (NSE). According to Moriasi et al. (2007), an R^2 value greater than 0.5 is generally considered acceptable, while an NSE value exceeding 0.5 indicates satisfactory model performance. These metrics provided quantitative validation of the model's predictive capability in simulating hydrological processes. The R^2 quantifies the proportion of variance in observed data that is explained by the model. The R^2 equation is given below in equation 2 (Michael and Jain, 2013):

$$R^2 = \frac{[\sum_{i=1}^{m}(q_{si}-\overline{q_s})(q_{oi}-\overline{q_o})]^2}{\sum_{i=1}^{m}(q_{si}-\overline{q_s})^2 \sum_{i=1}^{m}(q_{oi}-\overline{q_o})^2} \quad (2)$$

Where:

R^2 is the coefficient of determination, q_{si} is simulated flow, q_{oi} is observed flow, $\overline{q_s}$ and $\overline{q_o}$ are the average simulated and observed flow, respectively.

Similarly, the NSE quantifies the proportion of variance in observed data that is captured by the model, relative to the residual variance. The value of NSE can range from -∞ to 1.0, where values indicate poor model performance, and a value of 1 represents a perfect match between simulated and observed data. The NSE equation 3 (Nash and Sutcliffe, 1970) is given below:

$$NS = \frac{v_0 N - \sum_{i=1}^{m}(x_i-y_i)^2}{v_0 N} = 1 - \frac{\sum_{i=1}^{m}(x_i-y_i)^2}{\sum_{i=1}^{m}(x_i-\bar{x})^2} \quad (3)$$

Where the variance of the observed values is represented as v_0, m is the total number of data points to be analyzed, x_i is the observed value, y_i is the corresponding simulated value, and $\bar{x}$ is the average observed value for the study period.

Results and discussion

Model performance

The SWAT model was calibrated and validated for a monthly time scale in SWAT-SUFI2. Global sensitivity analysis prioritized sensitive parameters for flow as shown in Table 4. Table 4 presents the relative ranking of model parameters based on the student's t-stat and p-value. The ranking was assigned by prioritizing parameters with the highest absolute t-statistic, indicating greater sensitivity, and the lowest p-value, signifying higher statistical significance. The parameter exhibiting the largest t-statistic and the smallest p-value was designated as rank 1, reflecting its dominant influence on the model's performance, as shown in Table 4. The model parameter CN2 was a relatively more significant model parameter with a lower p-value at the catchment scale. The model parameter t-stat varied from -0.26 to 0.36. The outcome of the study identified that CN2 as most sensitive among 11 model parameters. Another sensitive parameter was base flow alpha factor (ALFA_BF) and Surface Runoff time lag (SURLAG).

Both R^2 and NSE were utilized to assess the SWAT model's performance in simulating flow during calibration and validation for the basin. The R^2 value, which ranges from 0 to 1, indicates the extent to which the model explains data variance. A value of 0 signifies no explanatory power, whereas a value of 1 represents a perfect fit (Arnold et al., 2012). Therefore, a higher R^2 value, approaching 1, implies a better model fit. According to Michael and Jain (2013), a model is considered to perform well if its indicator values exceed 0.5. NSE is a widely used metric in hydrological modeling to assess a model's ability to replicate observed data. According to Arnold et al. (2012), an NSE value greater than 0.75 indicates excellent performance, values between 0.36 and 0.75 suggest

satisfactory performance, and values below 0.36 reflect unsatisfactory performance. In this study, the R^2 and NSE values for calibration and validation in ARB and TRB remained above 0.75, signifying overall excellent model performance for monthly simulations.

The R^2 value for monthly flow during the calibration period was obtained as 0.95, accompanied by an NSE of 0.76, suggesting satisfactory model performance. However, during the validation period, the R^2 and NSE values dipped to 0.91 and 0.75, respectively. For flow calibration and validation in the basin, the model demonstrated excellent performance, with R^2 and NSE values consistently exceeding 0.75. The Figure 8 below shows the best fitted curves of flow out at sub-basin 18, i.e., Jalkundi station, during the calibration and validation period (Figure 7). The model simulated the flow pattern very well, and the hydrographs are in good agreement with the rainfall pattern. The scatter plot between observed flow and simulated flow also suggested that the model overestimated the base flow and underestimated the peak flows (Figure 8). Similar model performance is also evaluated for the SWAT model in Seti Gandaki Basin by KC et al. (2023), West Rapti Basin by Neupane and Pandey (2021), and Rapti River Basin by Kumari et al. (2024).

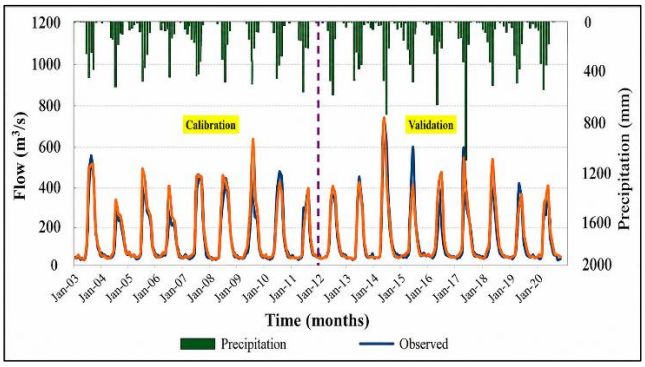

Figure 7, Calibration and validation curve

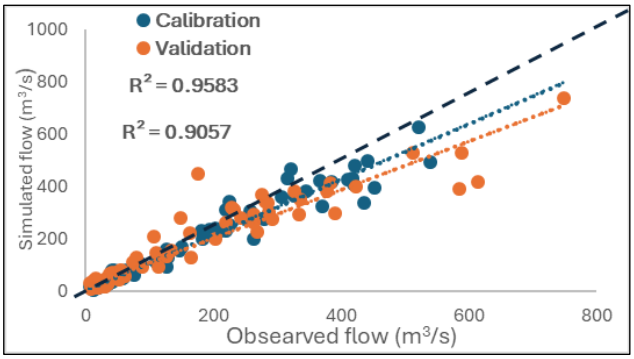

Figure 8, Scatter plot correlation

Table 4, Sensitive parameters for flow

Parameter	Description	Range	Fitting value	p-value	t-stat	Rank
R_CN2	Initial SCS runoff curve	67 to 90	68.72	0.72	0.36	1
R_ALFA_BF	Base flow alpha factor (days)	0.024 to 0.072	0.03	0.79	-0.26	2
A_SURLAG	Surface Runoff time lag (days)	0.05 to 24	23.40	0.80	0.24	3
R_SOL_AWC	Available Water Capacity (mm H2O/ mm soil)	0.0 to 1.0	0.675	0.84	-0.20	4
V_GWQMN	Threshold depth of water in the shallow aquifer required to start the return flow (mm H2 O)	0 to 2000	1450	0.93	0.08	5
V_LAT_TTIME	Lateral flow travel time (in days)	0 to 180	31.5	0.94	0.07	6
V_OV_N	Manning's "n" value for overflow flow	0.01 to 0.41	0.30	0.95	0.05	7
vV_SOL_Z	Depth from soil surface to bottom of layer (mm)	0 to 3500	3237.5	0.96	0.048	8
V_CH_K2	Effective hydraulic conductivity in main channel alluvium	0 to 150	71.25	0.97	0.043	9
V_GW_DELAY	Groundwater delay (days)	0 to 500	387.5	0.98	-0.022	10
R_CH_N2	Manning's "n" value for the main channel	0.01 to 0.3	0.0462	0.99	-0.012	11

Again, the calibration and validation for sediment involved the sensitive parameters as follows. Using the finalized sediment discharge rating equation, the sediment load (tonnes per day) was estimated. A daily data series was then generated, from which monthly sediment data were derived. This dataset was subsequently utilized for the calibration and validation of the SWAT model.

The R^2 value for monthly sediment during the calibration period was obtained as 0.65, accompanied by an NSE of 0.66, suggesting satisfactory model performance. However, during the validation period, the R^2 and NSE values dipped to 0.61 and 0.55, respectively.

SWAT model results

Hydrology and water balance

Spatial distribution of precipitation

Over the period of the 23-year run, the average annual precipitation distribution is estimated to be 1676.2 mm for the basin, with sub-basins 7 and 13 recording the highest amount (2617.7 mm) and sub-basins 10 and 11 experiencing the lowest (1092.2 mm) precipitation. 480.6 mm was the standard deviation of precipitation distribution among the sub-basins. Figure 11a shows

the spatial distribution of precipitation in the basin. Compared to the average precipitation that DHM observes, this simulated precipitation is somewhat exaggerated.

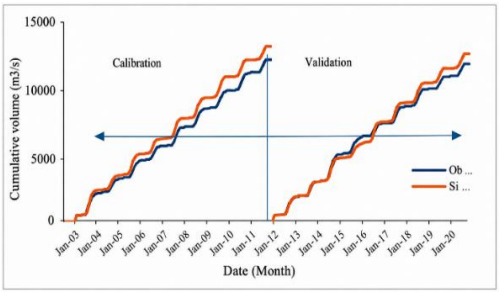

Figure 9, Cumulative flow volume curves

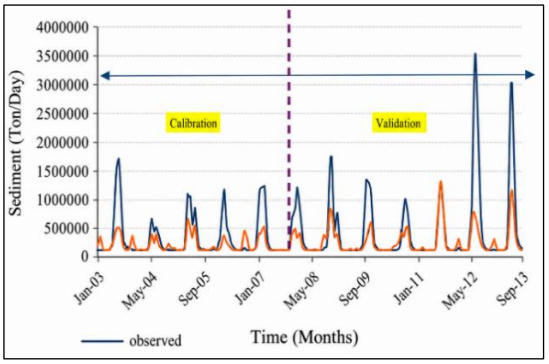

Figure 10, Calibration and validation curve for sediment

Table 5, Results of global sensitivity analysis and calibrated parameter values of the SWAT model obtained using the SUFI-2 algorithm in SWAT-CUP.

Parameter Name	Fitted Value	Min Value	Max Value	t-Stat	P-Value
V__CH_COV2.rte	0.408	0.36	1.00	-0.045048167	0.971340822
R__SOL_K(..).sol	-0.795	-0.94	1.22	-0.001688006	0.998925383
V__CH_K1.sub	7.75	0.00	10.00	0.056498201	0.964070325
R__SOL_BD(..).sol	-0.0495	-0.47	0.11	0.023819957	0.984838612
R__SLSUBBSN.hru	-0.30	-0.35	0.05	-0.052232961	0.966777656
V__OV_N.hru	2.38025	0.01	5.00	-0.121865253	0.922798843
V__CH_N1.sub	2.13225	-0.21	3.26	-0.041870080	0.973360239
V__CH_ERODMO(..).rte	0.435	-0.40	0.60	0.011318633	0.992794642
V__ADJ_PKR.bsn	1.5875	0.50	2.00	-0.008864086	0.994357096
R__SOL_Z(..).sol	0.38625	-0.03	0.42	0.000000000	1.000000000
R__USLE_K(..).sol	-0.2585	-0.19	0.27	0.033582860	0.978628519
R__HRU_SLP.hru	-0.12025	-0.15	0.02	-0.008472125	0.994606607
V__CH_S2.rte	0.537	0.24	0.68	0.023522648	0.985027778
V__PRF.bsn	0.5575	0.20	1.50	-0.065042844	0.958650684
R__CN2.mgt	-0.18975	-0.22	-0.11	0.059780293	0.961987921
V__CH_N2.rte	0.26375	0.01	0.30	0.034715605	0.977908231
V__CH_S1.sub	0.31725	-0.03	4.56	-0.084734476	0.946184908
R__USLE_P.mgt	-0.8225	-0.92	-0.66	0.033582860	0.978628519

The middle part of the river basin, which is primarily made up of the Jhimruk Khola watershed, experiences high precipitation. The denser forest cover and the upper Siwalik zone's tropical monsoonal regime may be attributed to the comparatively higher precipitation. The fact that this sub-basin is oriented in the windward zone of the Mahabharat range may be another factor. Because it is located in the semi-arid rain-shadow zone outside of the Mahabharat range, the western portion of the basin, or the downstream region, saw relatively less rainfall. At the same time, the leeward side of the Mahabharat Range and a few higher peaks cause less rainfall in the upstream portion of the West Rapti River, which is primarily in the districts of Rolpa and Salyan.

Spatial distribution of surface runoff

The average annual surface runoff was estimated as 573.4 mm in the model, with sub-basin 13 estimating the highest runoff (1180.1 mm) and sub-basin 11 estimating the lowest (276.2 mm). The standard deviation (284.7 mm) suggested variability in runoff distribution among the sub-basins of WRB. Figure 11b shows the spatial distribution of surface runoff in the basin.

Spatial distribution of water yield and evapotranspiration

With a low water output of 442 mm for sub-basin 10 and a high of 1845 mm for sub-basin 13, the average annual water yield in the basin was calculated to be 951.28 mm. Figure 11c shows the regional distribution of water yield in WRB. The Jhimruk Khola and downstream sub-basins were estimated to experience high evapotranspiration, with an average of 689.99 mm annually for the basin. The maximum was seen at sub-basin 19 and nearby sub-basins. These sub-basins, which have soil types of Je75-2a and Rd30-2b, are primarily composed of agricultural and mixed forest terrain contributed high evapotranspiration (Figure 11d).

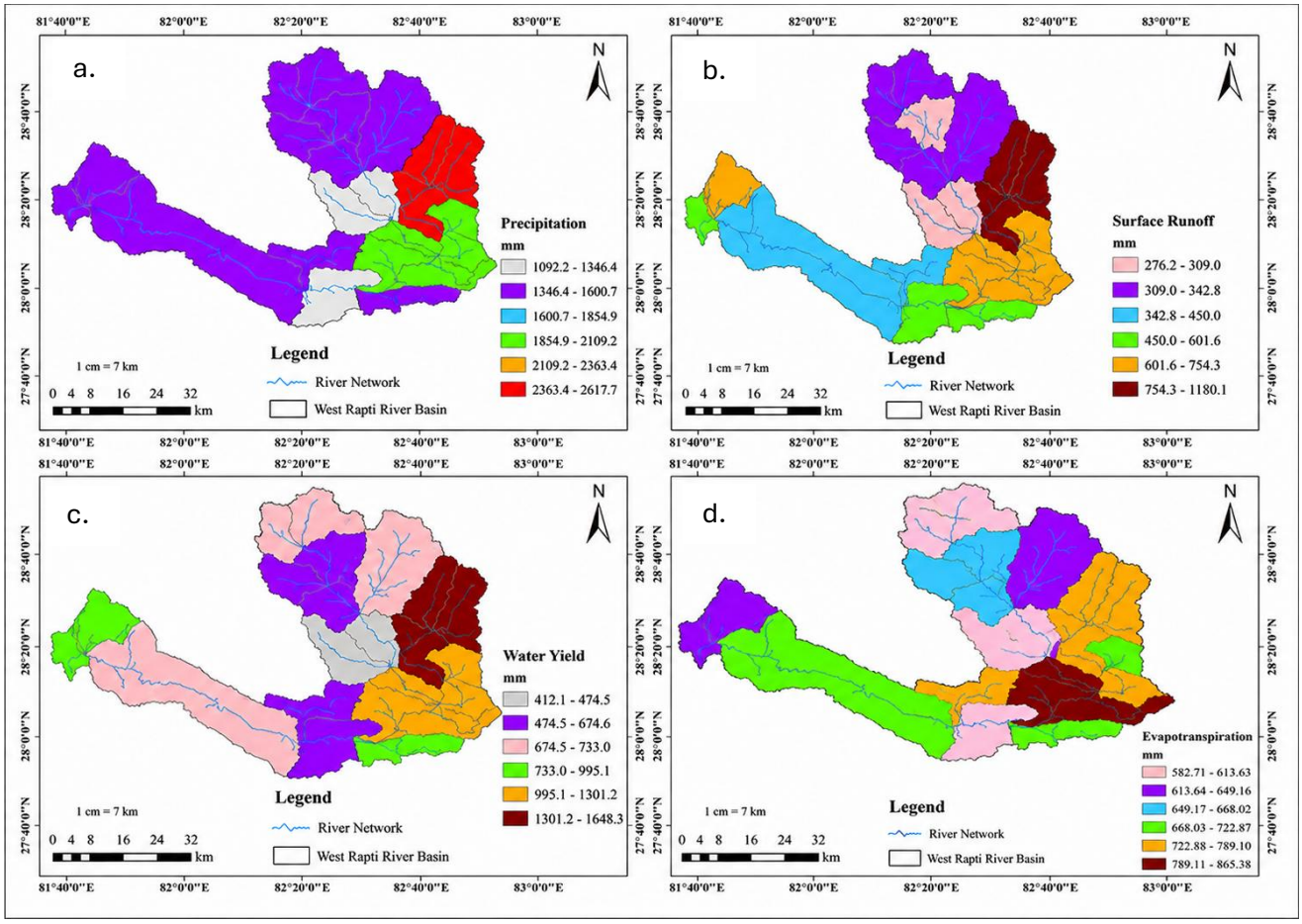

Figure 11, a. Precipitation and distribution map, b. Surface runoff and distribution map, c. Water yield distribution map, d. Evapotranspiration distribution map

Spatial distribution of sediment yield

The average annual sediment yield was determined to be 166 tonnes/ha by SWAT, with sub-basin 8 having the highest yield (468.05 tonnes/ha) and sub-basin 9 having the lowest (15.68 tonnes/ha) contribution. The standard deviation of sediment yield among the sub-basins was 32.06 tonnes/ha.

Figure 12 shows the spatial distribution of sediment yield in WRB. In the sub-basins, extremely high spatial diversity was noted. The Jhimruk Khola watershed region again attributed the highest yield of sediment to precipitation. This may suggest precipitation as a major erosion factor. This could also be due to the steeper topography of the Jhimruk Khola watershed. During the monsoon, surface runoff may potentially be the cause. Nonetheless, the Rapti River's downstream sub-basins made up a very small portion of the overall sediment budget.

Compared to the average sediment production of Nepalese river basins, this overall sediment yield or erosion rate is significantly higher (Sinha et al., 2019). Additionally, it exceeded the world average (Nepal et al., 2014).

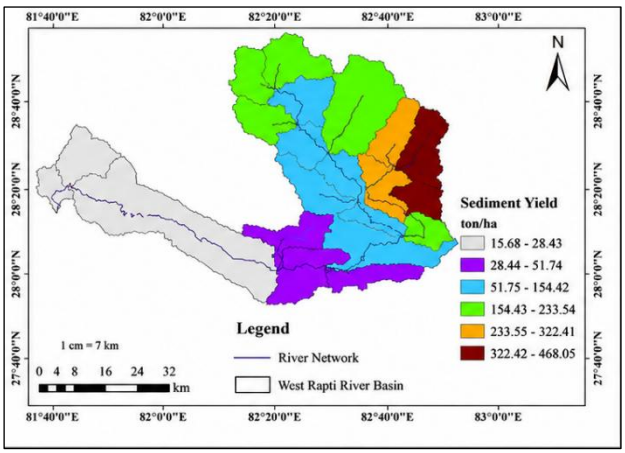

Figure 12, Sediment yield distribution map

Water balance in the West Rapti River basin

Out of the total precipitation that falls in the basin 55% flow as streamflow, 42% escape away as evapotranspiration. 55% contribute to streamflow. The remaining portion percolates to the aquifer (Figure 13).

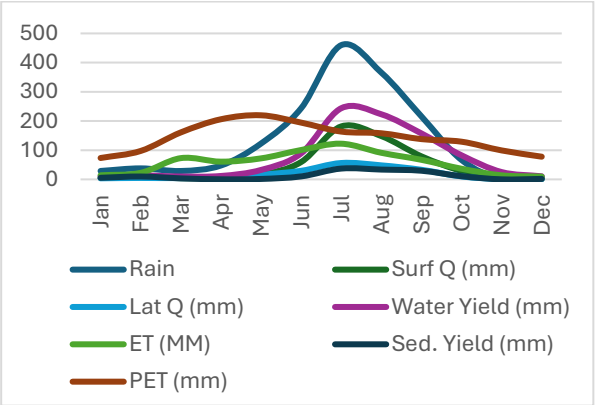

Figure 13, Water balance curves

Conclusion

This study successfully applied the SWAT model to simulate the baseline hydrology and water balance of Nepal's West Rapti River Basin, providing valuable insights into its hydrological processes and sediment dynamics. The model demonstrated strong predictive performance during calibration (R^2 = 0.95, NSE = 0.76) and validation (R^2 = 0.91, NSE = 0.75), accurately reproducing seasonal streamflow variability and sediment yield patterns. The most sensitive hydrological parameters were the curve number (CN2), baseflow recession coefficient (ALFA_BF), and surface runoff lag coefficient (SURLAG), emphasizing the combined influence of land use, soil characteristics, and runoff generation on basin hydrology. Long-term simulations (2000–2022) indicated a mean annual precipitation of 1,676 mm/yr, of which approximately 55% contributed to streamflow (951 mm/yr), while 42% was lost through evapotranspiration. Monsoon-driven surface runoff (573 mm/yr) dominated the hydrological regime, accounting for 68% of annual streamflow and approximately 85% of the annual sediment yield.

Sub-basin 8 was identified as the primary erosion hotspot, producing 468 t ha/yr because of its steep slopes (>40%) and highly erodible land use, highlighting the dominant role of topography in sediment generation. The spatial variability of evapotranspiration, surface runoff, and groundwater recharge reflected differences in land cover, soil properties, and terrain characteristics, resulting in distinct hydrological responses among forested, agricultural, and mixed land-use sub-basins. These findings demonstrate the basin's susceptibility to monsoon-driven hydrological extremes and land degradation, underscoring the need for targeted soil and water conservation measures in erosion-prone areas. The study provides a robust baseline for evaluating future climate and land-use change impacts and supports the development of sustainable watershed management strategies, including afforestation, soil conservation, and reservoir sedimentation control. Future research should integrate climate change projections and alternative land-use scenarios to assess long-term watershed resilience and guide adaptive water resource management.

Overall, the SWAT model proved to be an effective tool for quantifying the hydrology–sediment interactions of the West Rapti River Basin and provides a sound scientific basis for watershed planning and management in similar mountainous river basins.

References

Abdullah, M., and Al-Ansari, N. (2022). Missing rainfall data estimation: An approach to investigate different methods: Case study of Baghdad. Arabian Journal of Geosciences, 15(23), 1740. https://doi.org/10.1007/s12517-022-10995-6

Arnold, J. G., Moriasi, D. N., Gassman, P. W., Abbaspour, K. C., White, M. J., Srinivasan, R., Santhi, C., Harmel, R. D., Van Griensven, A., Van Liew, M. W., Kannan, N., and Jha, M. K. (2012). SWAT: Model use, calibration, and validation. Transactions of the ASABE, 55(4), 1491–1508. https://doi.org/10.13031/2013.42256

Arnold, J. G., Srinivasan, R., Muttiah, R. S., and Williams, J. R. (1998). Large-area hydrologic modeling and assessment: Part I. Model development. Journal of the American Water Resources Association, 34(1), 73–89. https://doi.org/10.1111/j.1752-1688.1998.tb05961.x

Ayele, G. T., Kuriqi, A., Jemberrie, M. A., Saia, S. M., Seka, A. M., Teshale, E. Z., Daba, M. H., Bhat, S. A., Demissie, S. S., Jeong, J., and Melesse, A. M. (2021). Sediment yield and reservoir sedimentation in highly dynamic watersheds: The case of Koga Reservoir, Ethiopia. Water, 13(23), 3374. https://doi.org/10.3390/w13233374

Basnet, N., Sitaula, S., Bohara, R., Bhattarai, S., Rawal, S., Uprety, M. P., Awasthi, M. P., Varol, M., Kayastha, S. P., and Pant, R. R. (2024). Hydro-chemical characteristics of Biring and Tangting rivers (Nepal) and evaluation of water quality for drinking and irrigation purposes. Environmental Research, 261, 119697. https://doi.org/10.1016/j.envres.2024.119697

Becker, A., and Braun, P. (1999). Disaggregation, aggregation and spatial scaling in hydrological modeling. Journal of Hydrology, 217(3), 239–252. https://doi.org/10.1016/S0022-1694(98)00291-1

Bekele, S., and Abate, B. (2020). Estimation of sediment yield using SWAT model: A case of Soke River Watershed, Ethiopia. International Journal of

Engineering Research and Technology, 9(12), 685–695.

Bhatta, B., Shrestha, S., Shrestha, P. K., Talchabhadel, R., 2019. Evaluation and application of a SWAT model to assess the climate change impact on the hydrology of the Himalayan River Basin. Catena, 181, 104082. https://doi.org/10.1016/j.catena.2019.104082

Bishwakarma, K., Wang, G., Zhang, F., Pant, R. R., Yuxuan, X., and Adhikari, S. (2024). Chemical weathering and CO2 consumption rates of the Koshi River Basin: Modeling and quantifying. Journal of Hydrology, 641, 131760. https://doi.org/10.1016/j.jhydrol.2024.131760

Bohara, R., Sitaula, S., Basnet, N., Awasthi, M. P., Rawal, S., Joshi, T. R., Byanju, R. M., and Pant, R. R. (2024). Hydrochemical characterization and water quality of perennial rivulets (Darchula), Sudurpashchim Province, Nepal. Tribhuvan University Journal, 39(2), 1–26. https://doi.org/10.3126/tuj.v39i2.72872

Chilagane, N. A., Kashaigili, J. J., Mutayoba, E., Lyimo, P., Munishi, P., Tam, C., and Burgess, N. (2021). Impact of land use and land cover changes on surface runoff and sediment yield in the Little Ruaha River Catchment. Open Journal of Modern Hydrology, 11(3), 54–74. https://doi.org/10.4236/ojmh.2021.113004

Chinnasamy, P., and Sood, A. (2020). Estimation of sediment load for Himalayan rivers: A case study of Kaligandaki in Nepal. Journal of Earth System Science, 129(1), 181. https://doi.org/10.1007/s12040-020-01437-6

de Oliveira Serrão, E. A., Silva, M. T., Ferreira, T. R., de Ataide, L. C. P., dos Santos, C. A., de Lima, A. M. M., da Silva, V. P. R., de Sousa, F. A. S., and Gomes, D. J. C. (2022). Impacts of land use and land cover changes on hydrological processes and sediment yield determined using the SWAT model. International Journal of Sediment Research, 37(1), 54–69. https://doi.org/10.1016/j.ijsrc.2021.04.002

Douglas-Mankin, K. R., Srinivasan, R., and Arnold, J. G. (2010). Soil and Water Assessment Tool (SWAT) model: Current developments and applications. Transactions of the ASABE, 53(5), 1423–1431. https://doi.org/10.13031/2013.34915

FAO (2002). FAO/UNESCO digital soil map of the world and derived soil properties (Land and Water Digital Media Series No. 1, Rev. 1). Food and Agriculture Organization of the United Nations, Rome.

FRTC (2022). Land cover of Nepal [Data set]. FRTC. https://doi.org/10.26066/RDS.1972729

KC, M., Aryal, I., Dhakal, N. R., and Marahatta, S. (2023). Application of SWAT hydrological model to simulate flow of the Seti-Gandaki Basin. Jalawaayu, 3(1). https://doi.org/10.3126/jalawaayu.v3i1.52060

Kumari, S., Singh, V., Suryavanshi, S., and Kumar, M. (2024). Application of the SWAT model for hydrological simulation of the Rapti River Basin. Journal of Experimental Agriculture International, 46 (6), 140-153. https://doi.org/10.9734/jeai/2024/v46i62466

Li, H., Yu, C., Qin, B., Li, Y., Jin, J., Luo, L., Wu, Z., Shi, K., and Zhu, G. (2022). Modeling the effects of climate change and land use/land cover change on sediment yield in a large reservoir basin in the East Asian monsoonal region. Water, 14(15), 1–19. https://doi.org/10.3390/w14152346

Liu, Y., and Jiang, H. (2019). Sediment yield modeling using the SWAT model: Case of the Changjiang River Basin. IOP Conference Series: Earth and Environmental Science, 234(1), 012031. https://doi.org/10.1088/1755-1315/234/1/012031

Michael, K. H., and Jain, M. (2013). Runoff and sediment modeling using SWAT in Gumera Catchment, Ethiopia. Open Journal of Modern Hydrology, 3(4), 196–205. https://doi.org/10.4236/ojmh.2013.34024

Moges, D., Moges, D. M., and Bhat, H. G. (2020). Watershed degradation and management practices in north-western highland Ethiopia. Environmental Monitoring and Assessment, 192(10), 664. https://doi.org/10.1007/s10661-020-08628-0

Moriasi, D. N., Arnold, J. G., Van Liew, M. W., Binger, R. L., Harmel, R. D., and Veith, T. (2007). Model evaluation guidelines for systematic quantification of accuracy in watershed simulations. Transactions of the ASABE, 50(3), 885–900. https://doi.org/10.13031/2013.23153

Nash, J. E., and Sutcliffe, J. V. (1970). River flow forecasting through conceptual models: Part I—A discussion of principles. Journal of Hydrology, 10(3), 282–290. https://doi.org/10.1016/0022-1694(70)90255-6

Nepal, J., Pant, R. R., Shrestha, S., Paudel, S., Bishwakarma, K., Awasthi, M. P., and Dhital, Y. P. (2024). Water balance estimation and runoff simulation of Chameliya Watershed, Nepal. Environmental Earth Sciences, 83(3), 117. https://doi.org/10.1007/s12665-024-11430-7

Nepal, S., Flügel, W.-A., and Shrestha, A. B. (2014). Upstream-downstream linkages of hydrological processes in the Himalayan region. Ecological Processes, 3(1), 19. https://doi.org/10.1186/s13717-014-0019-4

Neupane, S. N., and Pandey, A. (2021). Hydrological modeling of the West Rapti River Basin of Nepal using the SWAT model. In A. Pandey, S. Mishra, M. Kansal, R. Singh, and V. Singh (Eds.), Water management and water governance (Vol. 96, pp. XX–XX). Springer,

Cham. https://doi.org/10.1007/978-3-030-58051-3_19

Owens, P.N.(2020).Soil erosion and sediment dynamics in the Anthropocene: A review of human impacts during a period of rapid global environmental change. Journal of Soils and Sediments, 20(12), 4115-4143. https://doi.org/10.1007/s11368-020-02815-9

Pandey, V. P., Dhaubanjar, S., Bharati, L., and Thapa, B. R. (2019). Hydrological response of Chamelia Watershed in Mahakali Basin to climate change. Science of the Total Environment, 650, 365–383. https://doi.org/10.1016/j.scitotenv.2018.09.053

Pant, R. R., Varol, M., Phuyal, S., Bhattarai, S., Awasthi, M. P., Thakur, T. K., Bohara, R., and Afandi, G. E. (2025). How sand mining is shaping the Trishuli River in the Himalayas of South Asia. Earth Systems and Environment, 1–17. https://doi.org/10.1007/s41748-025-00569-3

Rahman, M. M., Harada, D., and Egashira, S. (2024). Sediment transport processes in the Sangu River Basin using a rainfall-sediment runoff model for sustainable river management. Proceedings of IAHS, 386, 109–114. https://doi.org/10.5194/piahs-386-109-2024

Ren,S., Zhang,B.,Wang, W.J.Yuan,Y.& Guo, C (2021). Sedimentation and its response to management strategies of the Three Georges River, Yangste River, China.Catena, https://doi.org/10.1016/j.catena.2020.105096

Schweizer, M., Dieterich, A., Corral Morillas, N., Dewald, C., Miksch, L., Nelson, S., Wick, A., Triebskorn, R., and Köhler, H. R. (2018). The importance of sediments in ecological quality assessment of stream headwaters: Embryotoxicity along the Nidda River and its tributaries in Central Hesse, Germany. Environmental Sciences, 30(1), 22 https://doi.org/10.1186/s12302-018-0150-4

Shi, X., Zhang, F., Lu, X., Wang, Z., Gong, T., Wang, G., and Zhang, H. (2018). Spatiotemporal variations of suspended sediment transport in the upstream and midstream of the Yarlung Tsangpo River (the upper Brahmaputra), China. Earth Surface Processes and Landforms, 43(2), 432–443. https://doi.org/10.1002/esp.4258

Shinde, V. M., Deshpande, P. K., and Kumthekar, M. B. (2013). Application of ASTER DEM in watershed management as flood zonation mapping in Koyana River of the Western Ghats. International Journal of Scientific and Engineering Research, 4(5), 297–301.

Sinha, R., Gupta, A., Mishra, K., Tripathi, S., Nepal, S., Wahid, S. M., and Swarnkar, S. (2019). Basin-scale hydrology and sediment dynamics of the Koshi River in the Himalayan foreland. Journal of Hydrology, 570, 156–166. https://doi.org/10.1016/j.jhydrol.2018.12.051

Srivastava, A., Deb, P., and Kumari, N. (2020). Multi-model approach to assess the dynamics of hydrologic components in a tropical ecosystem. Water Resources Management, 34, 327–341. https://doi.org/10.1007/s11269-019-02452-z

Subedi, S. R., Lamichhane, M., Dhungana, S., Chalise, B., Bhattarai, S., Chaulagain, U., and Khatiwada, R. (2024). Assessing the impact of climate change on streamflow in the Tamor River Basin, Nepal: An analysis using SWAT and CMIP6 scenarios. Discover Civil Engineering, 1, 135. https://doi.org/10.1007/s44290-024-00143-2

Thapa, B., Shrestha, R., Dhakal, P., and Thapa, B. S. (2005). Problems of Nepalese hydropower projects due to suspended sediments. Aquatic Ecosystem Health and Management, 8(3), 251–257. https://doi.org/10.1080/14634980500218241

Thomas, J., Joseph, S., Thrivikramji, K. P., and Arunkumar, K. S. (2014). Sensitivity of digital elevation models: The scenario from two tropical mountain river basins of the Western Ghats, India. Geoscience Frontiers, 5(6), 893–909. https://doi.org/10.1016/j.gsf.2013.12.008

Toma, M. B., Belete, M. D., and Ulsido, M. D. (2023). Hydrological components and sediment yield response to land use and land cover change in the Ajora-Woybo Watershed of Omo-Gibe Basin, Ethiopia. Air, Soil and Water Research, 16, 1–17. https://doi.org/10.1177/11786221221150186

Van Oost, K., Van Rompaey,A. Poesen, J.Grovers,G& Verstraeten,G.(2002).Evaluating an integrated approach to catchment management to reduce soil loss and sediment pollution through modeling. Soil Use and Manangement , 18(4)386-394. https://doi.org/10.1079/sum.2001.150

Vercruysse, K., Grabowski, R.C., & Rickson, R.J(2017). Suspended sediment transport dynamics in rivers: multi-scale drivers of temporal variation. Earth _ science Reviews, 166, 38-52. https://doi.org/10.1016/j.earscirev.2016.12.016

Technical Note DOI: https://doi.org/10.64862/ajeg.2025.202.05.268 Open Access

Structural Controls on Rock Slope Instability in the Bhotekoshi Corridor, Sindhupalchowk, Nepal, Following the 2015 Gorkha Earthquake

Bikash Adhikari[1], Ram Chandra Tiwari[2*] and Aanchal Tiwari[2]

[1]Department of Environmental Science and Engineering, Kathmandu University, Nepal
[2]Department of Civil Engineering, Institute of Engineering, Pulchowk Campus, Tribhuvan University, Lalitpur, Nepal

(*Corresponding E-mail: rct2075ce_rctiwari@pcampus.edu.np)

Received: July 08, 2025, Accepted: November 25, 2025

Abstract: This study critically examines the post-earthquake stability of a mountain slope in the Bhotekoshi Hydropower area, Sindhupalchowk District, one of the regions most affected by the 2015 Gorkha Earthquake of Mw 7.8. The weak geological formations of the area and steep terrain have repeatedly triggered slope failures, damaging highways, hydropower structures, and settlements along the Araniko Highway connecting Kathmandu to Tibet. Using Slope Mass Rating (SMR) and Stereographic Projection techniques, the study identifies key discontinuities, notably at 235°/67°, that control slope instability. The obtained RMR (27) and SMR (37.8) classify the slope as Class IV (Bad), denoting high instability and potential for large-scale planar and wedge failures. Stereographic analysis indicates that 57% and 28% of the area are critically prone to planar and wedge failures, respectively. These findings reveal significant structural weaknesses and emphasize the urgent need for systematic stabilization and continuous monitoring to safeguard hydropower infrastructure and communities in this seismically and geologically fragile region.

Keywords: ***Mountain slopes, Post-earthquake, Slope stability analysis, Slope stabilization, The 2015 Gorkha Earthquake.***

Introduction

Nepal Himalaya lies in a tectonically active region, characterized by fragile mountain and hill formations prone to slope instability. Landslides are common, causing loss of life, property, and infrastructure. This problem is particularly severe in Sindhupalchowk District, which was heavily affected by the 2015 Gorkha Earthquake, with most aftershocks concentrated in the district and nearby areas (Table 1). Roadside slopes along strategic routes, including the 115 km Araniko Highway connecting Kathmandu to Tibet, are highly vulnerable to traffic disruptions from slope failures triggered by steep terrain, weak geology, heavy rainfall, river floods, and seismic activity (Jha, 2014). The region's complex topography, combined with anthropogenic activities such as road haphazard construction and land use changes, further exacerbates slope instability and increases the risk of catastrophic failures.

Table 1, Major landslides in Nepal (DMG, 2018)

Year	Place	Loss
1967	Budhigandaki, Gorkha	9 died
1968	Budhigandaki, Gorkha	One bridge and 24 houses
1970	Tinau, Rupandehi	90 people lost
1971	Palakhu, Rasuwa	5 died
1976	Baglung	7 died and 3 bridges swept away
1982	Balefi, Sindhupalchowk	97 dead; many houses destroyed
1985	Trishuli, Rasuwa	-
1986	Tadi, Nuwakot	31 died; 24 houses and 3 bridge destroyed
1987	Sunkoshi, Sipa	98 people died; 229 houses, hydropower and highway destroyed
1988	Myagdi Khola, Myagdi	109 people died; 94 houses destroyed
1989	Aarukhola, Bajhang	16 people died; many houses destroyed
1996	Larcha, Sindhupalchowk	54 people lost; many houses destroyed
2010	Madikhola, Kaski	Fertile land and houses swept away
2014	Jure VDC, Sunkoshi	River blocked, claimed 156 lives, displaced hundreds, and caused extensive infrastructure and ecosystem damage.
2015	Mid Bhotekoshi and Upper Chaku	Damage Hydropower plants

The objective of this study is to assess the stability of mountain slopes affected by the Mw 7.8 2015 Gorkha Earthquake in Nepal, based on existing landslide inventories. The Bhotekoshi Hydropower area is selected as a case study due to its high landslide susceptibility and strategic importance for hydropower infrastructure. The study focuses on three specific

objectives: (1) review of existing landslide inventory in the study area, (2) slope stability analysis using Slope Mass Rating (SMR), and (3) slope stability assessment through Stereographic Projection techniques.

The findings are expected to contribute to improved landslide hazard management and mitigation strategies in earthquake-affected mountainous regions. Figure 1 shows the Bhotekoshi Hydropower area, illustrating different types of landslide activity: (a) rockfall, (b) debris flow, and (c) debris flow occurring along the highway.

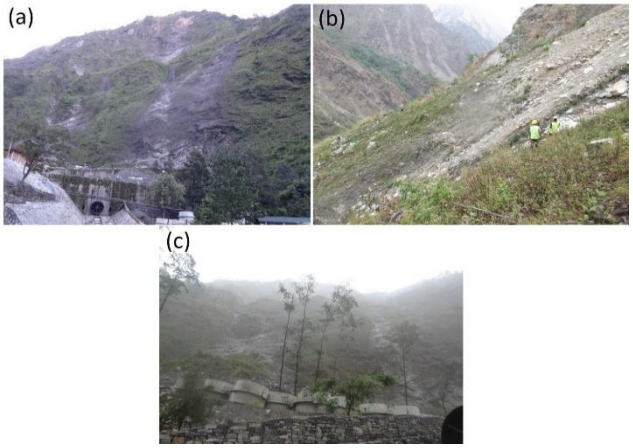

Figure 1, Bhotekoshi Hydropower area showing (a) rockfall, (b) debris slide, and (c) debris flow along the highway

Slope instability analysis

Slope stability was assessed using Rock Mass Rating (RMR) and Slope Mass Rating (SMR).

The RMR system, proposed by Bieniawski (1989) for tunneling and mining, has been extended to slope design. Bieniawski (1989) revised the ratings for various parameters. RMR classifies rock masses based on five field-determined parameters: (1) uniaxial compressive strength of intact rock, (2) Rock Quality Designation (RQD), (3) spacing of discontinuities, (4) condition of discontinuities, and (5) groundwater conditions. A sixth parameter, orientation of discontinuities, aids in assessing slope-specific stability issues.

The SMR modifies the RMR to account for slope-specific conditions, particularly discontinuity orientation relative to the slope face (Romana, 1991). It provides a more realistic assessment of slope stability in rock masses by incorporating geometric and kinematic factors. Key considerations include:

- Overall rock mass characterization (joint frequency, condition, water inflow)
- Difference between slope face strike and joint strike
- Joint dip versus slope dip, influencing potential planar or wedge failures
- Joint dip relative to normal joint friction on discontinuity surfaces

Stereographic projection

Stereographic projection is a graphical method for representing three-dimensional orientation data on a two-dimensional plane (Dahal, 2006). It is widely used in slope stability analysis and rock mass characterization to evaluate relationships between lines and planes. Projections are performed manually using a stereonet (Wulff net) or via computer, allowing visualization of discontinuity orientation and assessment of potential failure mechanisms.

Location and study area

The study area is situated in the Upper Bhotekoshi Valley within a run-of-the-river hydropower project on the Bhote Koshi River, a major tributary of the Sun Koshi River, in Sindhupalchowk District, central Nepal. It is located approximately 110 km northeast of Kathmandu, close to the Nepal–China border. The project includes a headworks with a side intake constructed about 500 m downstream of the confluence of the Bhote Koshi and Jung Khola near Tatopani. The powerhouse is located at Jhirpu Village, approximately 3.7 km downstream from the diversion dam. The project area is readily accessible via the Araniko Highway, which connects Kathmandu with the Nepal–China border at Kodari. The predominant rock types exposed in the study area include phyllite, schist, gneiss, quartzite, and minor metamorphic rocks.

Geological and geomorphological setting

Sherpa communities of Tibeto-Burmese origin. The valley experiences a monsoon-dominated climate, receiving approximately 2,500–3,000 mm of annual rainfall, of which 71–92% falls between June and September. Combined with elevations reaching 4,000 m asl and rugged topography with steep local relief, these conditions make the area highly susceptible to weathering, erosion, and slope instability. Geologically, the valley is underlain by steeply dipping phyllite, schist, gneiss, limestone, and quartzite, overlain by highly weathered colluvial and alluvial deposits. In the Himalaya, phyllite is considered the most landslide-prone lithology, followed by shale, schist, poorly cemented sandstone, limestone, gneiss, granite, and quartzite. Deeply weathered regolith is characterized by extensive gully erosion, while structurally controlled rockfalls commonly occur from steep phyllite cliffs. Large, slow-moving deep-seated translational landslides are widespread, rotational failures develop mainly where weathered schist is undercut, and channelized debris flows frequently occur along deeply incised tributaries. Based on the lithological classification (Table 2), the study area belongs to Group III, comprising slates, phyllites, and schists interbedded with quartzite and gneiss, indicating a moderate potential for lithology-controlled slope failure.

Nevertheless, road excavation and slope cutting have further increased the susceptibility of the area to landslides.

Table 2, Slide potential of rocks of Nepalese mountain (Krahenbunl and Wagner, 1983)

Group	Rock type of Nepal	Lithological slide potential
I	Slate, phyllite and schist, closely interbedded respected with calc-slate, calc Schist, limestone, dolomite and dolomite quartz	Very High (LCPS 16)
II	Slates, phyllites and schists	High (LCPS 10)
III	Slates, phyllites and schists closely interbedded respect with quarzite and gneiss	Medium (LCPS 5-10)
IV	Gneiss	Medium to Low(LCPS 1-5)
V	Quartzite	Low (LCPS 1)
VI	Massive limestone and dolomite	Very Low (LCPS 0-1)

Rock types

Slates, phyllites, and schists interbedded with quartzite and gneiss are the dominant rock types in the study area. The bedrock is composed predominantly of weak, highly weathered phyllite, although comparatively stronger schist is exposed in some locations. Phyllite is a foliated metamorphic rock formed through the progressive metamorphism of slate, in which very fine-grained white mica develops a preferred orientation. It is typically gray to light greenish-gray in color and exhibits well-developed foliation. Most of the exposed rock mass is moderately to highly weathered, resulting in reduced strength and increased susceptibility to failure.

The combination of steep natural slope angles, road-cut excavations, adverse discontinuity orientations, and advanced weathering constitutes the principal factors controlling slope instability in the study area. These conditions significantly reduce the stability of the rock mass and increase the likelihood of structurally controlled failures, particularly along foliation and joint planes.

Materials and methods

Initially, a desk study was conducted to plan the workflow. Relevant literature, including reports, books, and journals, was reviewed, followed by collection of secondary data from government agencies, primarily under the Ministry of Environment. Field visits were then conducted to gather primary data. Collected data were analyzed using standard slope stability approaches to achieve the study objectives. Finally, results were documented, disseminated, and compiled into a finalized report with regular reviews and updates.

Relevant reports, articles, and publications were collected from a variety of sources, including the Central Library of Tribhuvan University, Kathmandu University Library, and the Himalayan Conservation Group. Additionally, information was gathered from the Ministry of Environment, Science and Technology website, as well as from other relevant publications to ensure comprehensive coverage of the subject.

Field visits were conducted for direct observation and measurement using a Schmidt hammer, GPS, and Brunton compass. The following information were gathered: 1) the number of measurement stations (four); 2) criteria for choosing stations (ease of access, representation of exposure along the highway corridor, various rock types); 3) the tools employed (Schmidt hammer, Brunton compass, GPS); 4) procedure followed.

Collected data were analyzed for Rock Mass Rating (RMR), Slope Mass Rating (SMR), Stereographic Projection, and landslide mapping to evaluate slope stability.

Slope Mass Rating

Field visits and measurements of discontinuities are the main methods for finding the SMR. For this Bieniawski geomechanics classification of Rock Mass Rating (RMR) system has been used to find M. R. Romana's Slope Mass Rating (SMR). The basic five components of RMR i.e. uniaxial compressive strength of the intact rock, rock quality designation (RQD), spacing of discontinuities, conditions of discontinuities and ground water conditions. The rating was obtained by summing the values assigned for the first five components. Then, overall rating was made by a final adjustment by consideration of sixth parameter (orientation of discontinuities) depending upon the intended project type i.e. slope. Thus, the RMR was determined using following relationship:

$$RMR = \sum R \qquad (1)$$

Definition of RMR = R, where R is the summation of all the rating values for the five classification criteria (R1-R5) according to Bieniawski (1989).

Uniaxial compressive strength (UCS) of the intact rock was calculated by using Schmidt hammer test. Schmidt hammer was used to find Schmidt hardness of the rock for the calculating UCS of the intact rock.

Rock Quality Designation (RQD) was estimated using the joint data. Palmstrom (1982) suggested that number of discontinuities per unit volume helps to estimate value of RQD. Following formula given was used for the calculation:

$$RQD=115-3.3J_v \qquad (2)$$

Where, J_v is the sum of the number of joints (total joints seen) per unit volume and known as volumetric joint count.

Spacing of the discontinuities, condition of discontinuities, ground water condition and orientation of discontinuity was observed on site and estimated using Table described by Bieniawski (1989).

Joint dip angle, joint dip amount, slope dip angle and slope dip amount were measured with the help of Brunton compass for SMR system. Finally, SMR was calculated by the relationship defined by Romana (1991) as follows:

$$SMR=RMR+ (F_1*F_2*F_3) +F_4 \quad (3)$$

Where, RMR is Rock Mass Rating as obtained before.

F1 depends on parallelism between joints and slope face strikes. Its range is from 1.00 to 0.15 (Table 2). Romana gave these values empirically but he also proposed following relationship.

$$F_1= (1-SinA)^2 \quad (4)$$

Where A is the angle between the strike of the slope face and strike of discontinuities face.

F2 represents joint dip angle in the planar mode of failure. In a sense it is a measure of the probability of joint shear strength. Its value ranges from 1.00 to 0.15

F3 gives the relationship between the slope face and joint dip. In a planner mode of failure F3 refers to the probability that joints "daylight" in the slope face. Condition fair when slope face and joints are parallel. When the slope dips more than joints, very unfavorable conditions occur.

F4 is the adjustment factor for the method of excavation. Finally rated SMR values are classified as describes below:

Table 3, SMR classes defined (Romana, 1991)

Class	SMR	Description	Stability	Failures	Support
I	81-100	Very good	Completely stable	None	None
II	61-80	Good	Stable	Some Blocks	Occasional
III	41-60	Normal	Partially stable	Some joints or many wedges	Systematic
IV	21-40	Bad	Unstable	Planner or Big	Importance/ Corrective
V	0-20	Very bad	Completely Unstable	Big planner or soil like	Re-excavation

Stereographic projection

For slope stability analysis, the dip and dip direction of the natural slope surface and discontinuity planes were measured in the field using a Brunton compass. The collected structural data were analyzed using Stereonet software to evaluate the kinematic feasibility of slope failures and identify the potential failure mechanisms (Dahal, 2006).

Planar failure is considered possible when a discontinuity plane dips in the same general direction as the slope, with a strike difference of 20° or less, a dip angle lower than the slope angle, and a dip angle greater than the internal friction angle of the discontinuity.

Toppling failure is considered feasible when the discontinuity plane dips in the direction opposite to the slope face, the strike difference between the discontinuity and the slope is 20° or less, and the discontinuity dip exceeds the internal friction angle.

Wedge failure occurs when two intersecting discontinuity planes form a wedge whose line of intersection trends in the same general direction as the slope face.

Kinematic conditions for wedge failure are satisfied when the plunge of the line of intersection is less than the slope dip but greater than the internal friction angle, and the trend of the intersection line lies within approximately 20° of the slope dip direction.

Result and discussions

The data collected for RMR at different points above Bhotekoshi Hydropower project site are given below:

Station 1:

General description of rock = Hard schist

Number of joints = 20

Spacing between joints = 10 cm

Rock state = fresh/damp

Schmidt hammer value = 55

Station 2:

General description of rock = Weak phyllite

Number of joints = 25

Spacing between joints = 10-15 cm

Rock state = weathered/damp

Schmidt hammer value = 20

Station 3:

General description of rock = Weak phyllite rock

Number of joints = 22

Spacing between joints = 10-15 cm

Rock state = weathered/wet

Schmidt hammer value = 20

Station 4:

General description of rock = Weak phyllite rock

Number of joints = 8

Spacing between joints = 20 cm

Rock state = weathered/damp

Schmidt hammer value = 25

From above collected data from different location in the study area, RMR is calculated as per the standard chart, i.e. 27.

RMR for Location 1:

Rating for uniaxial compressive strength of axial load (R1) =12 (Using Schmidt hammer hardness and density of rock to find out Uniaxial Compressive Strength)

Rating for Rock quality designation (R2) = 8

Rating for Spacing between discontinuities (R3) = 8

Rating for Condition of discontinuities (R4) = 10

Rating for Groundwater Conditions (R5) = 20

Total RMR without orientation,

RMR=12+8+8+10+20 = 58

RMR with orientation for Slope (taking fair condition),

RMR= 58-25 = 33

RMR for Location 2:

Rating for uniaxial compressive strength of axial load (R1) = 4 (Using Schmidt hammer hardness and density of rock to find out Uniaxial Compressive Strength)

Rating for Rock quality designation (R2) = 8

Rating for Spacing between discontinuities (R3) = 8

Rating for Condition of discontinuities (R4) = 10

Rating for Groundwater Conditions (R5) = 20

Total RMR without orientation,

RMR=4+8+8+20+10 = 50

RMR with orientation for Slope (taking fair condition),

RMR= 50-25 = 25

RMR for Location 3:

Rating for uniaxial compressive strength of axial load (R1) =4 (Using Schmidt hammer hardness and density of rock to find out Uniaxial Compressive Strength)

Rating for Rock quality designation (R2) = 8

Rating for Spacing between discontinuities (R3) = 8

Rating for Condition of discontinuities (R4) = 7

Rating for Groundwater Conditions (R5) = 20

Total RMR without orientation,

RMR=4+8+8+20+7 = 47

RMR with orientation for Slope (taking fair condition),

RMR= 47-25 = 22

RMR for Location 4:

Rating for uniaxial compressive strength of axial load (R1) =4 (Using Schmidt hammer hardness and density of rock to find out Uniaxial Compressive Strength)

Rating for Rock quality designation (R2) = 17

Rating for Spacing between discontinuities (R3) = 10

Rating for Condition of discontinuities (R4) = 10

Rating for Groundwater Conditions (R5) = 10

Total RMR without orientation,

RMR=4+17+8+10+10 = 51

RMR with orientation for Slope (taking fair condition),

RMR= 51-25 = 26

Then, RMR = 27

The major discontinuities of slope in four different locations of the study area are given below:

Table 4, Major discontinuities of slope

No.	Dip Direction (Azimuth)	Dip Amount
1	304°	71°
2	235°	67°
3	231°	80°
4	230°	76°

The main discontinuity among them is 235°/67° and these joint sets could play main role in plane as well as wedge failures around the area.

Calculation of SMR

RMR from the calculation as per standard chart = 27

F1 = 0.7 (20°-10°)

F2 = 1 (dipping more than 45°)

F3 = -6 (difference is 0°-10°)

F4 = 15 (Natural Slope)

Then, SMR = 27 + (0.7 x 1 x (-6)) + 15 = 37.8

The calculated value lies on IV class (Bad), unstable having planner or big wedges failure of SMR and needs to be corrective measures in the slope.

Stereographic projection

Using 'Stereonet 8' graphical interpretation of slope stability is done. As shown in Figure 2 and 3, there is only presence of some plane failure and wedge failure according to the conditions for those failures.

The diagrams are based on stereographic projections created using Stereonet 8 in order to study the kinematic stability of slopes in the highway area near Bhotekoshi Hydropower Project site. Based on the plot of the orientation of the slope plane and the orientation of the major joint sets found at the site, the stereonets help us understand the potential failure mechanisms. The geometric relation between the great circles of the slope and the joints demonstrates the structural control of the stability, and shows that there are kinematically favorable conditions for plane and wedge failures.

Discussion

The rock slope investigated along the Bhotekoshi Hydropower Project corridor exhibits unfavorable stability conditions based on both the Rock Mass Rating (RMR) and Slope Mass Rating (SMR) classifications. The calculated SMR value of 37.8 places the slope within the Bad (Class IV) category, indicating an unstable rock

mass that is susceptible to structurally controlled failures.

According to the SMR classification proposed by Romana (1991), slopes in this category require appropriate stabilization and corrective measures before they can safely support engineering structures. The relatively low rock mass quality, combined with adverse discontinuity orientations, significantly increases the likelihood of instability.

The findings are consistent with those reported by Kafle (2010) for the Opi Landslide, which recorded an SMR value of 34, also falling within the Bad (Class IV) category. That study documented the occurrence of planar and large wedge failures, demonstrating that slopes with similar engineering geological characteristics are highly vulnerable to structurally controlled failure.

The Bhotekoshi Hydropower site shares many of the same geological and geomorphological attributes as the Opi Landslide, including steeply inclined slopes, weathered phyllite interbedded with gneiss and other metasedimentary rocks, a weak rock mass derived from clay-rich parent materials, and predominantly concave slope morphology. These similarities provide a valuable regional benchmark supporting the present interpretation that the investigated slope is inherently unstable.

Stereographic projection further confirmed the dominant failure mechanisms within the study area. Planar failure was identified in Figures 2(a), 2(c), 2(d), and 3(b), while wedge failure was recognized in Figures 2(b) and 3(c). Figure 3(a) showed no kinematically feasible failure. Overall, four of the seven stereographic analyses (57%) indicate planar failure, whereas two analyses (28%) indicate wedge failure. These results demonstrate that planar failure is the predominant instability mechanism, although wedge failure also represents a significant hazard in specific slope sections.

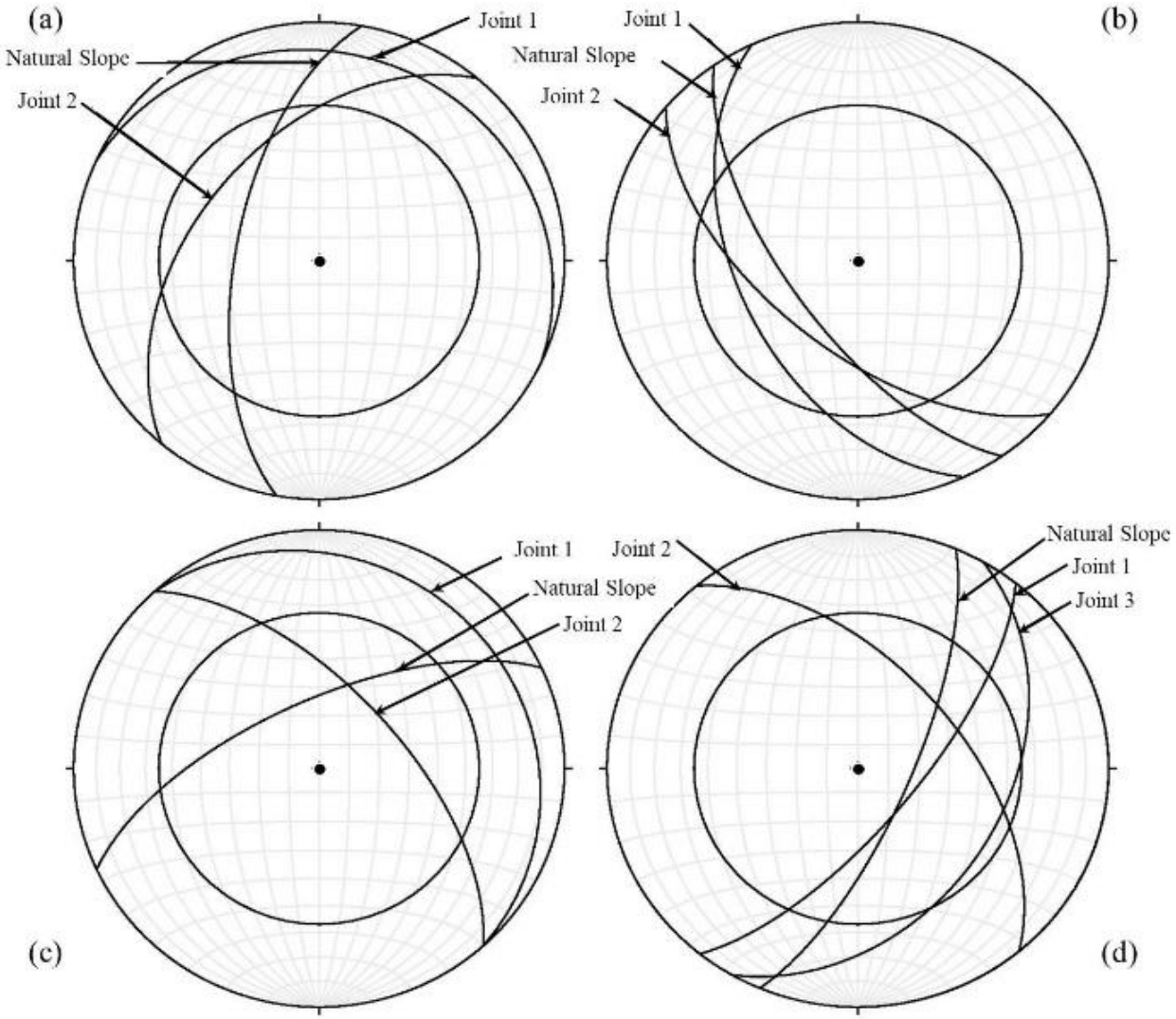

Figure 2, Stereographic projections of slope at Highway near Bhotekoshi Hydropower site: (a), (b), (c) and (d)

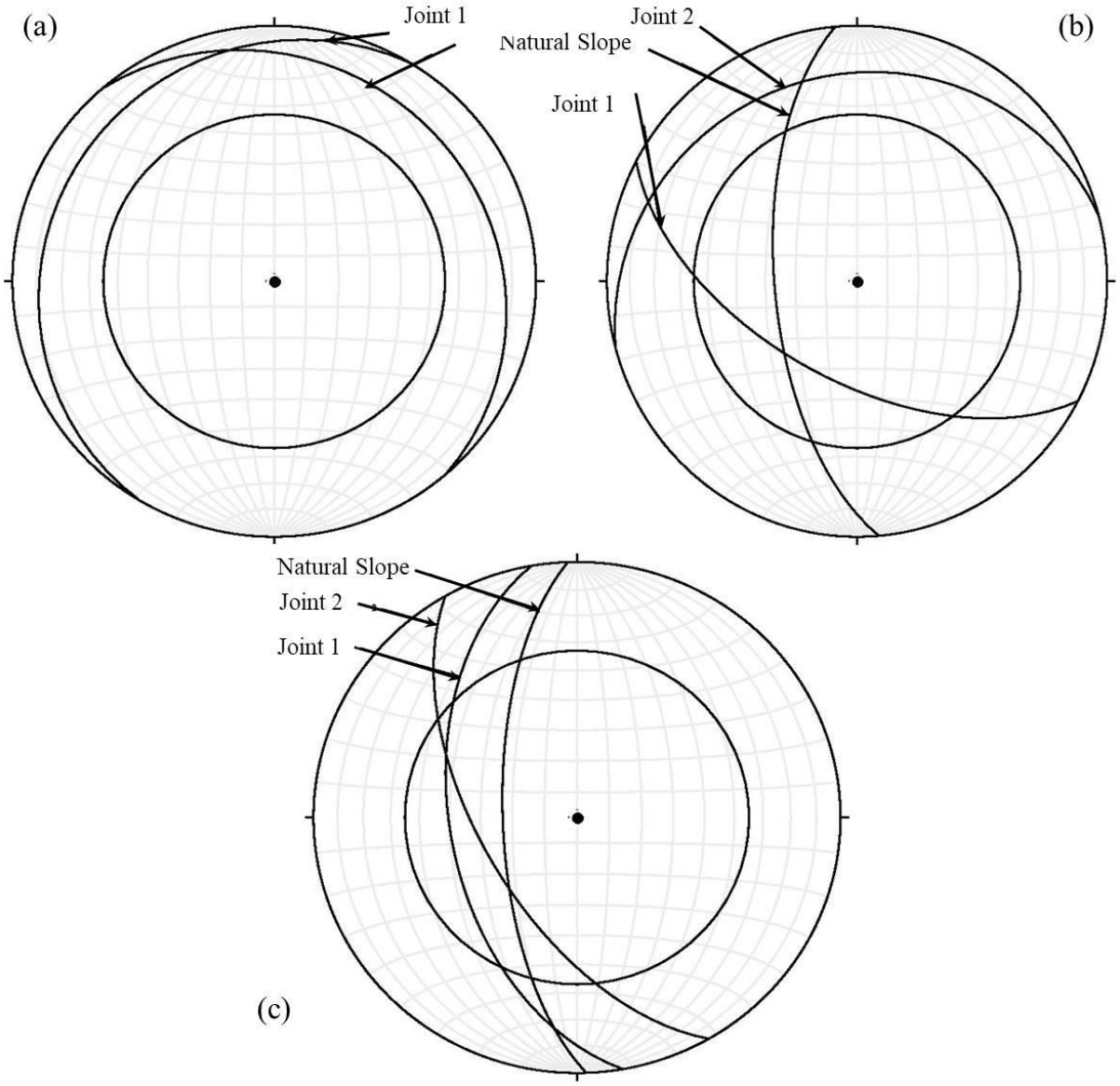

Figure 3, Stereographic projections of slope at Highway near Bhotekoshi Hydropower site: (a), (b) and (c)

The engineering implications of these findings are substantial. The calculated SMR value of 37.8 clearly indicates the need for stabilization measures, as recommended by Romana (1991).

The dominant discontinuity set (235°/67°) exhibits the greatest kinematic potential for sliding, making it the principal structural control on slope instability. Furthermore, the weathered phyllitic rock mass possesses reduced shear strength and durability, thereby increasing its susceptibility to failure under rainfall, seismic loading, and excavation activities.

Consequently, stabilization measures such as rock bolting, drainage improvement, retaining structures, rockfall protection systems, and systematic slope monitoring should be incorporated into the engineering design.

Quantitative stability analyses, including limit equilibrium and numerical modeling, are also recommended to complement the empirical classifications and provide a more comprehensive assessment of long-term slope performance.

Conclusion and recommendation

The exclusive conclusions drawn from this study, together with the major recommendations based on the engineering geological assessment and slope stability analysis, are presented in the following sections. These conclusions summarize the key findings of the investigation, while the recommendations provide practical guidance for future slope management, hazard mitigation, and infrastructure planning within the study area.

Conclusion

The rock slope stability assessment conducted in the Bhotekoshi Hydropower Project area using the Rock Mass Rating (RMR), Slope Mass Rating (SMR), and stereographic projection methods indicates that the investigated slopes are generally unstable and susceptible to structurally controlled failures. The RMR classification reveals that the rock mass quality ranges from fair to poor, reflecting the influence of highly

fractured rock masses, persistent discontinuities, and unfavorable geological conditions.

The calculated SMR values classify the majority of the investigated slopes as Class IV according to Romana (1991), representing an unstable slope condition with a high likelihood of failure unless appropriate stabilization measures are implemented. Kinematic analysis based on stereographic projection further demonstrates that planar failure is the dominant failure mechanism, occurring in approximately 57% of the analyzed slope sections where discontinuity orientations are favorably aligned with the slope face.

Wedge failure is identified as the second most significant failure mode, accounting for about 28% of the investigated locations due to the intersection of two or more discontinuity sets. The remaining slope sections are considered relatively stable with respect to the analyzed failure mechanisms.

Overall, the integrated application of RMR, SMR, and stereographic analysis provides a comprehensive evaluation of rock slope stability and highlights the critical role of geological structures in controlling instability within the Bhotekoshi Hydropower Project area.

Recommendation

Slope sections classified as SMR Class IV should be given high priority for continuous monitoring and detailed engineering geological investigation because they represent unstable rock masses with a significant potential for failure. Regular field inspections and periodic reassessment are recommended, particularly after intense rainfall or seismic events.

Rock slopes where planar and wedge failure mechanisms have been identified through stereographic projection should be evaluated individually using detailed structural mapping and site-specific stability analyses to better understand their failure potential and support appropriate mitigation planning.

Where kinematic analyses indicate the possibility of instability, suitable stabilization and protection measures, including rockfall barriers, retaining walls, rock bolting, shotcrete, drainage systems, and other engineered slope protection techniques, should be implemented based on detailed geotechnical investigations and sound engineering design principles.

Comprehensive geological, geotechnical, hydrogeological, and structural investigations should be carried out before the planning and construction of roads, hydropower projects, tunnels, and other infrastructure to ensure safe and sustainable development in the study area.

Future studies should incorporate quantitative slope stability analyses, including limit equilibrium and numerical modeling approaches, to complement the empirical stability classifications presented in this study and provide more reliable estimates of slope performance under both static and seismic loading conditions.

Article Note

This article is a full-length paper developed from **Extended Abstract #212**, entitled "**Stability of Mountain Slopes Affected by the 2015 Gorkha Earthquake: A Case Study of Bhotekoshi Hydropower, Sindhupalchowk, Nepal**", which was presented at the 15th Asian Regional Conference of the International Association for Engineering Geology and the Environment (ARC-15 of IAEG), held in Kathmandu, Nepal, from 27 to 29 November 2025.

References

Bieniawski, Z. T. (1989). Engineering Rock Mass Classifications: A Complete Manual for Engineers and Geologists in Mining, Civil, and Petroleum Engineering. John Wiley and Sons.

Dahal, R. (2006). Geology for Technical Students. Kathmandu: Bhrikuti Academic Publications, 756p.

DMG (2018). Landslide Inventory and Hazard Mapping of Nepal. Government of Nepal, Ministry of Industry, Commerce and Supplies, Department of Mines and Geology, Kathmandu, Nepal.

Jha, S. K. (2014). A case study on slope stability along Mid-Hill Highway, Dailekh, Nepal. International Symposium Geohazards: Science, Engineering and Management.

Kafle, K. R. (2010). Slope mass rating in Middle Mountain of Nepal: A case study on landslide at Rabi VDC, Opi village, Kavre. Kathmandu University Journal of Science, Engineering and Technology, 6, 28–38. https://doi.org/10.3126/kuset.v6i2.4009

Krahenbuhl, J. and Wagner, A. (1983). Survey, design, and construction of trail suspension bridges for remote areas. SKAT, Swiss Center for Appropriate Technology, St. Gallen, Switzerland.

Palmstrom, A. (1982). The volumetric joint count—a useful and simple measure of the degree of rock mass jointing. In IAEG Congress, New Delhi (Vol. 221). Available at: https://rockmass.net/ap/8_Palmstrom_on_Vol_joint_count_IAEG.pdf

Romana, M. (1991). SMR Classification. Presented at the 7th ISRM Congress, International Society for Rock Mechanics.

Asian Journal of Engineering Geology

Volume 2, No. 2

Table of Content

Quick Report

Original Articles

Technical Note

Official Journal of Nepal Society of Engineering Geology (NSEG)
Dhobighat, Lalitpur, Nepal
For Online Submission: https://ajeg.nseg.org.np